



universität
wien

DIPLOMARBEIT

Titel der Diplomarbeit

Optimizing extinction corrections in time series photometry

angestrebter akademischer Grad

Magistra der Naturwissenschaften (Mag. rer.nat.)

Verfasserin: Daniela Klotz
Matrikel-Nummer: 0308762
Studienrichtung
(lt. Studienblatt): Magisterstudium Astronomie UG2002
Betreuer: O. Univ. Prof. Dr. Michel Breger

Wien, im Juni 2009

Contents

| | |
|--|-----------|
| Abstract | 2 |
| 1 Introduction | 3 |
| 1.1 Why do some stars change their brightness? | 3 |
| 1.1.1 Pulsation mechanisms | 3 |
| 1.2 Modes of pulsation | 4 |
| 1.2.1 Quantum numbers | 5 |
| 1.2.2 Displacement | 5 |
| 1.2.3 Radial modes | 6 |
| 1.2.4 Nonradial modes | 7 |
| 1.2.5 p-modes and g-modes | 7 |
| 1.2.6 Mode identification | 9 |
| 1.3 The classical instability strip | 9 |
| 1.3.1 Cepheids | 9 |
| 1.3.2 W Vir stars | 9 |
| 1.3.3 RR Lyrae | 9 |
| 1.3.4 roAp stars | 9 |
| 1.3.5 γ Dor stars | 10 |
| 1.3.6 δ Scuti stars | 10 |
| 2 Photometer | 14 |
| 2.1 Single-channel photometer | 14 |
| 2.1.1 Layout | 14 |
| 2.1.2 Properties | 16 |
| 2.1.3 Advantages and disadvantages | 16 |
| 2.1.4 The noise problem | 17 |
| 2.1.5 Filters | 19 |
| 2.2 Wolfgang-Amadeus: the Vienna Twin Automatic Photoelectric Telescopes | 25 |
| 2.2.1 Observational restrictions | 25 |
| 2.2.2 Automatic telescopes | 26 |
| 2.2.3 Equipment | 26 |
| 2.3 The standard three-star technique | 27 |
| 2.3.1 Observation | 27 |
| 2.3.2 Selection of the comparison stars | 28 |

| | | |
|----------|---|-----------|
| 2.3.3 | Advantages of this technique | 28 |
| 3 | Data Reduction and Analysis | 30 |
| 3.1 | Julian Day Number and Julian Date | 30 |
| 3.1.1 | Calculation | 30 |
| 3.2 | True declination and right ascension | 31 |
| 3.2.1 | Calculation | 31 |
| 3.3 | Dark current correction | 32 |
| 3.4 | Dead time correction | 32 |
| 3.5 | Background correction | 32 |
| 3.6 | From counts per second to magnitude | 33 |
| 3.7 | Atmospheric extinction | 33 |
| 3.7.1 | Airmass | 33 |
| 3.7.2 | Sidereal time calculation | 34 |
| 3.7.3 | Extinction coefficient and intersection point | 34 |
| 3.8 | V – C1, V – C2, C1 – C2 | 35 |
| 3.9 | Heliocentric correction | 36 |
| 3.9.1 | Calculation | 37 |
| 4 | Frequency Analysis | 39 |
| 4.1 | Discrete Fourier Transform (DFT) | 39 |
| 4.2 | The Nyquist criterion | 41 |
| 4.2.1 | Example | 42 |
| 4.3 | Spectral window | 42 |
| 4.4 | Summary | 45 |
| 4.5 | Frequency-finding programs | 47 |
| 4.5.1 | Period04 | 47 |
| 4.5.2 | SigSpec | 48 |
| 5 | Results | 50 |
| 5.1 | Observational details | 50 |
| 5.1.1 | Instrument | 50 |
| 5.1.2 | Observing periods | 50 |
| 5.1.3 | Details on EE Cam and the comparison stars | 50 |
| 5.1.4 | Light curves | 51 |
| 5.2 | Data reduction | 54 |
| 5.2.1 | Heliocentric Julian Date correction | 54 |
| 5.2.2 | Extinction correction | 54 |
| 5.2.3 | Interpolation | 54 |
| 5.2.4 | Differential light curves | 55 |
| 5.2.5 | Elimination of individual data points | 55 |
| 5.2.6 | Frequency analysis | 55 |
| 5.2.7 | Restrictions | 56 |
| 5.3 | Determination of the appropriate extinction coefficient | 56 |
| 5.3.1 | Individual extinction coefficients – Method A | 57 |

| | | |
|----------|--|-----------|
| 5.3.2 | Constant intersection points – Method B | 57 |
| 5.3.3 | Constant extinction coefficients – Method C | 58 |
| 5.3.4 | Combination of constant and individual extinction coefficients – Method D | 58 |
| 5.3.5 | Further topics | 58 |
| 5.4 | Which extinction coefficient is correct? | 60 |
| 5.4.1 | First test: Residual light curves of EE Cam | 60 |
| 5.4.2 | Second test: Cycle-per-day periodicities | 61 |
| 5.5 | Discussion | 65 |
| A | Appendix | 67 |
| A.1 | Tables | 67 |
| A.1.1 | Extinction coefficients | 67 |
| A.1.2 | Observed residuals | 72 |
| A.2 | Figures | 76 |
| A.2.1 | Light curves of EE Cam | 76 |
| | References | 88 |
| | Acknowledgements | 91 |
| | Abstract – German | 92 |
| | Curriculum Vitae | 93 |

Abstract

The evolution and structure of pulsating stars is an interesting and fundamental field in astronomy. In order to get information on these properties it is crucial to study the inner part of a star, which is achievable by asteroseismology. Photometric data and theoretical model fitting to these data provide information on the change in brightness of a variable star and the opportunity to retrieve stellar parameters and describe physical processes by determining the frequencies. Frequency, amplitude and phase describe the sound waves, which can be used to gain information on the stellar interior. Observational data have to be corrected for several instrumental and atmospheric effects, and various sources of noise have to be taken into account to achieve a sufficient accuracy.

This thesis concentrates on the observational point of view. Instrumentation, data reduction and frequency analysis are explained, and common reduction algorithms are discussed. The major part of this work deals with the determination of the best extinction coefficients, in order to have the best correction for atmospheric extinction, which is caused by effects of absorption and scattering in the atmosphere. Four different methods to determine this coefficient are described and were tested using photometric data of the δ Scuti star EE Cam obtained during four (2006-2009) observing campaigns on one of the Vienna Twin Automatic Photoelectric Telescopes (APT), located in Arizona. Additionally, a frequency analysis of the data obtained in the first three observing campaigns was performed and the results are presented here.

An introduction to pulsating stars is provided in Chapter 1. Here, different types of pulsating variables, pulsation mechanisms and the inner structure are discussed. Chapter 2 deals with the instruments and filter systems used to obtain photometric data. The problem of instrumental noise is discussed and possible solutions are presented. As the APT was used to observe EE Cam, its properties are described in detail. A detailed description of the standard reduction steps is given in Chapter 3. The determination of frequencies, amplitudes and phases by using the Discrete Fourier Transform is finally discussed in Chapter 4. Two different software packages for frequency analysis are introduced. Information on the observations and the applied techniques is provided in Chapter 5, followed by a presentation and discussion of the results.

Chapter 1

Introduction

This chapter is a short introduction to the theory of pulsating stars, including pulsation mechanisms and modes. The classical instability strip and its members, with emphasis on δ Scuti stars, are presented.

1.1 Why do some stars change their brightness?

If the brightness of a star changes periodically, semi-periodically or even irregularly it is referred to as a variable star. There are several physical effects that can describe these variations. Variable stars can be assigned to different classes and sub-classes, depending on the physical effect causing the pulsation. Two different types of variables are known:

Intrinsic variables. The light variation is caused by physical changes in the inner part of the star. This type of variable stars can be divided into pulsating as well as eruptive variables.

Extrinsic variables. The variation in brightness is caused by either rotation or an eclipse of one star by another. They are divided into rotating stars and eclipsing binaries. Also exoplanetary transits may be responsible for extrinsic variations of stars.

This work concentrates on pulsating variables in the classical instability strip, where the pulsations can be radial (spherical symmetry is maintained) or nonradial (deviations from spherical symmetry). These stars expand and contract periodically causing the change in brightness. For many pulsating variables, the driving mechanism is the κ -mechanism. For solar-like oscillators the driving mechanism is convection. A third driving mechanism is the ε -mechanism.

1.1.1 Pulsation mechanisms

1.1.1.1 κ -mechanism

The κ -mechanism describes the pulsations in stars like δ Scuti or δ Cephei stars. The driving of this mechanism is the opacity

$$\kappa = \frac{1}{T} = \frac{I_0}{I}, \quad (1.1)$$

where T is the transmittance, I_0 the incident radiation and I the transmitted one. Thus, the opacity is a measure of the portion of radiation that cannot pass an atmospheric layer: the higher the opacity, the lower the fraction of transmitted radiation. The physical reason for this quantity is that radiation is scattered when penetrating the stellar material. The degree of opacity depends on pressure, temperature, and the chemical composition.

Pulsation will only occur if the opacity increases with temperature. Normally, an increase in temperature goes along with a decrease in opacity, because then the interaction of radiation and free electrons is less effective. This is valid for a constant number of free electrons. In the outer layers of a star single ionized and double or completely ionized atoms (e.g. He, H) are present. If the temperature increases (e.g. during compression), there will be more ionization and, consequently, the number of double ionized atoms is larger. Thus, more free electrons are available. Now more scattering will take place as there are more free electrons in the stellar material. An increase of the number of free electrons, therefore, goes along with a higher opacity. This blocks the radiation in the ionization layers. As a consequence, the radiation pressure increases. This retained pressure forces the star to expand. Due to expansion, the gas will cool down, less free electrons will be available and the opacity decreases, i.e., radiation can pass the stellar material more easily. The retained pressure can now escape and the radiation pressure decreases, which forces the star to contract.

1.1.1.2 Stochastic driving

This mechanism acts in the Sun, in solar-like stars as well as in red giants. If convection is effective enough, the convective layers will begin to oscillate. This type of pulsation is stable: the oscillation is damped in the atmosphere and can only survive thanks to stochastic re-excitation by convection.

1.1.1.3 ϵ -mechanism

The pulsation is caused by changes in the energy generation rate ϵ in the core of the star. The effect of this mechanism is very small and pulsation can therefore not be solely caused by the ϵ -mechanism.

1.2 Modes of pulsation

Kurtz (2006) wrote a detailed overview on stellar pulsation. Most of the information given in this section is adopted from his article.

The combination of frequency, amplitude and phase describes the sound waves. These frequencies are used to gain information on the stellar interior. The speed of sound, v_s , depends on the gas pressure, P , and the density, ρ , in a layer of the stellar atmosphere according to

$$v_s = \sqrt{\frac{\Gamma P}{\rho}}, \quad (1.2)$$

where Γ denotes the adiabatic exponent. For an ideal gas, pressure, density and temperature T are linked via

$$P = \frac{\rho k T}{\mu}, \quad (1.3)$$

μ denoting the molecular weight.

Substituting Eq. 1.3 for P in Eq. 1.2 yields

$$v_s = \sqrt{\frac{\Gamma k T}{\mu}}. \quad (1.4)$$

Changes in pressure invoke changes in temperature and density.

The sound speed is higher if the temperature is higher, because molecules are moving faster at higher temperatures.

The aim of asteroseismology is to measure the sound speed throughout a star in order to be able to understand the structure of the star. The interior speed of sound provides information on pressure, density, temperature, chemical composition and rotation. Thus, measuring the oscillation of a star permits to look inside the star.

1.2.1 Quantum numbers

The three-dimensionality of a star permits the oscillation modes to have nodes in three orthogonal directions (concentric radial shells, lines of latitude, lines of longitude). Consequently, there are three quantum numbers to describe these pulsation modes (see Fig. 1.1):

1. n is the number of radial nodes and is called the overtone of the mode if $m = 0$ (sometimes also referred to as k),
2. l is the spherical degree of the mode and defines the number of node lines on the stellar surface, $l \geq 0$,
3. m is the azimuthal order of the mode.

The number of surface nodes that are lines of longitude is

$$l - |m| \quad (1.5)$$

The values of m range from $-l$ to $+l$, i.e., there are $2l + 1$ m -modes for each degree l . Modes with $m > 0$ are travelling against the direction of rotation (retrograde), while modes with $m < 0$ are traveling into the direction of rotation (prograde). Modes with $m = 0$ are axisymmetric modes. A spherically symmetric star has the same frequencies for all $m = 2l + 1$. This is the so-called degeneration in $2l + 1$ folds.

1.2.2 Displacement

In theory, stellar pulsation is described by dividing the stellar atmosphere into (ideally infinitesimal) volume elements and examining the motion of each volume element. The

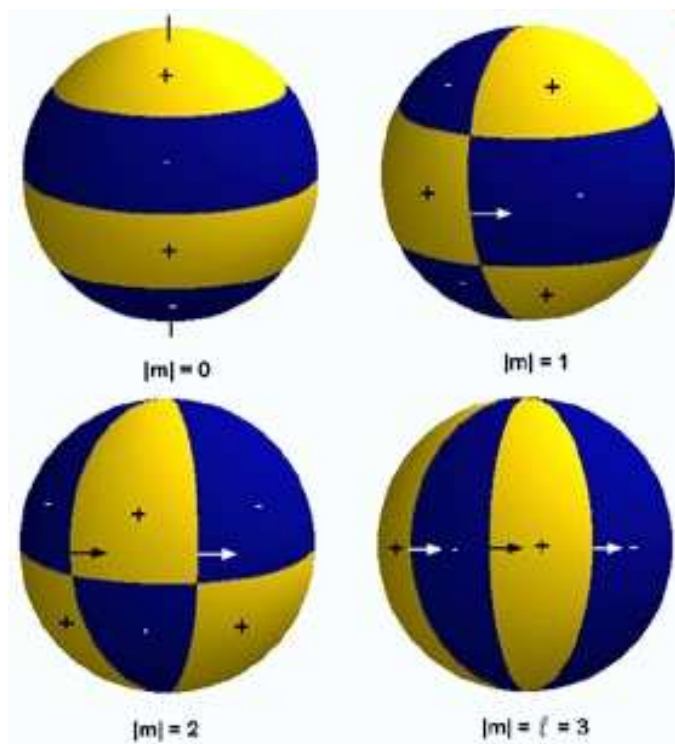


Figure 1.1: Pulsation of a star with $l = 3$. While the yellow areas are moving outwards, the blue areas are moving inwards. The arrows refer to the movement of the node lines (Zima 1999).

displacement is a vector that describes the position of a volume element with respect to a former position of this volume element. Consequently, displacement denotes the length of this vector connecting the starting point and the endpoint. Nodes and antinodes describe the vibrational pattern of a wave, where nodes denote the points of minimum and antinodes denote the points of maximum displacement. Imagine the case of a tube or pipe with one open end and one closed end. The closed end forms a node in the displacement of the air and the open end forms a displacement antinode (see Fig. 1.2).

1.2.3 Radial modes

The star oscillates around its equilibrium. While maintaining the spherical shape the stellar radius changes. Radial modes are the simplest modes, where the degree l of a radial mode is 0. For the fundamental radial mode, the number of radial nodes n is 0, too, where the core of the star is a node and the surface is a displacement antinode. Pulsations in only the fundamental radial modes are visible in RR Lyrae and Cepheid variables.

The first overtone radial mode has $n = 1$. So the node is an inert shell. Only the layers below and above this shell are moving in antiphase.

There are variable stars that oscillate simultaneously in both, fundamental and first overtone radial modes, e.g. the δ Scuti variables. In most of these stars the ratio of the first overtone and the fundamental is 0.77 (e.g. Kurtz 2006).

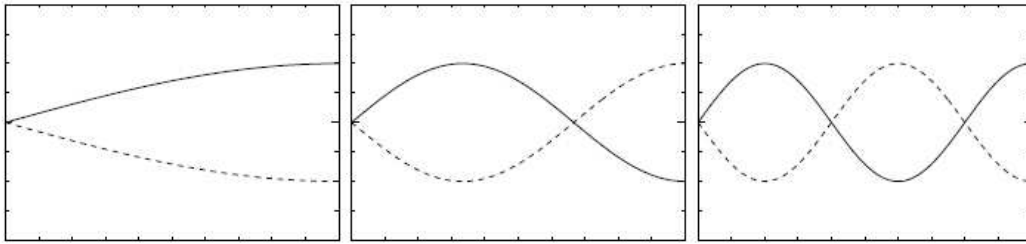


Figure 1.2: Figure showing the first three modes of an organ pipe. On the left hand side one can see the fundamental mode which has no node and no antinode. The graph in the middle shows the first overtone which has one node and one antinode. On the right hand side the second overtone with two nodes and two antinodes is shown. The open end in each graph is a displacement antinode and the closed end is a displacement node (Kurtz 2006).

1.2.4 Nonradial modes

Nonradial pulsation causes deviations from spherical symmetry. The axisymmetric dipole mode ($l = 1, m = 0$) is the simplest nonradial mode. In this case the equator is a node (see Fig. 1.3). While the upper hemisphere contracts, the lower hemisphere expands. One hemisphere heats up while the other cools down, and vice versa. Nonradial modes always have $n \geq 1$ if $l = 1$.

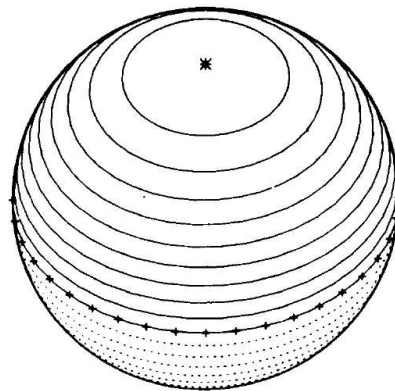


Figure 1.3: Simplest of nonradial modes ($l=1, m=0$) with an inclination angle of 45° towards the line of sight. The areas moving outwards are indicated by continuous lines while the areas moving inwards are indicated by dashed lines. The plus signs mark the equator. Figure courtesy of J. Christensen-Dalsgaard.

1.2.5 p-modes and g-modes

Acoustic waves are pressure modes (p-modes), since pressure is the primary restoring force. For gravity modes (g-modes), buoyancy acts as the restoring force. These modes

provide the possibility to see below the surface of a star and to sound its interiors.

Modes are trapped between the surface and an inner turning point. For low l values the turning point is close to the core of the star, whereas for higher l values it is closer to the surface of the star (see Fig. 1.4). As the sound wave propagates into the star, the lower part of this sound wave has a higher velocity. When travelling into the region with higher sound speed, the wave is refracted. Therefore, higher l modes have more reflection points but do not expand as deeply towards the center of the star as lower l modes.

While p-modes are more sensitive to conditions in the outer layers of the star, g-modes are more sensitive to the conditions near the core.

For higher n the frequencies of p-modes will increase, while the frequencies of g-modes will decrease. The frequencies of p-modes are in general higher than those of g-modes.

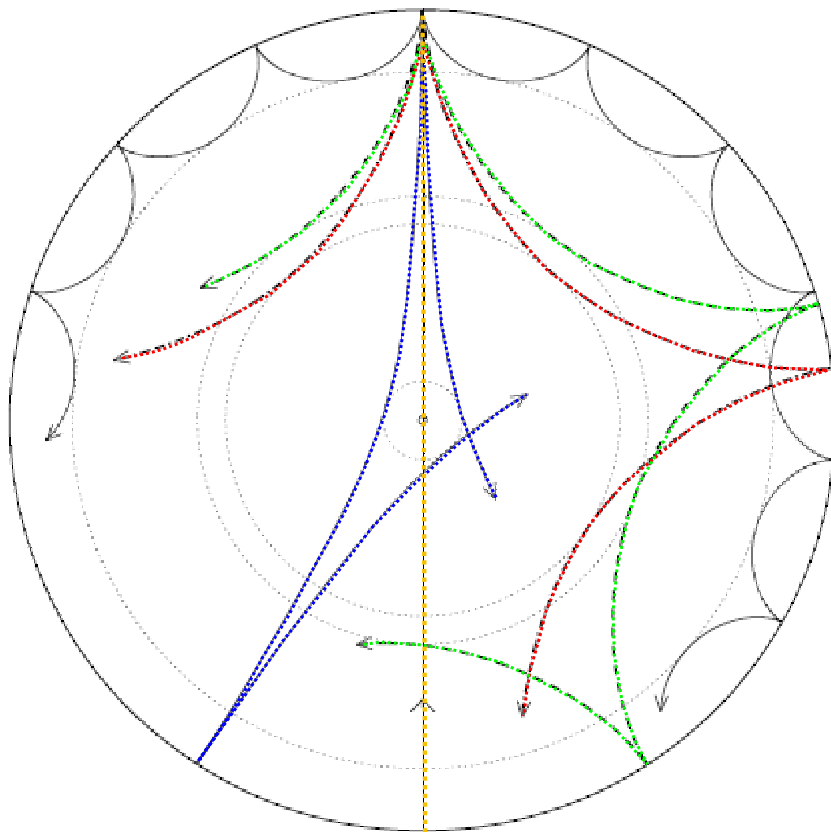


Figure 1.4: p-modes propagating into the star until they reach the inner turning point (dotted circles). The turning point is closer to the center of the star at small l values and closer to the surface at large l values ($l=0$ (yellow), 2 (blue), 20 (red), 25 (green), 75 (black)). Due to the decreasing density towards the surface, the waves are reflected. Figure courtesy of J. Christensen-Dalsgaard.

1.2.6 Mode identification

Mode identification is the determination of the quantum numbers l , m and n which describe the pulsation. Only mode identification can provide the astrophysical information astronomers are interested in. Spectroscopic data as well as multicolor photometry provide the possibility to determine the modes of pulsation. Phase shifts and amplitude ratios of photometric data in different filters provide the possibility to determine the degree l of the mode (Balona & Evers 1999). With spectroscopic data (e.g. Aerts 1996) l and m can be determined by investigating line profile variations (for high l values) or radial velocities (for low l values).

1.3 The classical instability strip

Pulsating stars are located in the classical instability strip on the right-hand side of the HR-diagram (see Fig. 1.5). The driving mechanism of these stars is the κ -mechanism. A short description of the different types of stars situated on the classical instability strip, with emphasis on δ Scuti pulsators, is provided subsequently.

1.3.1 Cepheids

Cepheids are so-called standard candles, as it is possible to determine their distances via the Period-Luminosity relation. They have periods ranging from 1 to 50 days and amplitudes between 0.1 and 2 mag. Spectral types are in the region of F5 – K5. Their masses typically range from 5 – 15 M_{Sun} .

1.3.2 W Vir stars

Periods and spectral types are comparable with the classical Cepheid stars. They are Population II stars. The amplitude variation lies between 1 – 2 mag. Masses range from 0.4 to 0.6 M_{Sun} .

1.3.3 RR Lyrae

RR Lyrae stars are Population II stars having periods of near 0.5 days and amplitudes of about 1 mag. Spectral types are A and early F stars. Typical masses are between 0.5 and 0.6 M_{Sun} . They are referred to as classical radial pulsators.

1.3.4 roAp stars

The rapidly oscillating Ap stars are A stars with a strong magnetic field and a peculiar chemical composition. These stars are multiperiodic, with periods between 4 and 15 minutes. The amplitudes are lower than 10 mmag in B . Masses range from 1.5 to 3 M_{Sun} . roAp stars pulsate in low degree, non-radial p-modes.

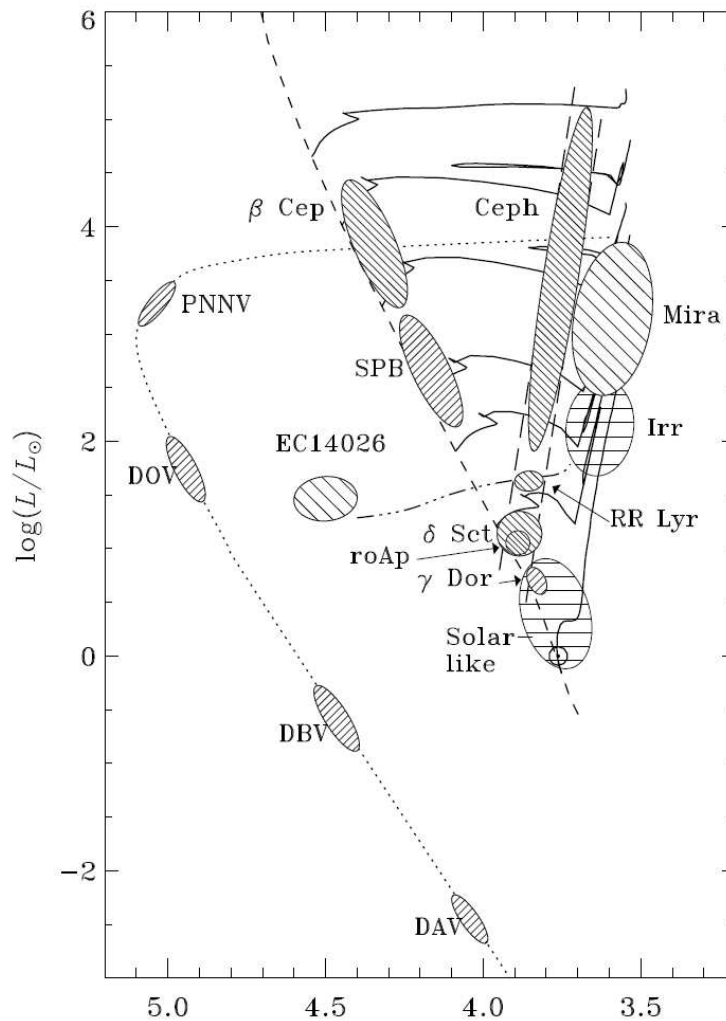


Figure 1.5: Theoretical HR diagram showing classes of pulsating stars. Figure courtesy of J. Christensen-Dalsgaard.

1.3.5 γ Dor stars

They have periods of 0.5 – 3 days. The observed amplitudes are below 0.1 mag and spectral types are late A or F stars. They pulsate in high-order, low-degree, nonradial g-modes.

1.3.6 δ Scuti stars

Smith (1955) suggested that a large fraction of RR Lyrae stars (periods shorter than 0.2 d) could have been misclassified. They seemed to differ in their Period-Luminosity-Relation and their higher metallicity. Thereupon Smith (1955) introduced the term “Dwarf Cepheids” to emphasize the low luminosity of these stars in comparison to the high amplitude RR Lyrae stars. For the first time, Eggen (1956) called stars with low amplitudes and short

periods after their prototype δ Scuti. Bessel (1969) suggested to call stars with amplitudes ranging from 0.3 to 0.8 mag AI Velorum stars, because "Dwarf Cepheids" might be confusing, since Cepheids are exclusively Population I stars. Breger (1979) proposed to term all these variables δ Scuti stars. In his opinion the division between Dwarf Cepheids and AI Velorum Stars was not clear enough so that it would be better to have one term instead of many confusing ones. Nowadays all of these stars are referred to as δ Scuti type stars.

δ Scuti stars are variables with spectral types A and F and luminosity classes ranging from III to V. Periods are between 0.02 and 0.25 days.

They are located in the classical instability strip, being main sequence (MS, see Fig. 1.5), slightly post-main sequence and even pre-main sequence stars (Marconi et al. 2002).

The instability is caused by the κ mechanism acting in the HeII ionization zone. δ Scuti stars have masses between 1.5 and 2.5 M_{Sun} (e.g. Lenz et al. 2008).

Delta Scuti stars pulsate with a large number of simultaneously excited modes. With ground-based telescopes and satellites these modes can be studied and detected, even though the photometric amplitudes of the dominant signal are sometimes only in the millimag range. Asteroseismologists aim to provide better models. Therefore, many astronomers concentrate on the same star to obtain a large amount of data and to derive a model which explains the pulsation of similar stars consistently.

1.3.6.1 Period-Luminosity-Color Relation

If the measured periods of a star are linked to its luminosity, a Period-Luminosity-Color Relation (PLCR) can be defined. The PLCR for δ Scuti variables was determined by Breger (1979) to be

$$M_v = -3.052 \log P + 8.456(b - y)_0 - 3.121(\pm 0.^m31), \quad (1.6)$$

where P refers to an average period for a multiperiodic star. Breger & Bregman (1975) confirmed that stars with different temperatures oscillate in different overtones, because the average pulsation constant Q decreases with increasing temperature, where Q is defined as

$$Q = P \sqrt{\frac{\rho_{\text{Star}}}{\rho_{\text{Sun}}}}, \quad (1.7)$$

with ρ_{Star} and ρ_{Sun} being the mean density of the star and the Sun, respectively. Q will be constant for a specific mode in all δ Scuti stars, but will change for different modes. These stars are known to pulsate in different modes, i.e. for each star exists more than just one Q value. The determination of these Q values is important for the comparison of the observed frequencies with theoretical models.

1.3.6.2 Subgroups of δ Scuti stars

δ Scuti can be divided into three subgroups:

1. Low-amplitude δ Scuti stars (LADS)
2. High-amplitude δ Scuti stars (HADS)
3. SX Phe variables

Low-amplitude δ Scuti stars. The low-amplitude δ Scuti stars represent the most common subgroup of δ Scuti stars showing predominantly nonradial p-mode pulsations and mixed modes (Breger 2000b). Low-amplitude δ Scuti stars are Population I members. As the name already suggests, they have low amplitudes (< 0.05 mag, e.g. Christiansen et al. 2007) and high rotational velocities (mean $v \sin i$ near 100 km s^{-1} , Solano & Fernley 1997).

High-amplitude δ Scuti stars. This subgroup contains Population I members with V peak-to-peak amplitudes higher than 0.3 mag. They have very low projected rotational velocities ($\leq 30 \text{ km s}^{-1}$, e.g. Breger 2007), but have period distributions, period-gravity relations and period ratios similar to δ Scuti stars with low amplitudes (Rodriguez 1994). They typically have periods ranging from 0.5 to 6 hours. Rodriguez (1994) stated that they pulsate only in the radial fundamental pressure mode and/or first overtone.

SX Phe variables. SX Phe stars are Population II and old disk population stars. They have typical periods of 0.03–0.08 d. These stars are metal poor while large-amplitude δ Scuti stars with similar light variations are metal rich (Kim et al. 2002).

1.3.6.3 Well-studied δ Scuti stars

44 Tau. Several campaigns of the Delta Scuti Network¹ focused on this star. The rotational velocity of $v \sin i = 2 \pm 1 \text{ km s}^{-1}$ (Zima et al. 2007) is stunningly low. Antoci et al. (2007) illustrated that this adverts to a pole-on view and/or intrinsic slow rotation. The second explanation was confirmed by Zima et al. (2007).

Antoci et al. (2007) detected 29 frequencies, of which 13 were independent. Breger & Lenz (2008) confirmed these frequencies and detected another 20 frequencies, 2 among them independent. The presence of both radial and nonradial oscillations was confirmed by Lenz et al. (2008).

Zima et al. (2007) derived an effective temperature of $7000 \pm 200 \text{ K}$ and $\log g = 3.6 \pm 0.1$. In this case a T_{eff} vs. $\log g$ diagram does not provide unambiguous information on the evolutionary state (MS vs. post-MS; Lenz et al. 2008). Thus main sequence as well as post-main sequence models have to be taken into account.

FG Vir. This star was a main target of the Delta Scuti Network. Breger et al. (2005) found 79 frequencies, 67 independent. Mantegazza et al. (1994) determined an effective temperature of $7500 \pm 150 \text{ K}$ and $\log g = 3.95 \pm 0.15$. FG Vir is in the second half of its main sequence evolution. The rotational velocity is $v \sin i = 21.3 \pm 1.0 \text{ km s}^{-1}$ (Mittermayer & Weiss 2003).

4 CVn. The Delta Scuti Network (Breger 2000a) found 34 frequencies, 22 independent. 4 CVn shows amplitude variability on long time scales. Breger (2000a) argues that this may be the case in all nonradially pulsating δ Scuti stars and that this variability can only be identified if data sets covering decades were available. 4 CVn is one of the few

¹Multisite campaign for short period variable stars

nonradial pulsating stars for which such extensive observation campaigns were carried out.

EE Cam. EE Cam is a little-studied δ Scuti star having amplitudes between those of HADS and LADS, i. e. ≈ 80 mmag peak-to-peak (Breger et al. 2007).

Nordström et al. (2004) determined $V = 7.753$ mag, an effective temperature of 6530 K and a metallicity [Fe/H] relative to the sun of 0.06. They also determined a mean radial velocity of 14.9 km s^{-1} . Breger et al. (2007) found a $v \sin i$ of $40 \pm 3 \text{ km s}^{-1}$. Since EE Cam is a star in the intermediate region of δ Scuti stars, it is a suitable object to study the astrophysical background.

Chapter 2

Photometer

2.1 Single-channel photometer

Information in this section was taken from Sterken & Manfroid (1992). There are several detectors that can be used to study radiation emitted by a star. While the input is the light of an astronomical object, the output is produced by the detector, which transforms the radiation into another kind of energy (depending on the detector). One such detector is the photometer, which counts the number of free electrons induced by incoming photons. This kind of detector belongs to the group of photo-emissive detectors, which collect the light on a photocathode. There are single-channel photometers with one aperture to observe only one star at the same time, and multi-channel photometers which permit simultaneous observations of different targets through multiple apertures. Here, mainly the properties of single-channel photometers are described, because only this type of photometer is of importance for the present work. For details concerning the properties of multi-channel-photometers, see Sterken & Manfroid (1992).

2.1.1 Layout

A typical single-channel photometer consists of two main parts: the photometer itself and the photomultiplier.

2.1.1.1 Arrangement of the photometer

Before the light can pass to the detector, it has to be collected and processed by a photometer. Fig. 2.1 illustrates the layout of a photometer. The incoming light falls on a movable mirror and is transported to the guider ocular, which is needed to identify the object of interest. When moving the mirror, the incoming light can pass on to the diaphragm wheel. The diaphragm is used to confine the incoming light, so that only the light from the object of interest is monitored (e.g. not light of nearby stars). A single-channel photometer uses one diaphragm at a time, where the diameter typically lies in the range of 10-60 arcsec. For brighter stars a diameter of 30-40 arcsec can be used (Handler, private communication). After passing the diaphragm wheel, the light falls on another movable mirror and

is transported to the centering ocular, which is needed to center the object of interest. By moving the mirror the light can be passed onto the filter wheel. The filter wheel normally consists of several filters (see 2.1.5), where the observer has to decide which filter to use for the measurements. After passing the filter wheel, the light is imaged onto the photocathode by the Fabry lens. The Fabry lens as well as the photomultiplier tube are located in a coldbox that keeps the temperature of the lens and the detector low and constant. The coldbox is used to reduce the thermal noise level.

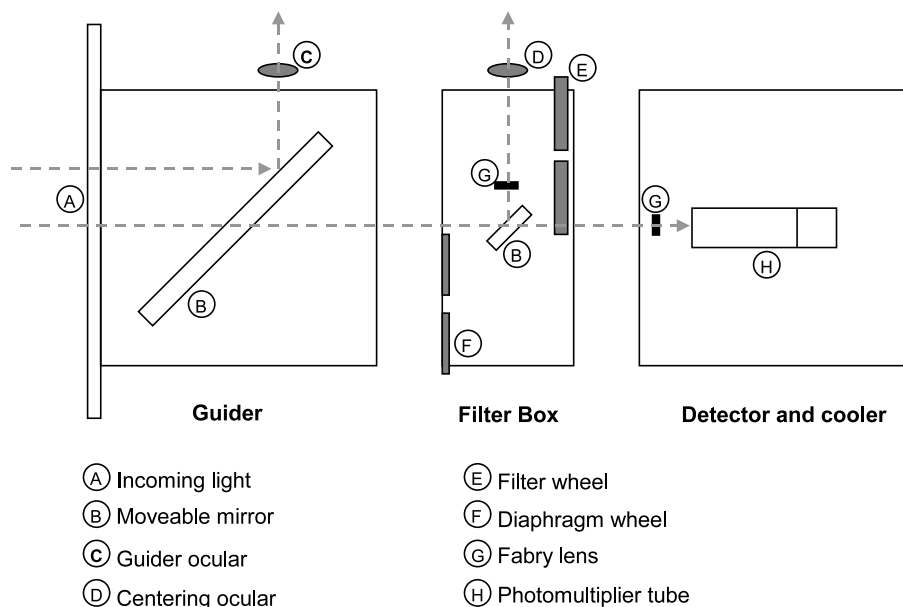


Figure 2.1: Schematic illustration of a single-channel photometer.

2.1.1.2 Arrangement of the Photomultiplier tube

The photomultiplier tube utilizes the photoelectric effect, e.g., a photon hits an atom or molecule and an electron is emitted. The photomultiplier tube allows secondary emission, e.g., some materials emit more than just one electron when they are hit by an electron. Especially in astronomy, secondary emission is important for photometric measurements, because the incoming radiation can be quite low. Fig. 2.2 illustrates the principle of a photomultiplier tube. When the light enters the photomultiplier tube, it strikes the photocathode which emits photoelectrons. These photoelectrons hit the first dynode, and secondary emission occurs. This happens for all dynodes, and more and more electrons are emitted. When these electrons hit the anode, a current is produced. This current is then transmitted to the voltmeter and is directly proportional to the incoming radiation intensity.

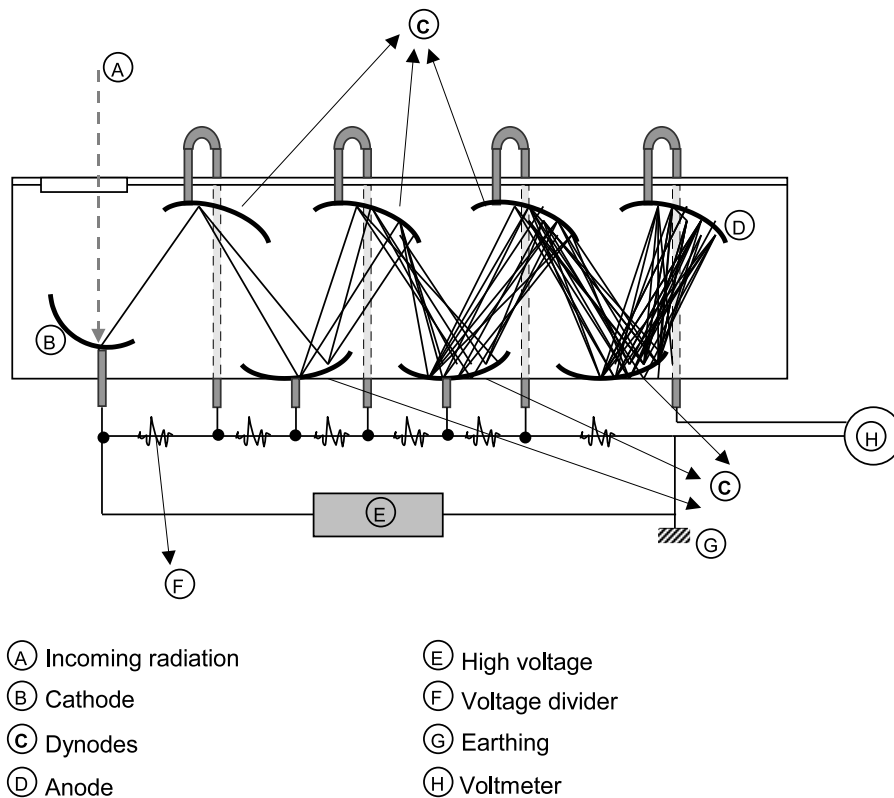


Figure 2.2: Schematic illustration of a photomultiplier tube.

2.1.2 Properties

Each detector has typical area sensitive to radiation. The sensitive area of a photomultiplier consists of one pixel, whereas a charge-coupled device (CCD) typically consists of several million pixels. The quantum efficiency of a detector is determined by

$$QE = \frac{P_{count}}{P_{ideal}}. \quad (2.1)$$

Where P_{count} is the number of photons counted and P_{ideal} is the number of photons that would have been counted if an ideal detector would have been used. The quantum efficiency of every detector differs with wavelength (see Fig. 2.3). Information on this dependency is essential to estimate the spectral range of the detector (the range where the detector can be used).

2.1.3 Advantages and disadvantages

Some advantages of the photomultiplier are

- the fast response time,
- the ability to measure very low radiation intensities thanks to the secondary emission. The detection limit is usually one photon.

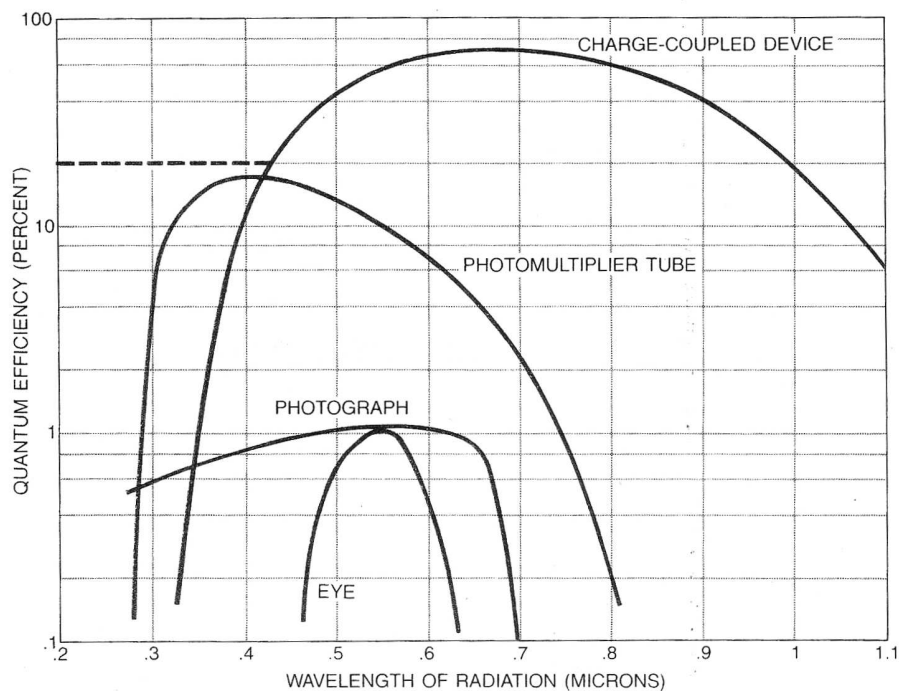


Figure 2.3: Illustration of the quantum efficiency of several detectors. Figure adapted from Kristian & Blouke (1982).

Some disadvantages are

- the narrow spectral range reaching from the near-UV (≈ 300 nm) to the near-IR (≈ 800 nm). This depends strongly on the type of tube.
- the susceptibility to drift. Drift means that the sensitivity¹ of the detector changes with time.
- The quantum efficiency is much lower than for a CCD.

2.1.4 The noise problem

Each physical measurement is associated with uncertainties. Even if an ideal detector was used, these uncertainties would not vanish. Hence it is impossible to detect all the signal coming from the light source.

2.1.4.1 Signal noise

Signal noise is caused by the quantum nature of light, background sources and effects that influence the signal, before it is measured.

¹ratio between the current measured by the anode and the radiation measured by the cathode

Quantum nature of light. The time interval between the emission of two consecutive photons is not constant. This is called photon noise. An exact prediction of how many photons will hit the detector in a time interval cannot be made. Even with a light source that illuminates two identical detectors, they will not measure the same number of incoming photons. A light source emits a mean photon number $n = \frac{N}{t}$ per unit time (usually 1 second). The probability that n photons are detected in a time interval t is described by a Poisson distribution

$$P(n, t) = \frac{(Nt)^n e^{-Nt}}{n!}. \quad (2.2)$$

The variance σ^2 is equal to the number of detected photons N in the time interval t . The photon noise can be therefore determined by

$$\sigma = \sqrt{Nt}. \quad (2.3)$$

Scintillation. The atmosphere of the Earth is not homogeneous and scatters stellar light. The brightness of the star varies due to these turbulences in the atmosphere. Planets are not effected by scintillation, because they are not point-shaped and so the light rays are no longer parallel. Scintillation is increasing with larger zenith distances. The effect of scintillation can be minimized with larger telescopes and locations for observations.

Seeing. In the lowest layers of the atmosphere, the effect of seeing is larger than in outer layers, because refraction depends on the density of the air. The effect is largest in the tropopause, where the turbulence is highest.

Sky background. The sky background is typically 20.5 mag/arcsec² in the optical wavelength range. However, this value is increased by the Moon. In this case, fainter stars are no longer visible.

2.1.4.2 Internal noise

Internal noise is caused by the detector. This noise can be induced by

Dark current. The noise added by the detector is called dark current (or dark noise). In photomultipliers the dark noise is produced by thermionic emission, i.e. by electrons that are emitted due to heat. These electrons cannot be distinguished from those emitted by the photoelectric effect. By cooling the photomultiplier, the dark current can be limited. The temperature has to be kept constant, because changes in temperature may cause variations in the spectral response of the photocathode. This noise is independent of the brightness of the light source and can be measured directly, if the detector is not illuminated. The mean dark current is subtracted from each measured intensity. The measurement of the individual dark current of every tube that is used is required, because even if the arrangement is the same, the dark current differs.

Thermal background. In the Infrared wavelength range the thermal background has to be taken into account, which may be neglected in the Optical. It is the thermal radiation emitted by the detector itself and the equipment located near the detector. One can minimize this noise by cooling the elements of the detector with liquid N₂ or He.

2.1.4.3 External noise

External noise is caused by erroneous detections, such as

Cosmic background radiation. Especially with CCDs cosmic background radiation has to be taken into account. This noise is produced by cosmic rays entering the detector.

2.1.4.4 Reduction noise

Reduction noise is caused by the reduction process, e.g. the digitalization.

2.1.4.5 Signal-to-noise ratio

Each observer and method is trying to reduce the source of disturbance or to correct for this disturbance by applying a reduction. It is possible to determine the ratio between the observed value and the true value (signal-to-noise-ratio, S/N).

Determination of S/N. As it is required to take separate measurements for the target and the sky background, one can determine the error for both. The error in the background count rate is given by

$$\sigma(B) = \left(\frac{B}{t_B} \right)^{0.5}, \quad (2.4)$$

where B is the count rate of the sky background and t_B is the integration time. The error in the target count rate can be determined by

$$\sigma(S + B) = \left(\frac{S + B}{t_{S+B}} \right)^{0.5}, \quad (2.5)$$

where $S + B$ is the count rate of the star and t_{S+B} is the integration time for the star. It is referred to as $S + B$, because every observation of the star includes the sky background. As the measuring error of S is needed rather than of $S + B$, the background has to be subtracted. This allows the determination of the error for the target count rate without background

$$\sigma(S) = \left(\frac{S}{t_{S+B}} + \frac{B}{t_{S+B}} + \frac{B}{t_B} \right)^{0.5}. \quad (2.6)$$

The signal-to-noise ratio is calculated by

$$\frac{S}{N} = \frac{S}{\sigma(S)}. \quad (2.7)$$

2.1.5 Filters

Filters are a very important part of the observing process as they can be adapted to specific requirements.

2.1.5.1 Photometric filter systems

A photometric filter system is used to obtain information on the spectral energy distribution of a star. This information is derived when making measurements with different filters covering the optical wavelength range. When using a filter system it is important to choose the appropriate bandwidth. Some standard photometric systems are described below.

Johnson-Morgan *UBVRI* system. Johnson & Morgan (1951) defined this system to provide the possibility to compare the results with the spectral classification scheme. Originally, they used three broad-band filters, where the *U* filter is located in the UV wavelength range, the *B* filter in the blue wavelength range and the *V* filter in the visual wavelength range. Johnson & Morgan (1951) decided to use three filters to get two color-indices (*B* – *V* correlating with the effective temperature, *U* – *B* gives the hydrogen line strength). Two other filters were added in 1965 (Johnson 1965; see Fig. 2.4 and Tab. 2.1), where the *R* filter covers the red wavelength range and the *I* filter covers the IR wavelength range.

Table 2.1: Effective wavelengths λ_{eff} and bandwidths $\Delta\lambda$ of the Johnson *UBVRI* system. The table was adopted from Sterken & Manfroid (1992).

| Filter | λ_{eff} [nm] | $\Delta\lambda$ [nm] |
|--------|-----------------------------|----------------------|
| U | 365 | 70 |
| B | 440 | 100 |
| V | 550 | 90 |
| R | 720 | 220 |
| I | 900 | 240 |

There are some disadvantages.

- A part of the spectral response of the *U* filter lies above the Balmer jump, i.e. measures the area where the energy distribution of a star changes significantly.
- The *U* filter has a certain transparency range that allows light at longer wavelengths (700 nm) to pass the filter. This red leak causes problems for cool stars. One solution is to additionally use a copper sulfate, which prevents red light from passing the filter.
- The spectral response of the *V* filter prevents blue light from passing. But light in the red wavelength range will pass the filter. To prevent this a blue tube² can be used. If a red tube is preferred, one can use special filters to avoid this problem.

Strömgren *uvby* system. This filter system belongs to the group of intermediate-band-systems. The goal of such systems is to measure well-defined spectral signatures of stars. It is possible to derive the surface gravity g , the effective temperature T_{eff} and, for A

²The cutoff of the detector is at 700 nm

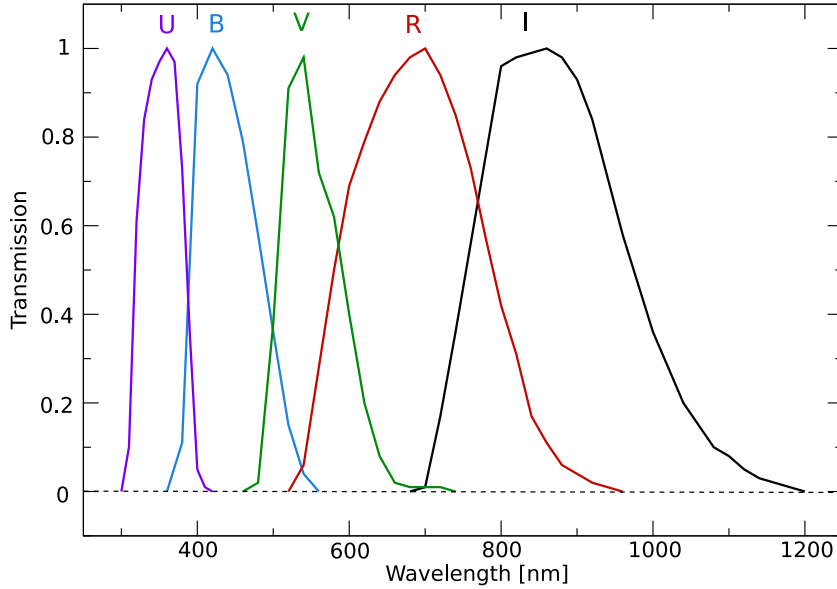


Figure 2.4: Spectral response of the Johnson *UBVRI* system. Figure adopted from Johnson (1965).

and F stars, the metallicity. The Strömgren filter system consists of four filters, where the *u* filter is sensitive to the UV wavelength range, the *v* filter to the violet wavelength range, the *b* filter to the blue wavelength range and the *y* filter in the yellow wavelength range (see Fig. 2.5). The filters *v* and *b* replace the Johnson *B* filter, and the *y* filter corresponds to the Johnson *V* filter. This system allows to use two $H\beta$ filters, where one is a wide (bandwidth) and the other one is a narrow (bandwidth) filter.

To indices can be derived

$$m_1 = (v - b) - (b - y) \quad (2.8)$$

and

$$c_1 = (u - v) - (v - b). \quad (2.9)$$

The index m_1 refers to the strength of the metal lines in A and F stars, c_1 represents the extent of the Balmer jump.

To apply this system, the stars have to be divided into three groups (Napiwotzki et al. 1992), depending on their T_{eff} :

- In cool stars ($T_{\text{eff}} \leq 8500$) the temperature can be defined by β , and the surface gravity corresponds to c_1 .

- In intermediate stars ($8500 \leq T_{\text{eff}} \leq 11000$), one has to define two additional parameters, because it is not possible to decide which index determines gravity and T_{eff} .
- In hot stars ($T_{\text{eff}} \geq 11000$) β is a gravity parameter and c_1 a temperature indicator.

Table 2.2: Effective wavelengths λ_{eff} and bandwidths $\Delta\lambda$ of the Strömgen *uvby* system. Table adopted from Sterken & Manfroid (1992).

| Filter | λ_{eff} [nm] | $\Delta\lambda$ [nm] |
|-------------|-----------------------------|----------------------|
| u | 350 | 34 |
| v | 410 | 20 |
| b | 470 | 16 |
| y | 550 | 24 |
| H β_w | 486 | 15 |
| H β_n | 485 | 3 |

Cousins $UBVR_C I_C$ system. The Johnson system is defined for the use with a PMT. The U , B and V filter characteristics are the same as those of the original UBV -system. Filter characteristics for the R_C and I_C filter are listed in Table 2.3, and Fig. 2.6 shows the transmission curves of these filters.

Table 2.3: Effective wavelengths λ_{eff} and bandwidths $\Delta\lambda$ of the Cousins $R_C I_C$ system (Lamla 1982).

| Filter | λ_{eff} [nm] | $\Delta\lambda$ [nm] |
|--------|-----------------------------|----------------------|
| R_C | 640 | 150 |
| I_C | 790 | 150 |

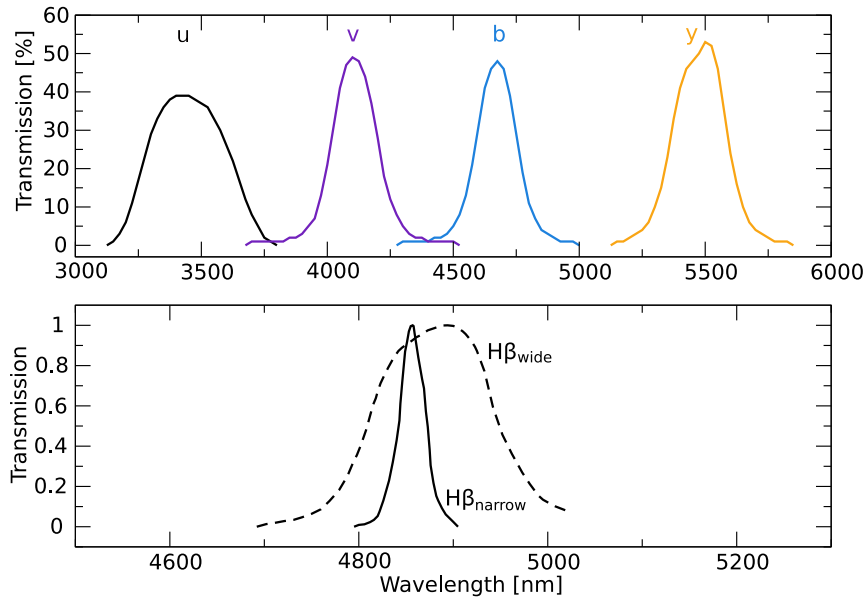


Figure 2.5: Spectral response of the Strömrgren $uvby\beta$ system. Figure adapted from Crawford & Barnes (1970).

2.1.5.2 Characteristics

The most important characteristics of filters are

- the central wavelength,
- the maximum transmission, indicating the ratio between transmitted flux and the incident flux on the filter surface,
- Full Width at Half Maximum (FWHM), indicating the spectral distance between the points with a transmission of 50% of the maximum,
- the optical thickness, where the same thickness for every filter in a filter set has to be used, otherwise the focus position will change,
- form and size,
- the temperature range, because filter characteristics are temperature dependent.

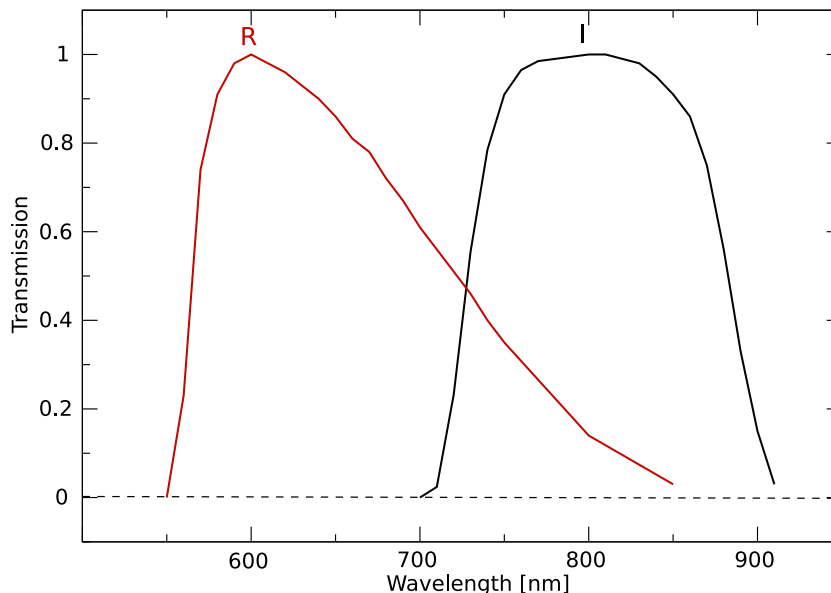


Figure 2.6: Spectral response of the Cousins $R_C I_C$ system. Figure adopted from Bessell (1990).

2.1.5.3 Subgroups

Sterken & Manfroid (1992) introduce three subgroups of filters, depending on the width of the wavelength range that is covered by the filter

- broad-band filters have a bandwidth ranging from 30 to 120 nm. An example for those filters is the UBV filter system.
- intermediate-band filters have a bandwidth ranging from 9 to 30 nm. An example is the Strömberg $uvby$ filter system.
- narrow-band filters have a bandwidth smaller than 9 nm. An example is the $H\alpha$ filter. $H\alpha$ filters are useful for the detection of planetary nebulae or HII regions, because these objects have a lot of hydrogen emission.

Additionally, astronomers often use circular variable filters or neutral density filters. Circular variable filters are interference filters with variable regional thickness. This allows a linear variation of the central wavelength. Neutral density filters are used if the object is too bright. If the telescope is too large for the object, over-exposure may even damage the detector. So it is necessary to use a neutral density filter to diminish the signal without distorting the spectral response.

2.1.5.4 Glass filters, gelatine filters and interference filters

In order to be able to observe in the ultraviolet wavelength range, filters are made of a transmissive glass. Glass and gelatine filters absorb the light inside the material. Interference filters cause transmission by interference. As gelatine filters have a lot of disadvantages, they are not frequently used in photometers.

Glass filters. They absorb or scatter the light. This process is wavelength-dependent. Additional energy can pass the filter at longer wavelengths. This is called red leak and is a problem when using the *U* filter of the Johnson filter system. For further details and solutions see 2.1.5.1. The characteristics of glass filters are temperature-dependent. Therefore, they have to be kept at constant temperatures.

Interference filters. They are combinations of Fabry-Perot interferometers. This interferometer consists of two semi-reflective surfaces. Only light at a certain wavelength can pass these surfaces. The remaining light is reflected. By tilting the filter, the light-transmissive range of the filter will change. As tilting avoids unwanted reflections, the tilting angle has to be considered when buying the filter. Changes in temperature can cause changes in the wavelength, too. However, these changes are smaller than the changes produced with glass filters. The characteristics depend on the thickness of the filter, the number of filters and the combinations used. Advantages of interference filters are the well-defined wavelength ranges, the fact that almost all wavelength ranges are possible and the high transmission of the filter. Disadvantages of interference filters are the high costs, the sensitivity to humidity and the dependence on the angle of incidence.

2.2 Wolfgang-Amadeus: the Vienna Twin Automatic Photoelectric Telescopes

Information in this section was taken from Strassmeier et al. (1997). The Vienna Twin Automatic Photoelectric Telescopes (APTs, see Fig. 2.7) were designed in 1992 by L. J. Boyd at Fairborn Observatory. In 1996 two robotic telescopes were handed over to the University of Vienna and were first located at Smithsonian Fred L. Whipple Observatory on Mount Hopkins. Half a year later they were moved to Fairborn Observatory at Washington Camp. This observatory is located in the Sonoran desert near Tucson, Arizona. Here it began to fully operate in autumn 1996.

2.2.1 Observational restrictions

Fairborn Observatory is located at a longitude of $-110^{\circ} 41' 41''$, a latitude of $+31^{\circ} 23' 12''$ and an altitude of 2700 m. Therefore, the observations are limited to a declination ranging from -35° to $+75^{\circ}$ and to airmasses below 2 in the northern hemisphere.

Furthermore, the 0.75m telescopes can only observe stars brighter than 13^m in Johnson.



Figure 2.7: The Vienna APT. Front: Wolfgang. Back: Amadeus

2.2.2 Automatic telescopes

The two telescopes as well as the whole observatory are automatic. This means that sensors monitor the weather conditions and the roof is operated by a computer. When the weather conditions are poor, the computer will not open the roof. There is another computer responsible for the telescope control. It runs the photometer and is responsible for the data input and output. The data output contains the Julian Date without heliocentric correction and the number of photoelectrons in each integration.

2.2.3 Equipment

Wolfgang and Amadeus are twin telescopes and therefore have almost the same equipment. The optical system consists of a 0.75 m Cassegrain primary mirror with a focal ratio of $f/8$ and a 0.2 m secondary mirror. The high slewing speed of about 10 degrees per second permits to switch between target and comparison star within 1 second. Each telescope has a CCD finder camera.

2.2.3.1 Photometer

The only difference between Wolfgang and Amadeus is that they have two different single-channel photoelectric photometers, where the filter combinations are optimized for use in the blue wavelength region for the Wolfgang photometer and for use in the red wavelength region for the Amadeus photometer.

2.2.3.2 Filters

The filter systems used are adapted to the spectral response of the photomultipliers. Both photometers provide four intermediate-band filters (*uvby*). Additionally, Amadeus has five broadband filters (*UVBRI*), two $H\alpha$ filters (wide and narrow) and one $H\beta$ (wide) filter, Wolfgang has only got 3 broad band filters (*UVB*) and a $H\beta$ filter (wide and narrow).

There are also neutral density filters in different magnitude ranges (1.25 mag, 2.5 mag, 3.75 mag, 5.0 mag) available, which reduce the incoming light. They have to be used when observing bright stars. For the APT neutral density filters have to be used when observing stars brighter than 6.0 mag in V .

2.2.3.3 How to acquire data with the APT

The Institute of Astronomy at the University of Vienna is responsible for the data files. This means, that astronomers send the data files, containing the informations necessary to start the observation, via internet to the APT. The data files produced from the APT, containing the data acquired during the observation, will be retrieved via internet. As the computer handles both input as well as output files, no staff is needed to operate the telescope.

The output files typically contain the ID number of the star, the Julian Date (note: without heliocentric correction), the integration time, the count rates and a lot of technical information that is not subject of the present discussion.

2.3 The standard three-star technique

For further information, the reader is referred to Breger (1993). A detailed description of the application of this technique is provided in Chapter 3. Many variable stars, such as δ Scuti variables, have variations in the millimag range. The three-star technique is a suitable method to study these variations. It can be applied to all variable stars with periods longer than 30 minutes. This limit is given by the fact that in one observing cycle the target, two comparison stars and the sky background are observed alternately in two different filters. Therefore, some time (approximately 10 minutes in the case of EE Cam and its comparison stars) passes until the target is observed again. To get all the information on the variability of the star, the period should not be shorter than half an hour.

2.3.1 Observation

One of the three stars observed is the variable star and the other two are the comparison stars. The variable star V , the first comparison star $C1$ and the second comparison star $C2$ should be observed with the same instrument. The integration times depend on the instrument used (e.g. size of the mirror) and on the star-to-background brightness ratio. The best signal-to-noise ratio can be achieved with a timing ratio of

$$ratio = \frac{t_{S+B}}{t_B} = \sqrt{\frac{S+B}{B}}, \quad (2.10)$$

where $S + B$ gives the count rate of the star (where the background B is included), t_{S+B} gives the integration time of the star, B denotes the count rate of the background and t_B is the integration time of the background. Thus, the fainter the background in comparison

to the star, the longer the star itself can be observed. If the target star as well as the comparison stars have equal brightnesses, the three stars should be observed equally often to obtain a sufficient accuracy. This timing ratio is only applied to faint stars and can therefore be neglected for EE Cam and its comparison stars.

At the APT, each observing run consists of a number of cycles. In each observing cycle every star is observed in a given order (e.g. first you observe C1, then C2, then V, see table 2.4). Depending on the phase of the moon, the background is observed at the beginning, the middle or the end of an observing cycle. One has to keep in mind that the uncertainties of the measurements are getting smaller with larger integration times.

Table 2.4: Example for how a cycle could look like.

| cycle | 1 | | |
|-----------------|-------------|--------|----------------------|
| observed object | JD | counts | integration time [s] |
| C1 | 4480.6224 | 76056 | 10 |
| | 4480.6231 | 76448 | 10 |
| | 4480.6280 | 76596 | 10 |
| C2 | 4480.6235 | 97972 | 10 |
| | 4480.6241 | 97392 | 10 |
| V | 4480.6245 | 160700 | 10 |
| | 4480.6251 | 161260 | 10 |
| | 4480.6259 | 159568 | 10 |
| | 4480.6265 | 160224 | 10 |
| sky background | 4480.622780 | 1880 | 10 |
| | 4480.6238 | 1800 | 10 |
| | 4480.6248 | 1796 | 10 |

2.3.2 Selection of the comparison stars

The variable star and both comparison stars should have comparable brightnesses and spectral types. The position in the sky plays an important role, too. The selection of stars close to each other improves the temporal resolution of the measurements and the accuracy of the extinction correction.

2.3.3 Advantages of this technique

The standard three-star technique has three major advantages.

- It allows to identify the variability (or non-variability) of the comparison stars.
- The use of two comparison stars is safer, because if one comparison star is variable there is still the other one available for successful data reduction. Additionally, the differential light curves (see Chapter 3) are likely to reveal the variable comparison star.

- The incorporation of a variable comparison star: Even if one of the comparison stars is variable, the difference $(C1 - C2)$ can still be used to find out which data points are less reliable. These points might then also be less reliable in $(V - C1)$ and $(V - C2)$.

Chapter 3

Data Reduction and Analysis

There will always be systematic errors in observational data which have to be corrected. This section gives an overview of the errors that can occur and the reduction steps that can be applied.

3.1 Julian Day Number and Julian Date

In 1582 Joseph Justus Scaliger proposed that the zero point of the Julian Day Number should be 1 January 4713 B.C. at 12:00 UT. So the Julian Day Number is the time in days elapsed since then (e. g. 1 January 2000 12:00 UT corresponds to JD 2451545.0).

Scaliger (McCarthy 1998) argued that a year can be distinguished by

- the position (S) within a 28-year solar cycle,
- the position (G) within the 19-year cycle of Golden Numbers (Numbers assigned to every year so that one can calculate the position of the year in the Metonic cycle),
- the position (I) within the 15-year cycle of Roman taxes.

As there are no common factors for these three numbers a given combination of these numbers will be repeated only after $28 \cdot 19 \cdot 15 = 7980$ years. So Scaliger defined these number as a Julian period. The year 1 B.C. has the numbers $S = 9$, $G = 1$, $I = 3$. So he calculated that the combination $S = 1$, $G = 1$ and $I = 1$ occurred in the year 4713 B.C..

The Julian Date gives the Julian Day Number as an integer and the hours, minutes and seconds passed as a floating point number (e. g. 1 January 2000 16:30 corresponds to JD 2451545.1875 in Greenwich). Especially in astronomy it is helpful to use this date, because there are no time shifts due to the summer time or the leap day.

3.1.1 Calculation

Gregorian Calendar to Julian Day Number

Montenbruck (2001) presents the following algorithm to calculate the JDN: if the month

$M \leq 2$, it is necessary to take $Y = Y - 1$ and $M = M + 12$, where Y denotes the year and M denotes the month. Otherwise Y and M are left unmodified. The Julian Day Number can be determined by

$$JD = INT(365.25 * (Y + 4716)) + INT(30.6001 * (M + 1)) + D + B - 1524.5. \quad (3.1)$$

Where A and B are given by

$$A = INT\left(\frac{Y}{100}\right), \quad (3.2)$$

$$B = 2 - A + INT\left(\frac{A}{4}\right). \quad (3.3)$$

Note that INT is the largest Integer $\leq x$ (e.g. $INT(3.2) = 3$, $INT(3.9) = 3$).

Julian Date

The floating point number, where the time of day is considered, can be calculated by

$$JD_{float} = \frac{\left(H + \frac{M}{60} + \frac{S}{3600}\right)}{24}. \quad (3.4)$$

Where H denotes the hour (note: the counting starts at 12:00, e. g. 16:00: $H = 4$, 10:00: $H = 22$, 12:00: $H = 0$), M denotes the minutes and S denotes the seconds. The Julian Date JD is calculated by

$$JD = JD_{float} + JDN. \quad (3.5)$$

3.2 True declination and right ascension

The declination δ is the angular distance (in degrees) of the star from the celestial equator. Positive values are assigned to the northern, negative values to the southern hemisphere. The right ascension α is the angular distance (in hours, minutes and seconds) of the star from the vernal equinox Υ along the equator.

The true values of these coordinates define the position of the star precisely. The lunisolar precession causes a change in the declination and right ascension of a star. Catalogues give the coordinates α_{eq} and δ_{eq} of stars for a given equinox eq and a specific Julian Day Number JDN (the standard equinox is $eq = 2000$, $JDN = 2451545.0$). Accordingly, these values have to be transformed to obtain the true values that correspond to the Julian Date JD of a measurement.

3.2.1 Calculation

According to Meeus (1998) the true values can be calculated by

$$\alpha = \alpha_{eq} + \frac{m + n \tan \delta_{eq} \sin \alpha_{eq}}{3600} \frac{JD - JDN}{365.25}, \quad (3.6)$$

$$\delta = \delta_{eq} + \frac{n \cos \alpha_{eq}}{3600} \frac{JD - JDN}{365.25}, \quad (3.7)$$

where

$$m = 46.085'', \quad (3.8)$$

$$n = 20.0431''. \quad (3.9)$$

Values for m and n are valid until the year 2100, when they have to be recalculated. These equations do not give a high accuracy, but can be applied if the epochs used are not far away from each other. Especially if the star is near the celestial poles it is not recommended to use this algorithm.

3.3 Dark current correction

Dark current is produced by the detector due to thermionic emission. More information is provided in 2.1.4.2.

3.4 Dead time correction

After receiving a signal, the system of the photomultiplier (PMT, see 2.1) will be blocked for a certain time (dead time). Within this time all additional signal will be ignored. If the count rate (intensity) is high enough (≥ 100000 counts), a dead time correction has to be applied.

For corrections $< 2\%$ the dead time correction is calculated by

$$I_{corr} = \frac{I_{count}}{1 - I_{count}\tau}. \quad (3.10)$$

For corrections $\geq 2\%$ the dead time correction is calculated by

$$I_{corr} = \frac{I_{count}}{1 - I_{count}\tau e^{-I_{count}\tau}}. \quad (3.11)$$

Where I_{count} denotes the measured countrate, I_{corr} the true count rate and τ the dead time in nanoseconds.

3.5 Background correction

Before subtracting the intensity of the sky background, a mean value for any star is determined. During one observing cycle, several measurements in different filters of the target, the comparison stars and the sky background are performed. These measurements have to be combined to one datapoint for each star in each filter.

The measured sky intensities must have the same JD as the star. It is required to apply an interpolation where the JD of the sky is converted into the JD of the star. Then the sky intensity is subtracted from the star's intensity. This correction has to be applied to all observed stars.

3.6 From counts per second to magnitude

The intensities I of the stars are given in counts per second. To convert these into magnitudes m , one can use the following equation:

$$m = -2.5 \log I + C. \quad (3.12)$$

3.7 Atmospheric extinction

The atmospheric extinction describes the effects of absorption and scatter in the atmosphere. Due to the different sizes r (0.1 nm to 100 μm) of the aerosols in the atmosphere¹ light coming from a star is scattered in different ways. The larger the scattering body, the larger the wavelength dependence of the scatter:

- If $r \ll \lambda$, the wavelength dependence will be $I \sim \lambda^{-4}$. This is called Rayleigh scatter and is responsible for the blue color of the sky.
- If $r \sim \lambda$, the scatter will be called Mie scatter, and the wavelength dependence is $I \sim \lambda^{-1}$.
- If $r \gg \lambda$, the scatter will be wavelength independent.

Absorption is caused by different types of molecule and atom transitions depending on the wavelength range. Molecular electronic transitions (e.g. CO , H_2O , CH_4) are dominant absorbers, because they are absorbing in a wide wavelength range and cover a large fraction of the molecules in the atmosphere. In the Infrared, water is the main absorber and is responsible for the variable transmission of the atmosphere. Most telescopes are located on mountains, because the absorption in many wavelength ranges, particularly in the Infrared, is decreasing with increasing altitude.

A transformation of the ground-based measurements into values that would be obtained outside the atmosphere provides a successful method to correct for these atmospheric effects.

3.7.1 Airmass

Light coming from a star has to pass the atmosphere before it reaches the telescope's surface. The airmass is a measure of the length of the light path through the atmosphere. Therefore, the airmass depends on the zenith distance of the target. For a star at the zenith, the value of the airmass is $X = 1$. On Earth values $X < 1$ cannot be reached. At larger zenith distances, the airmass increases because the light has to pass a larger fraction of air.

The airmass is calculated by

$$X = \sec z - 0.0018167(\sec z - 1) - 0.002875(\sec z - 1)^2 - 0.0008083(\sec z - 1)^3, \quad (3.13)$$

¹e. g. molecules, atoms, dust, water

$$\sec z = \frac{1}{\sin \Phi \sin \delta + \cos \Phi \cos \delta \cos h}, \quad (3.14)$$

with z denoting the zenith distance, Φ the geographic latitude, δ the declination, $h = \Theta - \alpha$ the hour angle, Θ the sidereal time (see 3.7.2) and α the right ascension. Note that the conversion of all values into consistent units is essential.

3.7.2 Sidereal time calculation

As a first step, one has to calculate the time period T elapsed since 1 January 2000 using

$$T = \frac{JD - 2451545.0}{36525}. \quad (3.15)$$

By means of this equation, the mean sidereal time (in degrees) in Greenwich can be directly calculated according to

$$\Theta_{mean} = 280.46061837 + 360.98564736629(JD - 2451545.0) + x$$

with

$$x = 0.000387933T^2 - \frac{T^3}{38710000}, \quad (3.16)$$

where 280.46061837 is the local sidereal time in Greenwich on 1 January 2000. The sidereal time in degrees can be calculated by

$$\Theta = \Theta_{mean} \pm \lambda. \quad (3.17)$$

The longitude λ is added if the location is east of Greenwich and is subtracted if the location is to the west of Greenwich.

Then the sidereal time in hours is given by

$$\Theta_{sid} = \frac{\Theta}{15}. \quad (3.18)$$

3.7.3 Extinction coefficient and intersection point

The extinction coefficient k is the quantity of light lost per unit airmass. It is determined from a Bouguer diagram (Fig. 3.1), in which magnitudes are plotted versus airmass. The data points should show a linear correlation. The slope of the linear regression is the extinction coefficient k . The linear correlation may be contaminated by variable extinction, instrumental changes or clouds. The point where the linear fit meets the y-axis at $X = 0$ is called the intersection point (see Fig. 3.1). This is the brightness of the star outside the atmosphere.

One can correct all light curves of a star for extinction by

$$m_{corr} = m - kX. \quad (3.19)$$

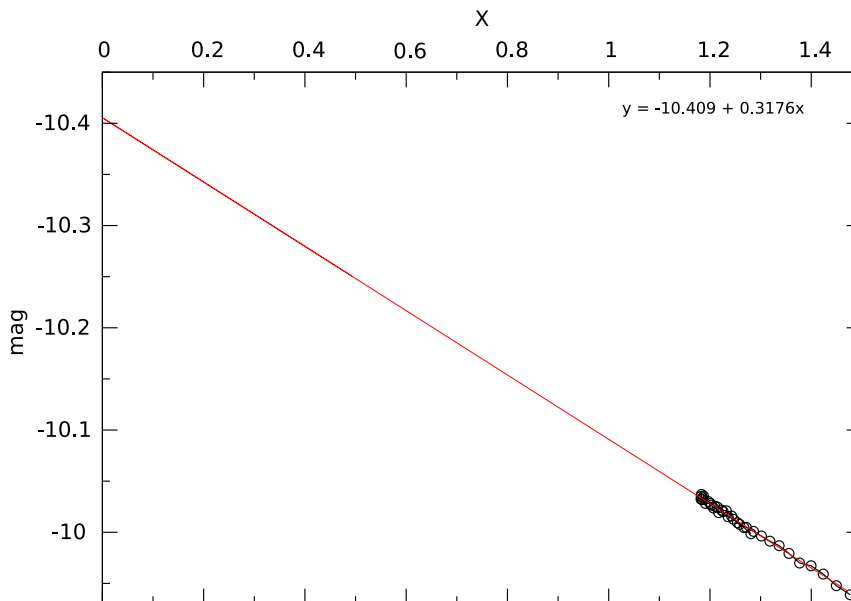


Figure 3.1: Bouguer diagram showing measurements of EE Cam over one night. This diagram allows the determination of the extinction coefficient k through linear regression.

3.8 V – C1, V – C2, C1 – C2

By means of the magnitudes corrected in the previous steps it is now possible to check the comparison stars for variability. The light curve of the comparison stars should be constant, but instrumental drifts occurring during one night can slightly change the light curve. Whether one or both of the comparison stars are variable or if both are constant can be found out by forming the differential light curves

- V – C1,
- V – C2,
- C1 – C2,

Where V is the magnitude of the target, C1 the magnitude of the first comparison star and C2 the magnitude of the second comparison star. Differential light curves are used rather than V, C1 and C2 itself, because instrumental errors, such as instrumental drifts, can be avoided. The instrumental errors would be present in all light curves and a subtraction involves a minimization of these effects. Additionally, by checking the differential light curve C1 – C2, data points with a low precision in V – C1 and V – C2 can be identified and removed.

The three-star technique relies on the minimization of most sources of error and avoids the drift problem experienced with multichannel instruments.

Before calculating these differences, it is required to interpolate to the same JD. In $V - C1$ and $V - C2$ it is common to interpolate to the time of the V measurement (see Fig. 3.2). In $C1 - C2$ it is common to interpolate the fainter target to the time of measurement of the brighter one.

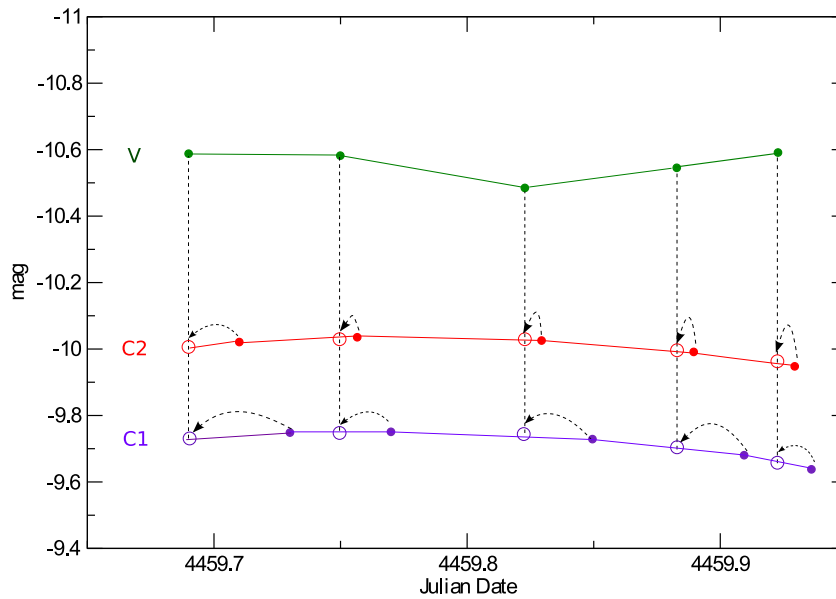


Figure 3.2: Interpolation to the same JD. The magnitudes of the comparison stars $C1$, $C2$ are interpolated to those of the variable star V . Solid circles mark the observed points. Open circles mark the interpolated $C1$ and $C2$ magnitudes.

3.9 Heliocentric correction

As the Earth is orbiting around the Sun, there is a time effect in the light coming from a star during a year: the Earth can be a few light minutes more distant from or closer to the star. This time shift has to be corrected. In the corresponding recalculation of the JD, the assumption that the star is observed from the center of the Sun is made. If the direction to the star is perpendicular to the ecliptic plane, the difference between JD and HJD will be zero. The size of the semimajor axis of the Earth is 8.3 light minutes. Consequently, the maximum value is $HJD - JD = +8.3$ minutes and is achieved if the star is in opposition to the Sun. In this case the light from the star will reach the Earth before it reaches the Sun. The minimum value of $HJD - JD = -8.3$ minutes is achieved if the Sun is located

between star and Earth. These maximum and minimum values will be achieved, if the star is on the ecliptic plane.

3.9.1 Calculation

According to Budding (1993), the heliocentric correction can be determined employing the rotation-matrix method. It is necessary to determine the x coordinate of the Sun (center of motion) when the x axis is pointing to the object. A geometrical explanation is given in Fig. 3.3. In the initial coordinate system, the x axis points to the Sun. The transformation (so that the x axis points towards the object) is applied by performing

$$x' = R_y(-\delta)R_z(\alpha)R_x(-\varepsilon)R_z(-\theta)x, \quad (3.20)$$

where α, δ denote the true coordinates of the variable star, ε describes the obliquity of the ecliptic and θ is the ecliptical longitude of the Sun.

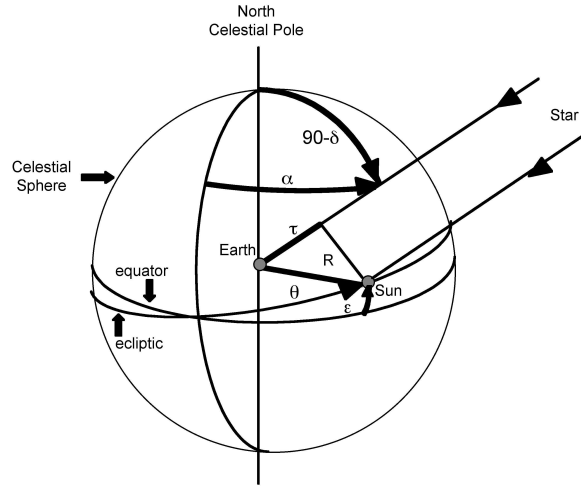


Figure 3.3: Heliocentric correction. Figure adopted from Budding (1993).

R_y , R_z and R_x denote the rotation matrices. They are defined as

$$R_x(\varphi) = \begin{pmatrix} 1 & 0 & 0 \\ 0 & \cos \varphi & \sin \varphi \\ 0 & -\sin \varphi & \cos \varphi \end{pmatrix}, \quad (3.21)$$

$$R_y(\varphi) = \begin{pmatrix} \cos \varphi & 0 & -\sin \varphi \\ 0 & 1 & 0 \\ \sin \varphi & 0 & \cos \varphi \end{pmatrix}, \quad (3.22)$$

$$R_z(\varphi) = \begin{pmatrix} \cos \varphi & \sin \varphi & 0 \\ -\sin \varphi & \cos \varphi & 0 \\ 0 & 0 & 1 \end{pmatrix}. \quad (3.23)$$

The coordinates of the Sun in the initial system are described by $r = (R, 0, 0)$, R denoting the radius vector Sun-Earth. By expanding the equation for x' the following equations are obtained

$$r' = \begin{pmatrix} R \cos \delta (\cos \alpha \cos \theta + \cos \varepsilon \sin \theta \sin \alpha) + R \sin \delta \sin \varepsilon \sin \theta \\ R \sin \alpha \cos \theta - R \cos \alpha \cos \varepsilon \sin \theta \\ R \sin \delta (\cos \alpha \cos \theta + \cos \varepsilon \sin \theta \sin \alpha) - R \cos \delta \sin \varepsilon \sin \theta \end{pmatrix}. \quad (3.24)$$

As only the x coordinate is needed, one can calculate the heliocentric correction by

$$x' = -\tau (R \cos \delta (\cos \alpha \cos \theta + \cos \varepsilon \sin \theta \sin \alpha) + R \sin \delta \sin \varepsilon \sin \theta), \quad (3.25)$$

where $\tau = 0.0057755$ d is the time the light needs to travel from the Earth to the Sun.

Finally, the HJD is calculated by

$$HJD = JD - x'. \quad (3.26)$$

Chapter 4

Frequency Analysis

The Fourier Transform is a common tool to interpret periodicities in a function of time as a superposition of sinusoids. Since astronomy deals with discrete data sets (time series) rather than continuous functions of time, the appropriate technique to examine periodic variations is the Discrete Fourier Transform. This chapter contains an introduction to the DFT, and two programs for time series analysis are presented and discussed. Most of the content was taken from Reegen (2000), Lenz (2005) and Deeming (1975).

4.1 Discrete Fourier Transform (DFT)

In general, the linear correlation between a time series

$$x_k = x(t_k) \quad (4.1)$$

and a fit function

$$f_k = f(t_k) = \sin(\omega t_k + \phi) \text{ with } k = 1, \dots, K, \quad (4.2)$$

is described by the covariance

$$\text{cov}(x_k, f_k) = \frac{1}{K} \sum_{k=1}^K x_k f_k = \frac{1}{K} \sum_{k=1}^K x_k \sin(\omega t_k + \phi). \quad (4.3)$$

In this context, x_k is assumed to be averaged to zero, and the fact that the mean value of the sinusoid may deviate from zero in special cases is neglected, since this approach is intended as a motivation.

If the covariance is 0, then there is no linear relationship, but there may be a non-linear one. A positive covariance means that higher (lower) values of x_k tend to pair with higher (lower) values of f_k , respectively. A negative covariance means that higher (lower) values of x_k tend to pair with lower (higher) values of f_k .

Eq. 4.3 contains two free parameters. As this may correspond to a high computational effort in practical applications, $f_k = \sin(\omega t_k + \phi)$ is replaced by $f_k = e^{i\omega t_k}$. The covariance now writes as

$$\text{cov}(x_k, f_k) = \frac{1}{K} \sum_{k=1}^K x_k e^{i\omega t_k} = \frac{1}{K} \sum_{k=1}^K x_k (\cos \omega t_k + i \sin \omega t_k). \quad (4.4)$$

This is a two-dimensional representation with coordinates $a(\omega) := \frac{1}{K} \sum x_k \cos \omega t_k$, $b(\omega) := \frac{1}{K} \sum x_k \sin \omega t_k$, where the amplitude spectrum is defined as the length of the Fourier vector, and the phase is the angle between this vector and the axis $a(\omega)$ (see Fig. 4.1). The amplitude spectrum is denoted $A(\omega)$ and defined by

$$A^2(\omega) = \frac{1}{K^2} \left[\left(\sum_{k=1}^K x_k \cos \omega t_k \right)^2 + \left(\sum_{k=1}^K x_k \sin \omega t_k \right)^2 \right], \quad (4.5)$$

with $\omega \in [-\infty, \infty]$. As the amplitude is an even function, because x_k is real $\forall k$, and

$$A(\omega) := A(\omega) + A(-\omega) = 2A(\omega), \quad (4.6)$$

it is sufficient to consider non-negative frequencies through

$$A^2(\omega) = \frac{4}{K^2} \left[\left(\sum_{k=1}^K x_k \cos \omega t_k \right)^2 + \left(\sum_{k=1}^K x_k \sin \omega t_k \right)^2 \right]. \quad (4.7)$$

As the amplitude spectrum follows the concept of the covariance, peaks indicate frequen-

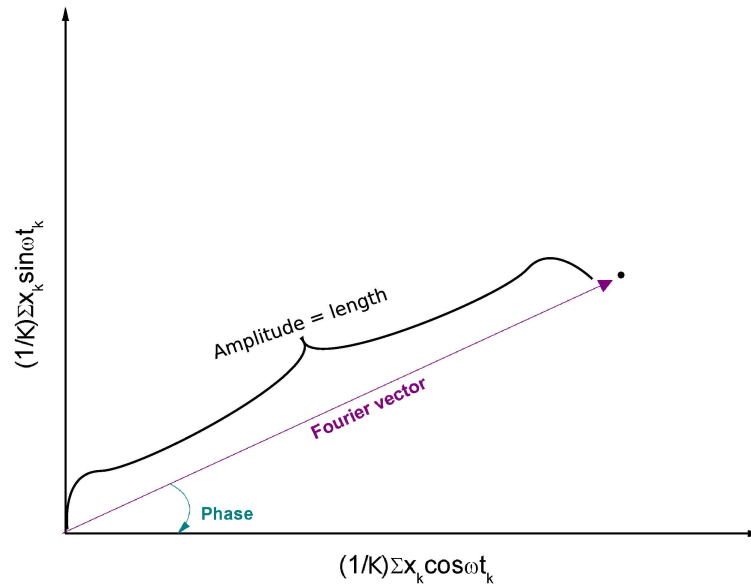


Figure 4.1: Two-dimensional representation of the Fourier vector, the phase and the amplitude.

cies where the sinusoid is in good agreement with the data. The peaks in the amplitude spectrum contain the information an astronomer is interested in, namely the frequencies, amplitudes and phases. These parameters are important to get information on the energy transport, the element abundances and the mass and temperature distributions. Even the radius, mass, effective temperature, and the age of the star can be derived.

4.2 The Nyquist criterion

Writing Eq. 4.7 in terms of a double sum, yields

$$A^2(\omega) = \frac{4}{K^2} \sum_{k=1}^K \sum_{l=1}^K x_k x_l (\cos \omega t_k \cos \omega t_l + \sin \omega t_k \sin \omega t_l), \quad (4.8)$$

which reduces to

$$A^2(\omega) = \frac{4}{K^2} \sum_{k=1}^K \sum_{l=1}^K x_k x_l \cos \omega(t_k - t_l). \quad (4.9)$$

Each pair of measurements contributes a periodic term in ω to the sum, the period of which is $\frac{2\pi}{|t_l - t_k|}$. For an equidistantly sampled time series, $t_k := k\delta t$, where δt is the sampling rate, this yields

$$A^2(\omega) = \frac{4}{K^2} \sum_{k=1}^K \sum_{l=1}^K x_k x_l \cos \omega \delta t(k - l). \quad (4.10)$$

Replacing ω by $\omega + \frac{2\pi}{\delta t}$, yields

$$\cos\left(\omega + \frac{2\pi}{\delta t}\right) \delta t(k - l) = \cos(\omega \delta t(k - l) + 2\pi(k - l)) = \cos \omega \delta t(k - l). \quad (4.11)$$

Now all contributions to the sum have an unique period

$$\Delta\omega = \frac{2\pi}{\delta t}, \quad (4.12)$$

i.e., the amplitude spectrum recurs every $\frac{2\pi}{\delta t}$ in ω or every $\frac{1}{\delta t}$ in frequency.

Lets now use $\frac{2\pi}{\delta t} - \omega$ instead of ω . Then the backmost part of Eq. 4.10 is

$$\cos\left(\frac{2\pi}{\delta t} - \omega\right) \delta t(k - l) = \cos(\omega \delta t(k - l) - 2\pi(k - l)) = \cos \omega \delta t(k - l). \quad (4.13)$$

Again, the same result is achieved and a symmetry with respect to

$$\frac{1}{2} \frac{2\pi}{\delta t} = \frac{\pi}{\delta t}. \quad (4.14)$$

is obtained. This corresponds to $\frac{1}{2\delta t}$ in frequency and is called the Nyquist criterion. Therefore, if the signal is measured with a unique sampling rate δt , the amplitude spectrum is unique only for frequencies $f \in \left[0, \frac{1}{2\delta t}\right]$. Outside this interval, the amplitude spectrum is an exact repetition of this range and called alias.

4.2.1 Example

Assuming a signal of 18 Hz and a sampling rate of 0.1 s for an unlimited time series, the Nyquist frequency will be 5 Hz. So, a peak at 2 Hz would be present. Due to the axes of symmetry at $\frac{1}{2\delta t} = 5\text{Hz}$ and its multiples, there will be additional peaks at 8, 12, 18, 22, etc. Hz (see Fig. 4.2). As the period is $\frac{1}{\delta t} = 10\text{Hz}$ the amplitude spectrum will recur every 10 Hz. So, a suitable sampling rate is required, i.e. the sampling should be dense enough. This density depends on the frequency interval that is investigated.

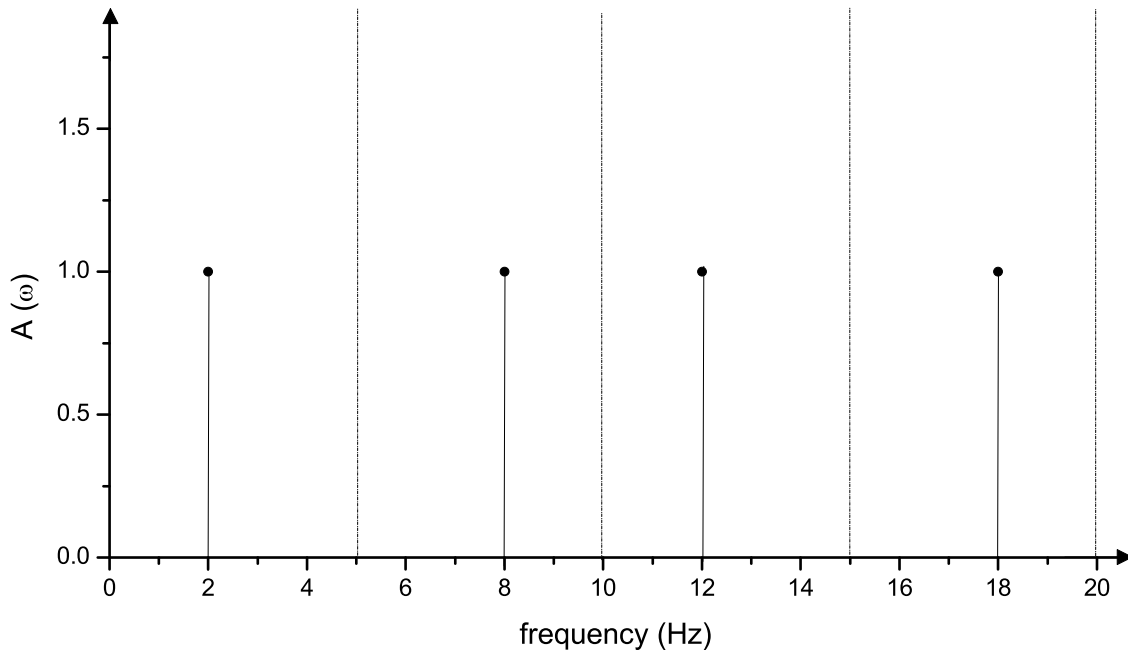


Figure 4.2: Amplitude spectrum of a signal with 18 Hz and a sampling rate of 0.1 s for an unlimited time series. The Nyquist frequency is at 5 Hz, and the spectrum repeats every 10 Hz. Solid lines mark the frequency peaks. Dashed lines mark the axes of symmetry.

4.3 Spectral window

Given a continuous function of time $x(t)$ on the interval $t \in \left[-\frac{\Delta t}{2}, \frac{\Delta t}{2}\right]$, the corresponding series expansion is

$$x(t) = \sum_{n=0}^{\infty} c_n e^{i\omega_n t}. \quad (4.15)$$

If $\omega_n = \frac{2\pi n}{\Delta t}$, Eq. 4.15 transforms into

$$x(t) = \sum_{n=0}^{\infty} c_n \exp\left(2i\pi n \frac{t}{\Delta t}\right). \quad (4.16)$$

Postulating

$$c_m = \frac{1}{\Delta t} \int_{-\Delta t/2}^{\Delta t/2} dt x(t) \exp\left(-2\pi i m \frac{t}{\Delta t}\right). \quad (4.17)$$

Employing Eq. 4.16, yields

$$c_m = \frac{1}{\Delta t} \sum_{n=0}^{\infty} c_n \int_{-\Delta t/2}^{\Delta t/2} dt \exp\left(2i\pi(n-m)\frac{t}{\Delta t}\right). \quad (4.18)$$

Now, two cases are possible: (i) $n \neq m$; (ii) $n = m$.

(i) $\mathbf{n} \neq \mathbf{m}$. Integration of Eq. 4.18 yields

$$\begin{aligned} c_m &= \frac{1}{\Delta t} \sum_{n=0}^{\infty} c_n \frac{\Delta t}{2\pi i(n-m)} \exp\left(2\pi i(n-m)\frac{t}{\Delta t}\right) \Bigg|_{-\Delta t/2}^{\Delta t/2} = \\ c_m &= \frac{1}{\Delta t} \sum_{n=0}^{\infty} c_n \frac{\Delta t}{2\pi i(n-m)} \left[e^{\pi i(n-m)} - e^{-\pi i(n-m)} \right] \\ c_m &= \frac{1}{\Delta t} \sum_{n=0}^{\infty} c_n \frac{\Delta t}{2\pi i(n-m)} [2i \sin \pi(n-m)] = 0. \end{aligned} \quad (4.19)$$

(ii) $\mathbf{n} = \mathbf{m}$. Integration of Eq. 4.18 results in $c_m = 1$. The general annotation incorporates the Kronecker symbol δ_{mn} and writes as

$$c_m = \sum_{n=0}^{\infty} \delta_{nm} c_n. \quad (4.20)$$

This leads to four important conclusions:

1. The Fourier coefficients c_n are orthogonal.
2. The frequency resolution is $\delta\omega = \frac{2\pi}{\Delta t}$ in ω and $\delta f = \frac{1}{\Delta t}$ in frequency. This is also referred to as the Rayleigh criterion.
3. There is a symmetry: if the time domain is bounded, then the frequency domain is discrete, and vice versa.
4. Consequently, if the time domain is discrete and bounded, then the frequency domain is discrete and bounded, too.

If the time series $x(t)$ represents a product $x(t) = y(t)z(t)$, where

$$y(t) = \sum_{n=0}^{\infty} a_n e^{i\omega_n t}, \quad \omega_n = \frac{2\pi n}{\Delta t} \quad (4.21)$$

and

$$z(t) = \sum_{m=0}^{\infty} b_m e^{i\omega_m t}, \quad \omega_m = \frac{2\pi m}{\Delta t}, \quad (4.22)$$

then $x(t)$ is given by

$$x(t) = \sum_{m=0}^{\infty} \sum_{n=0}^{\infty} a_n b_m \exp\left(2\pi i(m+n)\frac{t}{\Delta t}\right). \quad (4.23)$$

Now a new index $k := m + n$ is defined. Eq. 4.23 then re-writes as

$$x(t) = \sum_{k=0}^{\infty} \sum_{n=0}^k a_n b_{k-n} \exp\left(2\pi i k \frac{t}{\Delta t}\right) = \sum_{k=0}^{\infty} c_k \exp\left(2\pi i k \frac{t}{\Delta t}\right). \quad (4.24)$$

with

$$c_k = \sum_{n=0}^k a_n b_{k-n}. \quad (4.25)$$

This is defined as the convolution theorem. In terms of Fourier transforms represented by the tilde “~”, it writes as

$$(\widetilde{f\tilde{g}})(\omega) = \int_{-\infty}^{\infty} d\omega' \tilde{f}(\omega') \tilde{g}(\omega - \omega'), \quad (4.26)$$

i.e. the Fourier transform of the convolution of two functions is equal to the product of the Fourier transforms. Let us consider $z(t)$ a rectangular function

$$z(t) = \begin{cases} 1 & \forall t \in [t_1, t_2] \\ 0 & \text{else.} \end{cases} \quad (4.27)$$

The Fourier transform of the rectangular function is the sinc function $\text{sinc}(\omega)$. Therefore, the Fourier spectrum of a continuous function of time on a finite time interval is a convolution of the Fourier spectrum of the corresponding function on an infinite interval with the Fourier spectrum of the rectangular function, where the Fourier spectrum of the rectangular function is called the spectral window. So, even for a continuous function on a bounded interval a spectral window exists, and also for discrete time series.

Fig. 4.3 shows the spectral windows of an equidistant time series (upper graph) and the APT photometry of EE Cam (2006-2009) (i.e. non-equidistant sampling, lower graph). Both have the same Nyquist frequency f_v (red dashed-dotted line). One can see that the spectrum is mirrored at this frequency. As explained before, the spectrum is unique between 0 and f_v . Fig. 4.4 and Fig. 4.5 zoom the range around $f = 0$ and around $f = 1$. The non-equidistant time series (lower graphs) clearly shows annual as well as daily aliases. The equidistant time series (upper graphs) consists of equidistant peaks, where each Fourier coefficient is a root because of the orthogonality (Eq. 4.20).

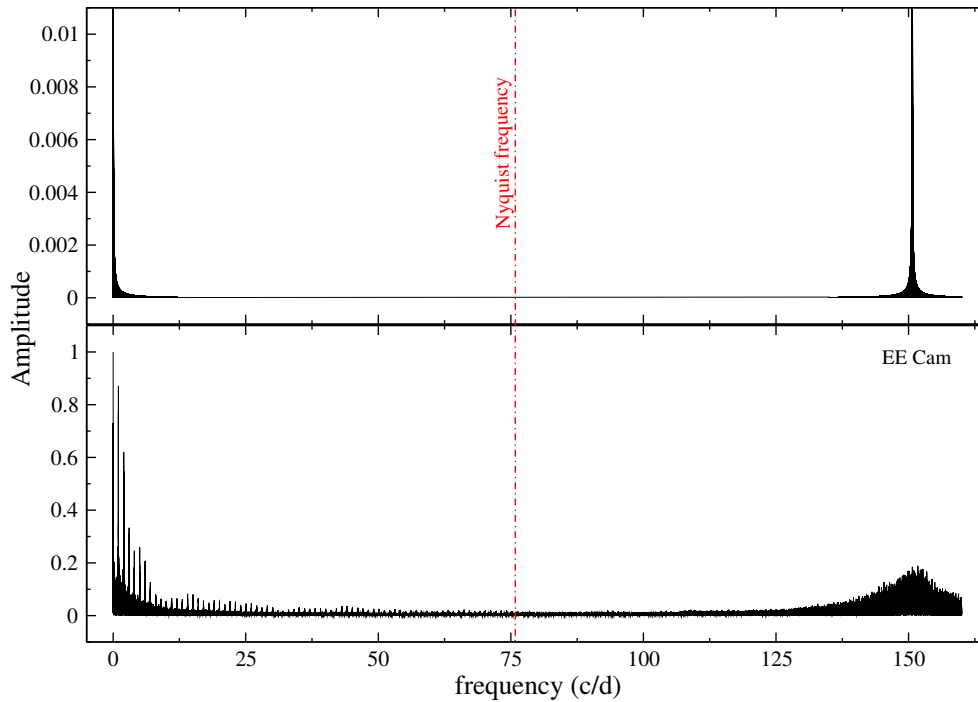


Figure 4.3: Spectral windows of an equidistant (upper) time series and the non-equidistant (lower) time series of EE Cam. Both have the Nyquist frequency $f_v = 75.5$ c/d marked by the dash-dotted line. Amplitude axes have different scalings for better visibility.

4.4 Summary

Table 4.1 contains the main differences between the Fourier transform, the Fourier analysis and the DFT.

Table 4.1: Summary.

| | f | \hat{f} |
|--------------------------|------------------------|---------------------------------------|
| Fourier transform | continuous & unbounded | continuous & unbounded |
| Fourier analysis | continuous & bounded | discrete & unbounded (Fourier series) |
| DFT | discrete | (continuous &) bounded |

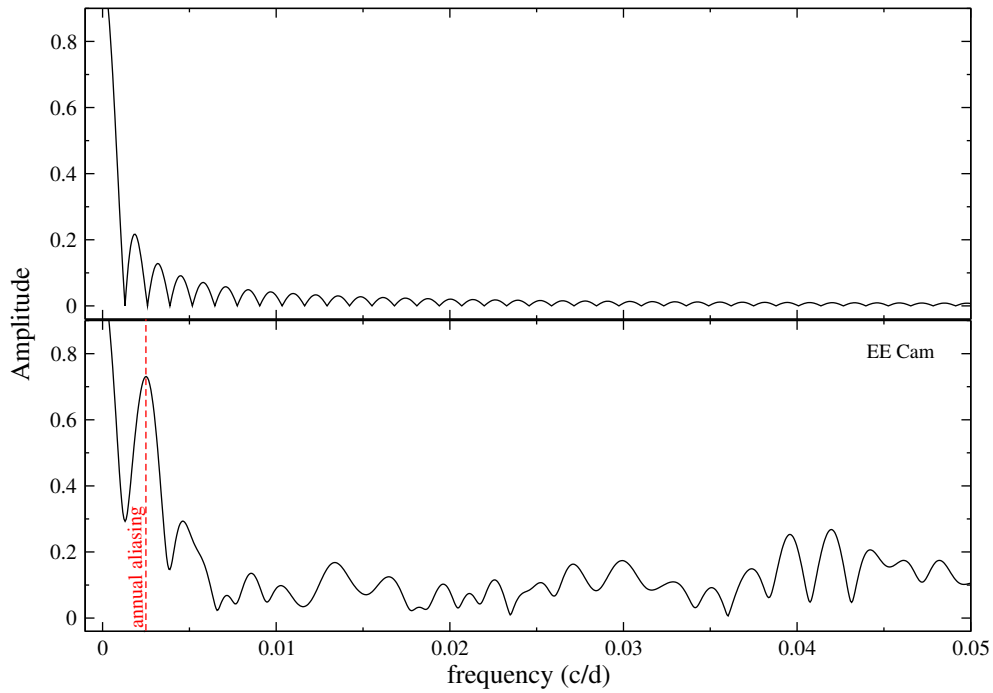


Figure 4.4: Spectral windows of an equidistant (upper graph) and non equidistant (lower graph) time series focusing on frequencies around 0 c/d. Annual aliasing is present in the non-equidistant data set. Amplitude axes have different scalings for better visibility.

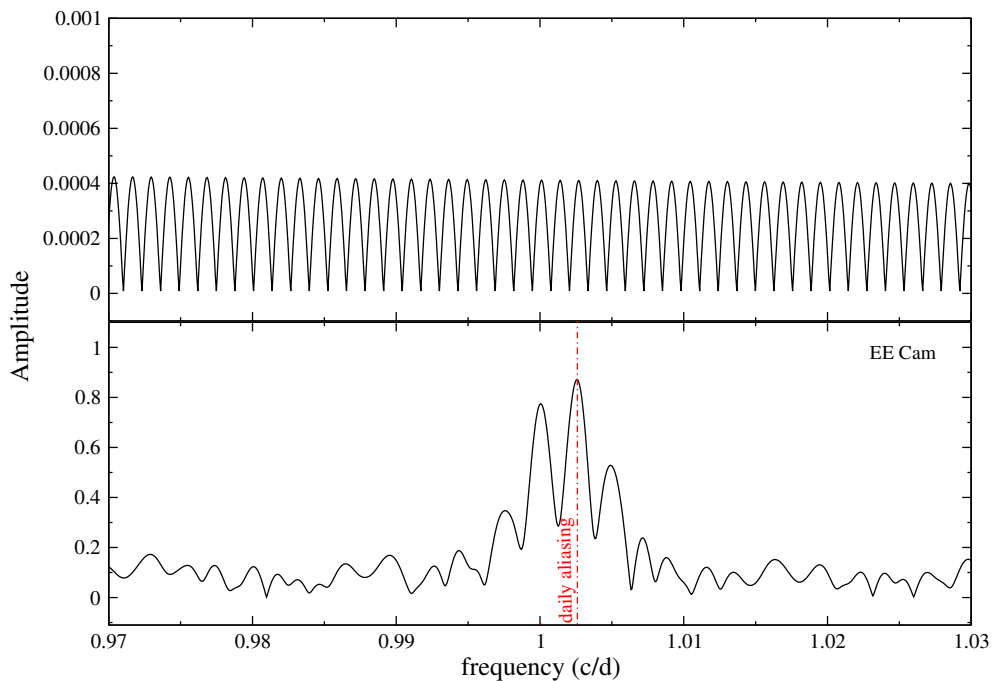


Figure 4.5: Same as Fig. 4.4 but focusing on frequencies around 1 c/d. Daily aliasing (1 cycle per sidereal day, lower figure) is present in the non-equidistant data set. Amplitude axes have different scalings for better visibility.

4.5 Frequency-finding programs

There are many programs and algorithms that can be used to find the significant frequencies, amplitudes and phases of a data series. Here, two programs and methods are presented. I chose these two programs, because they will be used for the determination of the best extinction correction method (see Chapter 5).

4.5.1 Period04

Period04 is a program for the analysis of astronomical time series (Lenz & Breger 2005). It can also be applied to data sets containing gaps.

4.5.1.1 The modules and its methods

The program has an user interface and consists of three modules:

- Time string module
- Fourier module
- Fit module

4.5.1.2 Properties of the Time string module

In this module the time string data obtained during observations can be imported. Additionally, one can split the data into subgroups, combine time strings or add other data. The time string plot and the appropriate Fourier-Fit can be inspected.

4.5.1.3 Properties of the Fourier module

In this module a Fourier calculation is performed in order to obtain frequencies fitting the data. This program uses a DFT algorithm. Lenz & Breger (2005) argue that FFTs (Fast Fourier Transform) are not suitable for astronomical time string data, because of the unequal spacing of these data.

Every step carried out can be checked or exported with the Log tab.

4.5.1.4 Properties of the Fit module

This module computes least-squares fits using the obtained frequencies. The fitting formula is

$$A_0 + \sum A_i \sin(2\pi(\omega_i t + \Phi_i)). \quad (4.28)$$

It is also possible to calculate amplitude/phase variations, to include periodic time shifts and to calculate the signal-to-noise-ratio of the frequencies or the noise spectrum. The calculated noise can be higher than the uncertainty of the measurements because of aliasing effects and intrinsic signal below the noise level. In addition, frequencies can be imported and the obtained frequencies exported. The goodness-of-fit can be checked by calculating the uncertainties with a Monte Carlo simulation.

4.5.1.5 How does it work?

For a given data set `Period04` first computes an amplitude spectrum and determines the maximum amplitude. Then one has to decide whether this frequency is significant or not. This can be done by computing the signal-to-noise ratio, S/N, the residuals and/or the spectral window (check for aliasing). If this frequency is regarded as significant by the user then the sine function is prewhitened from the data set. The residuals are then used for the next iteration, i.e. everything starts from the beginning. This will be done as long as the amplitude S/N is ≥ 4.0 , because that is, according to Breger et al. (1993), the limit for the significance of an independent frequency. So the program, or the user who decides whether it is wise to continue or not, stops if the significance of the maximum amplitude is below this limit. This method provides the detected frequencies, amplitudes and phases that can be used to identify pulsation modes.

4.5.2 SigSpec

`SigSpec` (Reegen 2000, 2007) is a program that focuses on the determination of the significance of a peak in the Discrete Fourier Transform. Unlike `Period04` it has no user interface. The data are read in and the results are written out by the program automatically.

4.5.2.1 The method

By means of an analytical solution for the probability density function of white noise in Fourier space it calculates how likely it is that a given peak amplitude is caused by noise. This probability distribution is important, because any misinterpretation of a peak amplitude will lead to inaccuracies in the subsequent analysis. The probability distribution can be described by a Probability Density Function. The integral over this Probability Density Function gives the False-Alarm Probability Φ_{FA} , describing how likely it is that a peak is an artifact. The False-Alarm Probability gets lower for higher peak amplitudes in the spectrum, so it is less likely that a high peak is an artifact.

Reegen (2007) defines a new term called spectral significance which depends on frequency, phase and amplitude in the Discrete Fourier Transform. It is the logarithm of the inverse False-Alarm-Probability (Scargle 1982)

$$\text{sig}(A) = -\log[\Phi_{FA}(A)]. \quad (4.29)$$

The spectral significance is the number of cases in one out of which the peak is an artifact, on a logarithmic scale. The spectral significance is the formally exact representation of what is estimated by the S/N. If the maximum amplitude of the spectrum is above a given limit it can be considered significant. The S/N limit of ≥ 4.0 (Breger et al. 1993) used in `Period04` corresponds to a spectral significance of 5.46. This means that the amplitude is reliable if the probability is larger than this value. As `SigSpec` is a black box, the author recommends to check the results for reliability. A peak that is regarded as significant can still be an instrumental or atmospheric artifact instead of a description of a physical process.

4.5.2.2 How does it work?

This information was taken from Reegen (2000). As Period04, SigSpec performs many iterations. It first calculates the significance spectrum based on which it determines the peak with the maximum significance. For the corresponding frequency it calculates a least-squares fit of the amplitude and phase. Then the sinusoidal component with the maximum significance is prewhitened. After this, a next iteration is started. SigSpec allows the user to choose between different outputs (after each step of prewhitening): (i) a Fourier spectrum as well as a significance spectrum (plot of spectral significance vs. frequency); (ii) a time series that corresponds to the residuals; (iii) a file containing the results (the identified signal components). If the significance of the maximum peak is below a defined limit, the program exits the loop.

Chapter 5

Results

5.1 Observational details

5.1.1 Instrument

EE Cam was observed by the Vienna Automatic Photoelectric Telescope (APT, Strassmeier et al. 1997), located in Arizona. Wolfgang, one of the two telescopes, contains a photometer optimized for the use in the blue wavelength region and is therefore suitable for the observations of EE Cam in the Strömgren v and y filters.

5.1.2 Observing periods

EE Cam was observed in 2006, 2007, 2008 and 2009 in four observing periods. Table 5.1 gives the beginning, end, duration and the number of data points of each observing period. Additionally, a list of the comparison stars that were used in the distinct observing periods is provided. In the fourth observing period C2 was exchanged after a few nights because of suspected variability. Therefore, this observing period is referred to as OP4 (old C2) and OP4' (new C2). A detailed list containing the HJD and the observation time in each night is provided in Table 5.3 and 5.4.

5.1.3 Details on EE Cam and the comparison stars

As the three-star technique was used (see 2.3), two comparison stars were observed. In OP4' the second comparison star was replaced because of suspected variability. All necessary information on EE Cam (HD 37857) and the comparison stars HD 35606 and HD 32745 (HD 37420 for OP4') is provided in Table 5.2. Right ascensions and declinations are given for the equinox 2000 and taken from the Hipparcos Catalogue (Perryman et al. 1997). The brightness and effective temperature of EE Cam are given by Nordström et al. (2004). The $v \sin i$ was determined by Breger et al. (2007) and the spectral type by Olsen (1980).

Table 5.1: Beginning, end, duration, number of data points as well as the observed comparison stars of the individual observing periods.

| | OP1 | OP2 | OP3 | OP4 | OP4' |
|------------------------------|------|-------|-------|------|-------|
| HJD start (245 0000+) | 3791 | 3997 | 4370 | 4728 | 4767 |
| HJD end (245 0000+) | 3810 | 4189 | 4566 | 4760 | 4888 |
| number of nights | 9 | 80 | 47 | 21 | 45 |
| total time (hours) | 16.2 | 291.1 | 148.1 | 53.3 | 178.4 |
| number of data points | | | | | |
| raw v | 104 | 1858 | 886 | 331 | 1057 |
| raw y | 104 | 1858 | 890 | 335 | 1064 |
| reduced v and y | 104 | 1822 | 850 | 314 | 1027 |
| HD 35606 | C1 | C1 | C1 | C1 | C1 |
| HD 32745 | C2 | C2 | C2 | C2 | – |
| HD 37420 | – | – | – | – | C2 |

Table 5.2: Information on EE Cam, HD 35606, HD 32745 and HD 37420.

| Parameter | EE Cam (V) | HD 35606 (C1) | HD 32745 (C2) | HD 37420 (C2) |
|---------------------------|----------------------|-------------------------|-------------------------|-------------------------|
| RA [h m s] | 05 45 54.99 | 05 30 35.52 | 05 09 45.95 | 05 42 38.66 |
| DEC [° ' ”] | +63 17 46.56 | +63 57 17.87 | +63 50 00.08 | +61 36 10.93 |
| Spectral type | F3 | F8 | G0 | F5 |
| V [mag] | 7.753 | 8.15 | 8.21 | 7.78 |
| T_{eff} [K] | 6530 | – | – | – |
| $v \sin i$ [kms^{-1}] | 40 ± 3 | – | – | – |

5.1.4 Light curves

Fig. A.1 (see Appendix) visualizes the differential light curve V – C1 obtained in v and y in all four observing periods. When referring to four observing periods OP4 and OP4' are regarded as one (the fourth) observing period.

Table 5.3: Dates and durations of the observations obtained during the first (OP1) and second (OP2) observing period between spring 2007 and spring 2008.

| HJD 245 0000+ | length [h] | HJD 245 0000+ | length [h] | HJD 245 0000+ | length [h] | HJD 245 0000+ | length [h] |
|------------------|---------------|------------------|---------------|------------------|---------------|------------------|---------------|
| OP1 | | OP2 | | | | | |
| 3791.6 | 3.30 | 3997.9 | 3.13 | 4077.7 | 2.33 | 4158.6 | 3.23 |
| 3796.7 | 0.80 | 4000.9 | 2.07 | 4079.7 | 1.94 | 4160.6 | 3.03 |
| 3797.6 | 1.18 | 4003.9 | 3.61 | 4080.7 | 2.28 | 4161.6 | 2.07 |
| 3798.6 | 1.82 | 4005.9 | 3.76 | 4081.7 | 7.59 | 4169.6 | 1.60 |
| 3799.6 | 2.78 | 4010.8 | 3.76 | 4084.9 | 0.48 | 4170.6 | 2.23 |
| 3803.6 | 1.50 | 4023.9 | 3.17 | 4090.6 | 6.77 | 4171.6 | 2.23 |
| 3808.6 | 1.60 | 4024.8 | 5.19 | 4093.6 | 5.04 | 4172.6 | 2.07 |
| 3810.6 | 1.82 | 4025.8 | 5.20 | 4094.6 | 6.85 | 4173.6 | 2.08 |
| | | 4028.8 | 5.51 | 4095.6 | 3.13 | 4174.6 | 1.91 |
| | | 4029.8 | 5.51 | 4100.6 | 6.88 | 4175.6 | 1.91 |
| | | 4030.8 | 5.52 | 4101.6 | 5.04 | 4178.6 | 1.28 |
| | | 4031.8 | 5.66 | 4102.6 | 6.81 | 4185.6 | 0.80 |
| | | 4035.8 | 5.84 | 4103.6 | 6.81 | 4187.6 | 0.80 |
| | | 4038.9 | 3.98 | 4104.6 | 6.96 | 4189.6 | 0.64 |
| | | 4048.7 | 2.33 | 4105.6 | 6.86 | | |
| | | 4049.7 | 2.33 | 4108.6 | 6.95 | | |
| | | 4050.7 | 2.33 | 4116.6 | 6.48 | | |
| | | 4054.7 | 2.33 | 4117.6 | 6.47 | | |
| | | 4055.7 | 2.17 | 4124.6 | 5.74 | | |
| | | 4056.7 | 2.33 | 4127.6 | 5.57 | | |
| | | 4057.7 | 2.33 | 4128.6 | 5.39 | | |
| | | 4058.7 | 2.33 | 4134.6 | 4.94 | | |
| | | 4059.7 | 2.17 | 4135.6 | 3.79 | | |
| | | 4060.7 | 2.17 | 4136.6 | 4.83 | | |
| | | 4061.7 | 2.33 | 4140.6 | 4.55 | | |
| | | 4062.7 | 2.33 | 4143.7 | 2.23 | | |
| | | 4064.7 | 2.33 | 4146.6 | 2.82 | | |
| | | 4067.7 | 2.17 | 4147.7 | 1.43 | | |
| | | 4069.7 | 2.33 | 4152.6 | 3.67 | | |
| | | 4070.7 | 2.17 | 4153.6 | 2.23 | | |
| | | 4071.7 | 2.33 | 4154.6 | 3.51 | | |
| | | 4072.7 | 2.23 | 4156.6 | 3.35 | | |
| | | 4074.7 | 2.33 | 4157.6 | 3.27 | | |

Table 5.4: Dates and durations of the observations obtained during the third (OP3) and fourth (OP4 & OP4') observing period between autumn 2007 and spring 2009.

| HJD 245 0000+ | length [h] | HJD 245 0000+ | length [h] | HJD 245 0000+ | length [h] | HJD 245 0000+ | length [h] |
|------------------|---------------|------------------|---------------|------------------|---------------|------------------|---------------|
| OP3 | | | | OP4 | | | |
| 4370.9 | 2.66 | 4516.6 | 4.56 | 4728.9 | 1.44 | 4785.8 | 4.47 |
| 4397.8 | 5.77 | 4523.6 | 4.05 | 4729.9 | 1.59 | 4786.8 | 4.47 |
| 4402 | 0.32 | 4524.6 | 3.94 | 4730.9 | 1.60 | 4787.8 | 5.09 |
| 4404 | 0.48 | 4530.6 | 2.15 | 4731.9 | 1.60 | 4788.8 | 3.71 |
| 4406 | 0.64 | 4533.6 | 2.81 | 4734.9 | 1.85 | 4789.8 | 4.41 |
| 4413 | 1.11 | 4536.7 | 1.43 | 4736.9 | 2.07 | 4790.8 | 5.10 |
| 4414 | 1.12 | 4544.6 | 2.04 | 4737.9 | 2.06 | 4800.8 | 5.12 |
| 4416 | 1.28 | 4550.6 | 1.6 | 4738.9 | 2.20 | 4801.8 | 4.63 |
| 4419 | 1.6 | 4551.6 | 1.59 | 4740.9 | 2.29 | 4810.7 | 5.21 |
| 4423 | 1.91 | 4553.6 | 1.27 | 4743.9 | 1.76 | 4821.7 | 4.55 |
| 4426 | 1.76 | 4555.6 | 1.12 | 4745.9 | 2.63 | 4822.7 | 4.46 |
| 4427.9 | 2.08 | 4564.6 | 0.64 | 4746.9 | 2.68 | 4830.7 | 4.36 |
| 4437.9 | 1.9 | 4565.6 | 0.48 | 4747.9 | 2.78 | 4831.7 | 0.48 |
| 4438.9 | 1.91 | 4566.6 | 0.48 | 4752.9 | 3.32 | 4832.7 | 3.65 |
| 4439.9 | 1.92 | | | 4753.9 | 3.29 | 4833.7 | 5.08 |
| 4459.7 | 6.06 | | | 4754.9 | 3.33 | 4838.7 | 3.32 |
| 4460.7 | 5.73 | | | 4755.9 | 3.50 | 4839.7 | 4.45 |
| 4461.7 | 5.7 | | | 4756.9 | 2.56 | 4840.6 | 4.10 |
| 4462.7 | 5.41 | | | 4757.9 | 3.66 | 4841.6 | 0.48 |
| 4465.7 | 6.1 | | | 4758.9 | 3.55 | 4842.6 | 0.48 |
| 4466.7 | 4.58 | | | 4760.9 | 3.59 | 4844.6 | 5.13 |
| 4476.6 | 6.11 | | | 4767.8 | 4.36 | 4846.6 | 5.12 |
| 4482.6 | 2.55 | | | 4768.8 | 4.03 | 4856.6 | 5.08 |
| 4483.6 | 5.84 | | | 4769.9 | 4.29 | 4860.6 | 4.91 |
| 4484.6 | 4.3 | | | 4770.8 | 4.15 | 4861.6 | 0.48 |
| 4485.6 | 5.64 | | | 4771.8 | 4.77 | 4862.6 | 0.64 |
| 4486.6 | 5.1 | | | 4772.8 | 1.75 | 4863.6 | 4.80 |
| 4502.6 | 4.12 | | | 4773.8 | 4.76 | 4864.6 | 3.67 |
| 4503.6 | 5.47 | | | 4774.8 | 3.60 | 4865.6 | 4.95 |
| 4504.6 | 5.38 | | | 4775.8 | 3.72 | 4873.6 | 4.24 |
| 4505.6 | 5.3 | | | 4776.8 | 5.11 | 4875.6 | 4.16 |
| 4508.6 | 5.08 | | | 4777.8 | 5.14 | 4881.6 | 3.55 |
| 4509.6 | 5.03 | | | 4778.8 | 5.10 | 4888.6 | 3.27 |

5.2 Data reduction

The APT data output can be retrieved via internet. It contains the ID number of the observed stars, the Julian Date without heliocentric correction, the integration time and the measured photon counts. Peter Reegen, who is responsible for the administration and operation of the APT, performed a standard reduction of the EE Cam photometry according to the procedure outlined in Chapter 3. Additionally, he provided Julian Date and instrumental magnitudes¹, based on which it was my task to examine and compare alternative extinction correction methods, as described below.

5.2.1 Heliocentric Julian Date correction

The rotation of the Earth around the Sun causes a time shift in the observed data, because the distance between the Earth and the star varies. The Heliocentric Julian Date is the recalculation of the Julian Date, corrected for these variations. My Fortran program is based on the Java code ‘Heliocentric Julian Date Converter’ by Dan Bruton² and relies on the description provided in 3.9.1.

5.2.2 Extinction correction

Computing a linear regression in a Bouguer Diagram (magnitude vs. airmass), one can determine the slope and the intersection point. The slope is the extinction coefficient used to apply the extinction correction, where the intersection point denotes the brightness of the star outside the atmosphere. There are various methods that can be used. As my thesis mainly concentrates on the determination of the extinction coefficient, more detailed information on this topic is provided in 5.3.

5.2.3 Interpolation

The telescope is not able to observe more than one star at the same time. Therefore, the stars are observed at slightly different times. To avoid errors caused by this difference, an interpolation has to be applied, where the HJD of the comparison star is interpolated to the HJD of the object of interest. This means that the time and magnitude of the comparison stars C1 and C2 are interpolated to those of EE Cam. For the three-star-technique the differential light curve C1–C2 is required, too. Therefore, it is required to interpolate one to the other. Concerning the comparison stars it is common to interpolate the fainter one to the brighter one, i.e., here C2 is interpolated to the time of C1. The Fortran program calculates the interpolation by a *distance-weighted average* (Reegen et al. 2006)

$$mag_1(t) = \sum \frac{mag(t_i)}{[t - t_i]^2}, \quad (5.1)$$

¹Photon counts, corrected for dark current and deadtime, after sky subtraction and conversion into magnitudes.

²<http://www.physics.sfasu.edu/astro/javascript/hjd.html>

$$mag_2(t) = \sum \frac{1}{[t - t_i]^2}, \quad (5.2)$$

$$mag(t) = \frac{mag_1(t)}{mag_2(t)}, \quad (5.3)$$

where t_i denotes the distinct times during one night of the star (STAR 2) that is interpolated and t is one data point in time of one night of the star (STAR 1) that is interpolated to. The final magnitude of STAR 2 is given by $mag(t)$. This calculation is repeated for each data point in time t in a given night of STAR 1. It has to be repeated for each single night. The final outputs are two sets of measurements at equal times.

5.2.4 Differential light curves

Now, the differential light curves V–C1, V–C2 and C1–C2 can be computed. This is the concept of the three-star-technique. With differential light curves one can examine the variability of the comparison stars. C1–C2 should be a constant value if the comparison stars are not variable. The examination of C1–C2 using HD 35606 and HD 32745, respectively revealed variability. Breger et al. (2007) found that C2 is a long-term variable. A variable comparison star eliminates the final use of the three-star-technique and the data reduction has to solely rely on C1. But nevertheless the differential light curve C1–C2 can still be used to check the significance of individual data points.

5.2.5 Elimination of individual data points

First, one or two frequencies of the differential light curve C1–C2 have to be calculated using Period04 or SigSpec. Afterwards it is possible to plot the residuals of the least-squares-fitting-method. Upper and lower values for the residuals can be defined. All points beyond these boundaries are candidates for elimination. But, of course, it is still necessary to have a look at the differential light curve V–C1 and to decide on rejection for each single data point. This has to be done for each filter. It needs to be emphasized that only extremely deviant points are eliminated and no statistical bias is introduced.

5.2.6 Frequency analysis

Once there is a set of differential light curves available, the next step is the determination of frequencies, amplitudes and phases of the signal components intrinsic to the star. The frequency analysis of the obtained EE Cam data was performed with Period04 (Lenz & Breger 2005) as well as SigSpec (Reegen 2007). The results are presented and discussed in 5.5. Note that the frequency analysis was only performed for the first three observing periods and the best extinction correction.

5.2.7 Restrictions

5.2.7.1 Variability of comparison stars

As already mentioned before, the three-star technique cannot be applied if one or both comparison stars are variable. Therefore, a careful examination of the variability is crucial. If one of the comparison stars is variable, the whole reduction process has to be remade relying on the constant comparison star only.

5.2.7.2 Airmass

In order to obtain an accurate extinction coefficient for one night, the observations should cover a sufficiently wide range of airmasses. Note that too high airmasses lower the accuracy. In most cases a wide airmass interval can be realized by observing several hours per night. But with the APT only airmasses below 2 (Strassmeier et al. 1997) are available in the northern hemisphere. In the case of EE Cam, most of the nights have airmass intervals ≤ 0.5 . As this reduces the accuracy of the extinction coefficient determination, a detailed inspection is crucial (see 5.3).

5.2.7.3 Time base

As the time base during one night is correlated with the accuracy of the extinction coefficient determination, the observation should be as long as possible. But there are several factors that can limit the time base, such as weather conditions, limited observing time on the telescope, observability of the star, etc. To get a good accuracy, the observation length should, in the present case, preferably be ≥ 4 hours per night. As one can see from Tables 5.3 and 5.4, only 38 % of the nights have observations for more than 4 hours. The fourth observing period was the best with a time base ≥ 4 hours for 48% of the nights.

5.3 Determination of the appropriate extinction coefficient

Atmospheric extinction is the reduction of radiation intensity due to scattering and, to a lower extent, absorption. The different sizes of the scattering bodies in the atmosphere lead to a change in the wavelength dependence of the scattering. Due to this wavelength dependence the v filter is much more sensitive to extinction than the y filter, because the mean extinction is higher at 410 nm (central wavelength of v filter) than at 550 nm (central wavelength of y filter).

As the atmosphere of the Earth is not constant during one night, the extinction varies. Even in clear nights the peak-to-peak variation of the extinction caused mainly by scattering ranges from 0.2 to 0.3 mag per unit airmass (Rufener 1986). To correct these effects, ground-based measurements have to be transformed to values that would have been obtained outside the Earth's atmosphere. This can be achieved by means of a Bouguer diagram: plotting magnitudes M_{obs} versus airmass X , there should be a linear correlation

between the data points of one night. A linear fit reveals the extinction coefficient k (slope) and the stellar brightness outside the atmosphere M_0 (intercept).

It is common to use one extinction coefficient per night. Sometimes, having few data points, a short observation or a small airmass interval, it is common to use the mean extinction coefficient of one night before and afterwards. The EE Cam data contain almost solely nights with very narrow airmass intervals and time bases ≤ 4 h per night.

It is not possible to know a priori whether the extinction coefficients k are really variable from night to night. The observed variations in k may be caused by instrumental effects or may depend on the short time base. Therefore several methods (A - D), described in the next subsections, were tested.

5.3.1 Individual extinction coefficients – Method A

The atmospheric extinction should constant during one observing night. Therefore, it is reasonable to use one constant extinction coefficient individually determined for each night (referred to as individual extinction coefficients). This is the common method for the extinction correction.

The calculated individual extinction coefficients for the EE Cam observations are given in Table A.1 (see Appendix).

5.3.2 Constant intersection points – Method B

Assuming a perfect set of data, the extinction coefficient should be vary from night to night (because of different atmospheric conditions). However, the brightness of the star outside the atmosphere, i.e. the intersection point of the Bouguer graph, should be constant. Since no data set is perfect, the intersection points may change slightly from night to night. It has to be examined whether this scatter stil permits an accurate extinction correction.

This method is applied according to the following steps.

- **Step 1:** The individual extinction coefficient can be determined by $M_{\text{obs}} = kX + M_0$, where M_{obs} denotes the observed magnitude, X the calculated airmass, k the extinction coefficient and M_0 the intersection point. The atmospheric extinction is characterized by a pair of an extinction coefficient and an intersection point for each night. The first step is to calculate the average of all intersection points of the first comparison star C1 in both filters. If two constant comparison stars were available, the same had to be done for C2.
- **Step 2:** The average intersection point is then subtracted from the observed magnitudes M_{obs} of C1 (and eventually C2). The result is denoted M_{diff} .
- **Step 3:** The outputs are data sets of C1 and C2 containing the calculated airmass X and M_{diff} . From these the extinction coefficient k_{new} can be derived by

$$k_{\text{new}} = \frac{\sum XM_{\text{diff}}}{\sum X^2}. \quad (5.4)$$

Having two constant comparison stars, the extinction coefficient is derived by calculating the mean value of k_{C1} and k_{C2} . The obtained extinction coefficients are listed in Table A.1 (see Appendix).

- **Step 4:** The extinction correction described in 3.7.3 can now be applied, where the value $k_{\text{new}}X$ is subtracted from the observed magnitudes M_{obs} of EE Cam, C1 and C2 in both filters.

5.3.3 Constant extinction coefficients – Method C

Since the observing length of the EE Cam data are rather short, it is not clear if individual extinction coefficients are the best choice. Therefore, an analysis with constant extinction coefficients was performed to check if these would yield better results. In one observing period the extinction coefficient should not change significantly, if the atmospheric conditions remain the same. One constant extinction coefficient was calculated for each observing period and each filter. For the determination of this coefficient the point weighted average of all extinction coefficients derived in 5.3.1, belonging to nights with more than 9 data points, was calculated. The derived coefficients are listed in Table A.1 (see Appendix).

5.3.4 Combination of constant and individual extinction coefficients – Method D

Normally, individual extinction coefficients are used. It is possible that a constant coefficient has to be used for a number of nights. This coefficient is usually the average of the coefficients derived for one night before and afterwards. But also average coefficients over the entire observing period can be used (see 5.3.3). Another possibility is to use extinction coefficients derived from other measurements. This is only possible if the measurements were taken during the same night as well as with the same instrument. In the case of EE Cam, some nights are shared with Gerald Handler, who observed other stars on the APT and whose measurements cover a longer time base.

According to Fig. 5.1, coefficients belonging to nights shorter than 4 hours tend to larger variations (0.342 ± 0.088) than coefficients belonging to longer nights (0.329 ± 0.049). Therefore, for nights ≤ 4 hours a constant extinction coefficient (derived in 5.3.3) was used to correct the EE Cam data for extinction. If a coefficient obtained from measurements of other stars in the same night was available and if the time base was ≥ 4 hours, this coefficient was used instead. A detailed list of the chosen coefficients is given in Table A.1 (see Appendix).

5.3.5 Further topics

5.3.5.1 Dependence of the extinction coefficient on dust

As the APT is located in the Sonoran desert, the measurements are possibly contaminated by dust effects. This dust descends in the atmosphere during the night and affects mainly

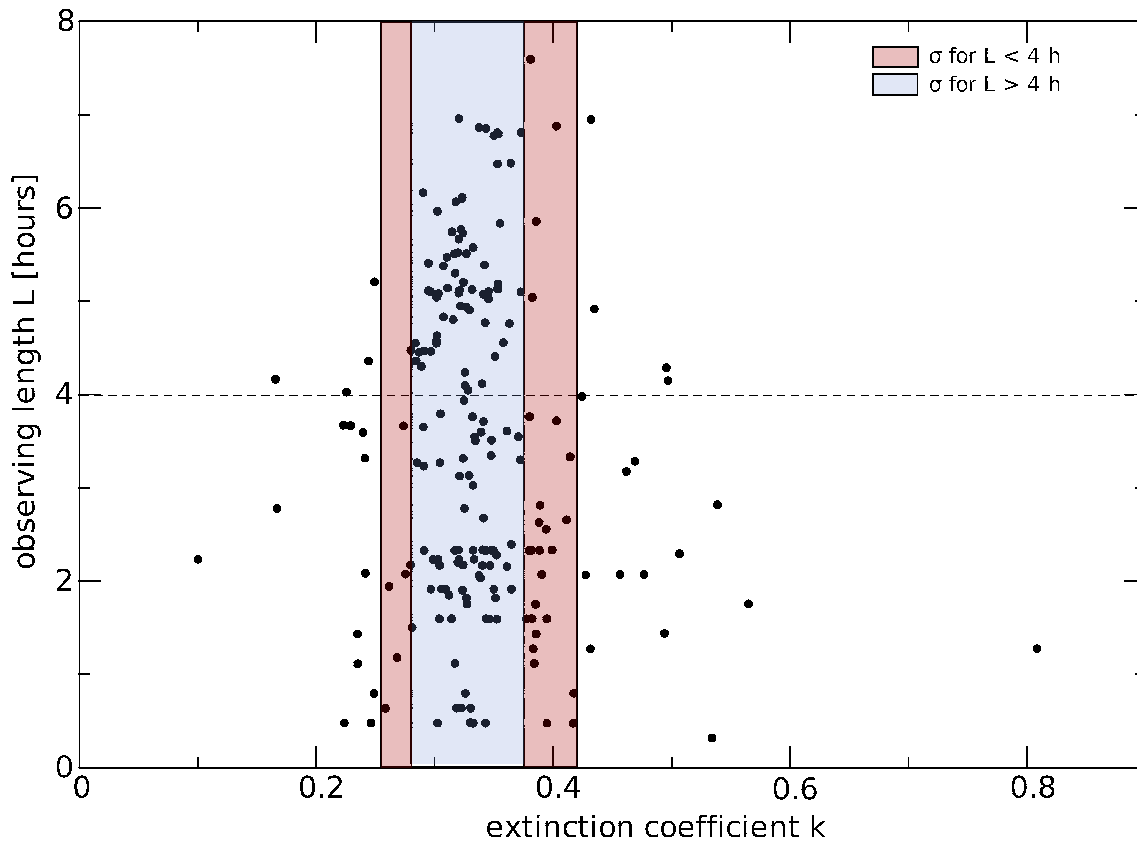


Figure 5.1: Determined extinction coefficients for EE Cam in v plotted versus length of the observations. The dots represent the individual coefficients obtained during all four observing periods. The black dashed line marks the limit of 4 hours. The red and blue boxes refer to the standard deviations of extinction coefficients for short and long nights, respectively.

the first hours of observation. This results in different extinction coefficients depending on the part of the night. To study the effects due to dust, observations covering several hours per night, especially including the beginning of the night, are required. Unfortunately, most of the EE Cam photometry was performed in the middle and towards the end of the night. Thus, only a few nights were useful for this investigation. In these nights, the extinction coefficients of ascending vs. descending stars do not show a significant trend, which is considered evidence against dust contamination. Given the low number of suitable nights, the responsibility of dust variations for the higher residuals (see Table 5.5) in the v filter cannot be confirmed.

5.3.5.2 Dependence of the extinction coefficient on seasons

The extinction coefficient may show seasonal changes due to weather conditions (e.g. temperature, humidity). In Fig. 5.2 the EE Cam data show a slight correlation between the seasons and the distribution of the extinction coefficients.

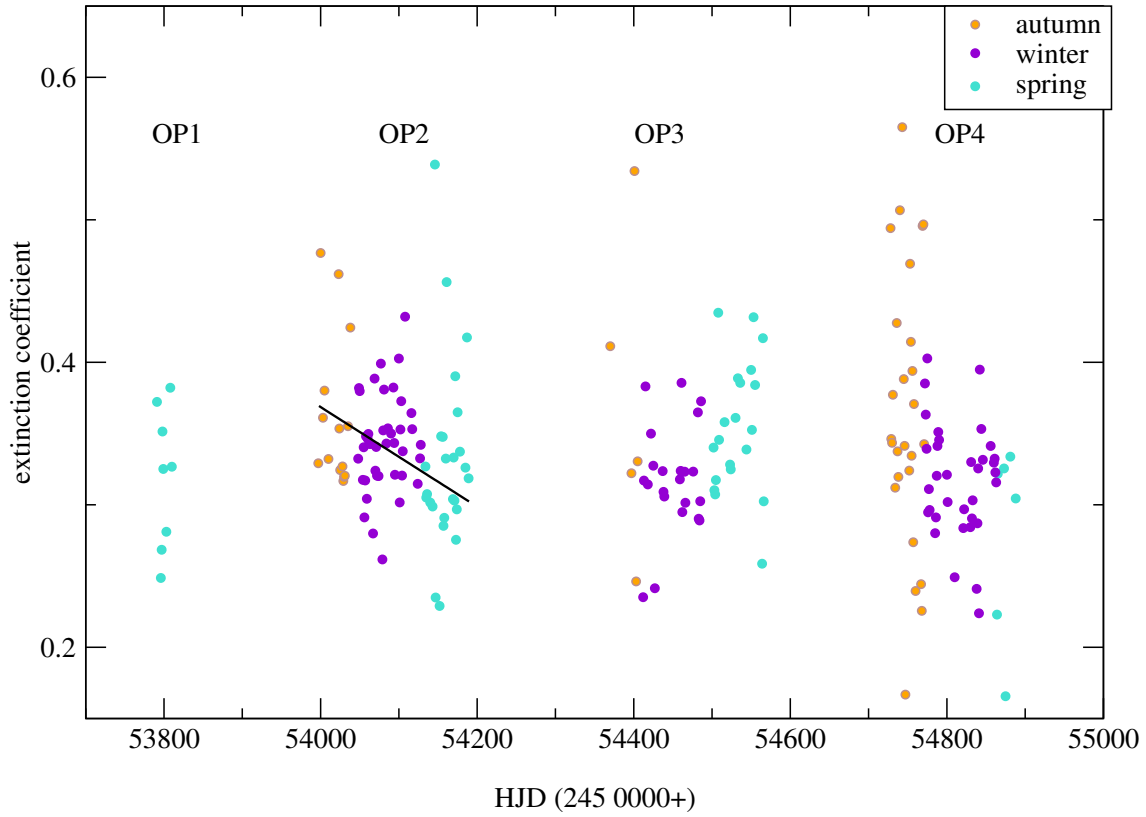


Figure 5.2: Dependence of the extinction coefficient on seasons. The color-coding refers to the derived extinction coefficients in v in spring, autumn and winter from 2006 to 2009. The black line displays the linear dependence of the coefficient in the second observing period.

5.4 Which extinction coefficient is correct?

The results from each method A – D obtained in 5.3 were used to check which extinction coefficients give the best results. Two independent tests were performed with Period04 and SigSpec respectively.

5.4.1 First test: Residual light curves of EE Cam

For each method A – D a frequency analysis was performed with Period04 using the data of OP1, OP2 and OP3 together. The resulting fit will be slightly different for these methods. By examining the residuals r_i with $i = 1, \dots, N$ between the measurements and the fit it is possible to decide which method works best, i.e., the method with the lowest average residuals r_{av} defined as

$$r_{av} = \sqrt{\frac{\sum r_i^2}{N}}, \quad (5.5)$$

according to the error propagation law. The average value of the observed residuals in both filters for all four methods is given in Table 5.5 and a list of all residuals in the y filter is provided in Table A.2 (see Appendix). The average values are higher than predicted by the photon statistics. Breger et al. (2007) state that this is due to unresolved frequencies. The power spectrum of the residuals (see Fig. 5.6) clearly shows an excess between 3 and 15 c/d that is likely to be caused by such unresolved frequencies.

One can see from Table 5.5 that the lowest average residuals are obtained when using Method D. To confirm this choice, another frequency analysis was carried out with the data of the fourth observing period (see Table 5.5). The average residuals are almost the same for all methods, Method D being slightly better. This confirms the results obtained for the first three observing periods.

A detailed frequency analysis was performed for the method that revealed the best rms residuals. Results are provided in 5.5.

Table 5.5: Average residuals determined for all four methods in both filters. The residuals were determined by performing a frequency analysis of the data obtained in the first, second and third observing period. A separate analysis was performed for the data of the fourth observing period.

| | Filter | Method A | Method B | Method C | Method D |
|--------------------------------|--------|----------|----------|----------|----------|
| Average Residuals [mag] | y | 5.641 | 5.493 | 5.343 | 5.115 |
| OP1, OP2, OP3 | v | 8.069 | 7.818 | 7.747 | 7.474 |
| Average Residuals [mag] | y | 5.482 | 5.501 | 5.496 | 5.488 |
| OP4 | v | 7.808 | 7.852 | 7.764 | 7.754 |

5.4.2 Second test: Cycle-per-day periodicities

The correct extinction correction for the constant comparison stars would produce a horizontal line in the time domain. An erroneous extinction correction can lead to cycle-per-day periodicities in the amplitude spectrum. Imagine a data set with an erroneous extinction correction. The light curves of the comparison stars will look like a sinusoidal bump in each night showing a peak at 1 c/d. Depending on the deviation of the used extinction coefficient from the "real" one, the bump in the light curve may be sharp enough to produce additional peaks at integer multiples of 1 c/d. Fig. 5.3 displays the data of one night of C1 without extinction correction (red dots). The star was observed for 5.6 hours. A frequency analysis yields a frequency of 3 c/d (black line). Calculating the significances of these cycle-per-day periodicities is a good test for the determination of the best extinction coefficient, the method with the lowest significances. The advantage of this method is that it works even in case of intrinsic variabilities if their frequencies are not too close to the cycle-per-day multiples considered here. Even in such a case the examination of these peaks provides reasonable information, if one relies on a reference method and examines the deviations in the spectra from the reference spectrum.

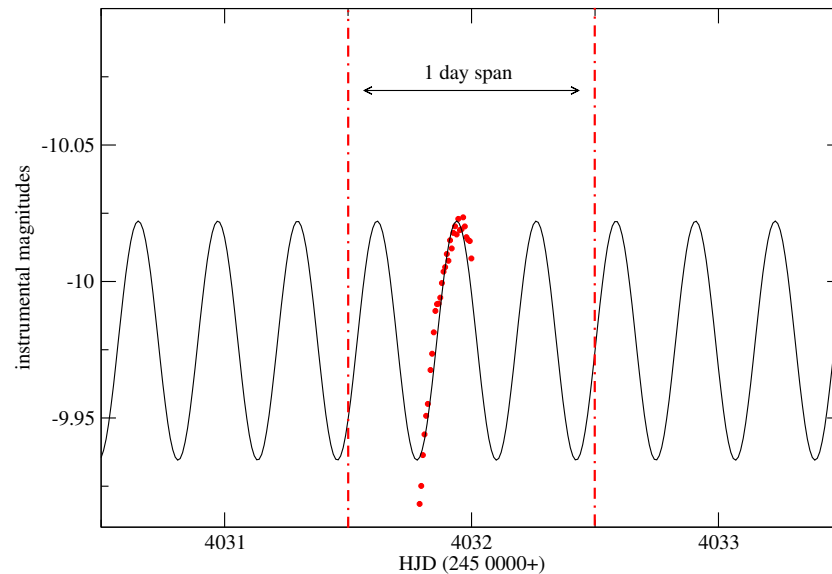


Figure 5.3: Observed data points (red dots) without extinction correction of C1 for one night. A frequency analysis yielded a 3 c/d periodicity (black curve). The red dashed-dotted lines mark the one day span.

Spectral significances of the 1 c/d aliases were calculated applying SigSpec to Methods A, B and C. The differential light curve $V - C1$ for each method was split into two sets: one containing the nights with a time base shorter than 4 hours and the other one containing the nights longer than 4 hours. Method D (individual as well as constant coefficients) was not used, because it corresponds to Method C (constant coefficients) in short and Method A (variable) in long nights and would therefore give the same results. The method with the lowest average significance can be considered as the best one. The resulting significances of Method A were subtracted from the significances of the other methods in order to provide a better comparison. Negative values denote a lower significance than in Method A (namely Method A is worse) and positive values denote a higher significance than in Method A (namely Method A is better). Fig. 5.4 shows the results obtained using the data of OP1, OP2 and OP3. Fig. 5.5 visualizes the results of OP4. Additionally, for the purpose of clarity, each graph contains a box showing the average value of the data plotted in the graph. The lowest average value indicates the best method.

The upper graph in Fig. 5.4 clearly shows that for long nights it is better to use individual extinction coefficients. The lower graph suggests to use constant extinction coefficients for short nights. In both graphs of Fig. 5.5 the average significance is almost the same for all methods. Period04 yielded exactly the same results. The circumstance that in the fourth observing period all methods are equal can be explained by the comparison stars: as in this observing period both comparison stars are constant and could be used to reduce the data, an improved accuracy in the determination of the extinction coefficient was achieved.

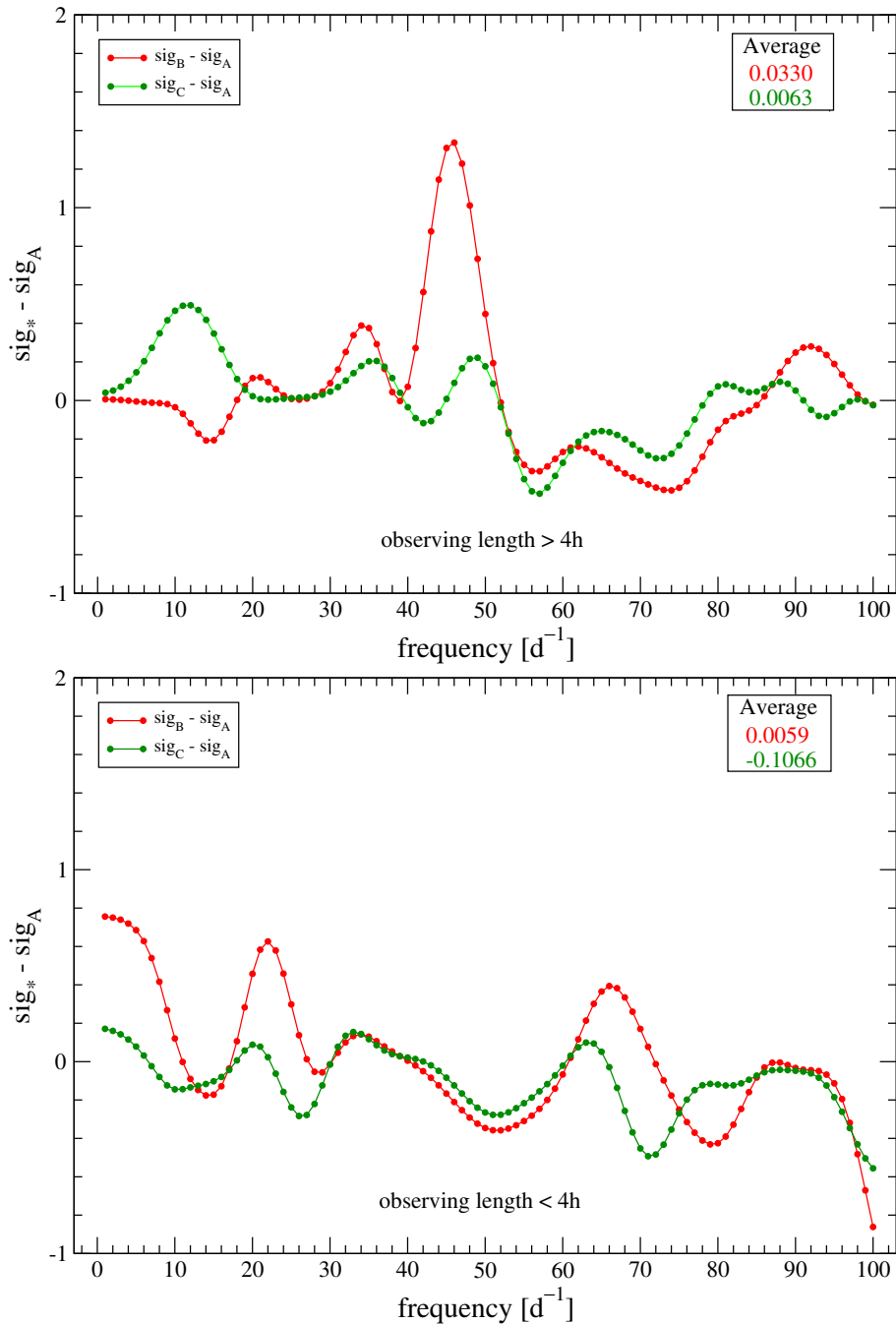


Figure 5.4: Upper graph: Comparison of Methods A, B and C for OP1, OP2 and OP3 using significances determined with a frequency spacing of 1 c/d and for nights with observations longer 4 hours. The significance of Method A was subtracted from the significances of Methods B and C. The average value is given in the right corner of each graph. The lower average value denotes the better method. Lower graph: same as upper graph but for nights with observations shorter 4 hours.

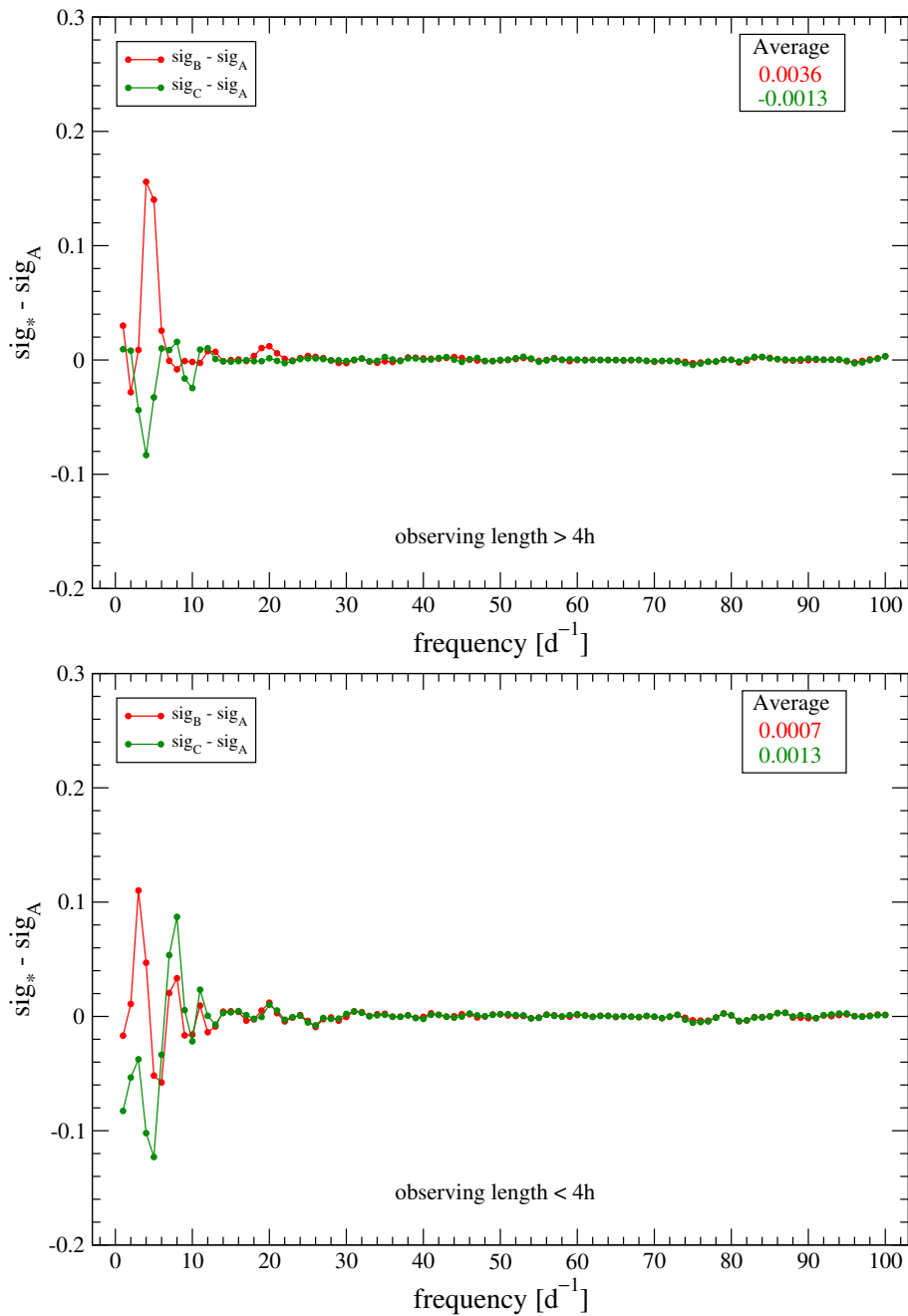


Figure 5.5: Upper graph: Comparison of Methods A, B and C for OP4 using significances determined with a frequency spacing of 1 c/d and for nights with observations longer 4 hours. The significance of Method A was subtracted from the significances of Methods B and C. The average value is given in the right corner of each graph. The lower average value denotes the better method. Lower graph: same as upper graph but for nights with observations shorter 4 hours.

5.5 Discussion

The aim of this work was to find the best extinction correction for the photometry of EE Cam by the Vienna APT. As can be seen in Tables 5.5 and Fig. 5.4, it is best to use both constant and individual extinction coefficients (Method D). A detailed frequency analysis was performed by combining the data obtained in the first, second and third observing period. The frequency analysis of the fourth observing period as well as an astrophysical interpretation of all observing periods are still outstanding, but are not subject of this work. Further investigation on the seasonal dependence of the extinction coefficients could be interesting. Instead of using a single, constant coefficient for a whole observing period, it may be considered a linear function of Julian Day Number, according to the linear regression in Fig. 5.2.

A frequency analysis was performed with Period04 as well as SigSpec. Only frequencies that are found by both computer programs were considered significant. Concerning Period04, the data have been checked for daily and annual aliasing (i.e. 1 c/d as well as 0.0027 c/d). Table 5.6 contains the significant³ frequencies, their signal-to-noise ratio obtained with Period04 and their significance obtained with SigSpec. The corresponding power spectra obtained with Period04 are displayed in Fig. 5.6. The excess power, visible as a bump in the 16-frequency solution, suggests that more frequencies are present, but yet below the detection limit.

Table 5.6: Detected frequencies of EE Cam in the y filter. The signal-to-noise ratio was calculated using ± 2 c/d frequency ranges. The error of the y filter amplitude is ± 0.0001 .

| ID | Frequency [c/d] | Detection S/N | sig | y filter Amplitude [mag] | Notes |
|-----|-----------------|---------------|--------|--------------------------|-------|
| F1 | 4.934 | 126.8 | 407.73 | 0.0363 | |
| F2 | 5.214 | 68.2 | 367.44 | 0.0201 | |
| F3 | 8.333 | 20.1 | 101.86 | 0.0072 | |
| F4 | 9.839 | 15.4 | 104.78 | 0.0058 | |
| F5 | 4.938 | 14.9 | 71.50 | 0.0043 | |
| F6 | 8.456 | 13.3 | 71.33 | 0.0047 | |
| F7 | 4.765 | 10.2 | 46.15 | 0.0029 | |
| F8 | 7.905 | 9.5 | 49.56 | 0.0033 | |
| F9 | 9.867 | 7.9 | 52.97 | 0.0030 | 2F1 |
| F10 | 10.147 | 7.7 | 53.93 | 0.0029 | F1+F2 |
| F11 | 8.266 | 7.2 | 36.18 | 0.0026 | |
| F12 | 9.476 | 7.0 | 45.04 | 0.0026 | |
| F13 | 7.666 | 6.4 | 32.86 | 0.0022 | |
| F14 | 8.512 | 5.8 | 29.37 | 0.0021 | |
| F15 | 6.204 | 5.7 | 28.42 | 0.0018 | |
| F16 | 10.318 | 4.0 | 24.32 | 0.0016 | |

³Detection limit signal-to-noise ratio ≥ 4 (Breger et al. 1993). This corresponds to a power signal-to-noise ratio of 12.6 (Horne & Baliunas 1986, Reegen 2007).

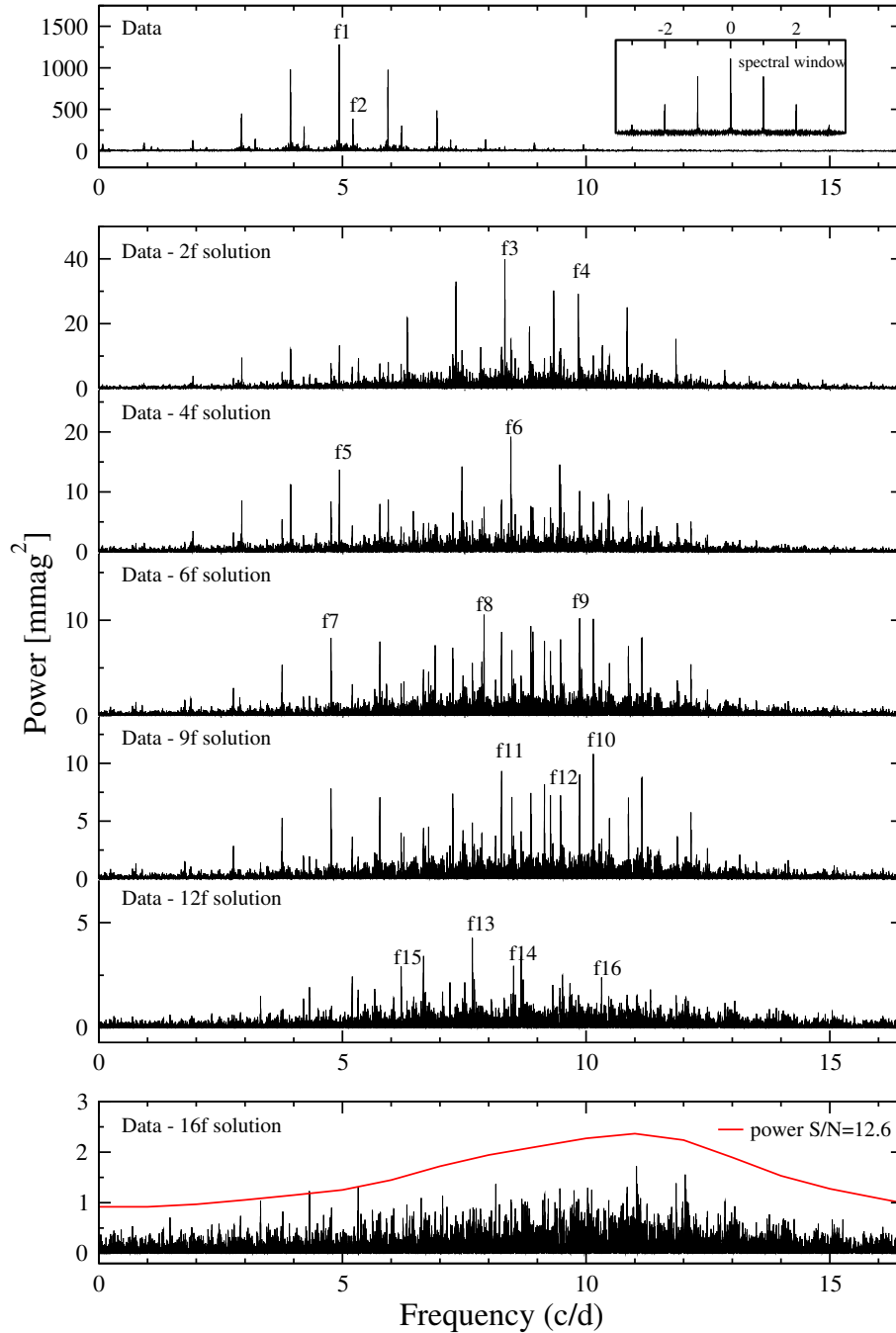


Figure 5.6: Top panel: power spectrum of EE Cam. Mid panels: after subtracting the first 2, 4, 6, 9 and 12 frequencies, respectively. The spectral window (small panel in top panel) clearly shows a 1 c/d aliasing pattern. Bottom panel: Residual spectrum after subtraction of 16 frequencies.

Appendix A

Appendix

A.1 Tables

A.1.1 Extinction coefficients

Table A.1: Determined extinction coefficients in mag per airmass in the v and y filter using different methods (A: individual k , B: constant intersection points, C: constant k , D: constant and individual k).

| HJD (245 0000+) | Methods | | | | | | | |
|--------------------|---------|-------|-------|-------|-------|-------|-------|-------|
| | A | | B | | C | | D | |
| | k_v | k_y | k_v | k_y | k_v | k_y | k_v | k_y |
| 3791.7 | 0.167 | 0.372 | 0.054 | 0.254 | 0.146 | 0.337 | 0.146 | 0.337 |
| 3796.7 | 0.100 | 0.249 | 0.083 | 0.304 | 0.146 | 0.337 | 0.146 | 0.337 |
| 3797.6 | 0.131 | 0.268 | 0.037 | 0.234 | 0.146 | 0.337 | 0.146 | 0.337 |
| 3798.7 | 0.124 | 0.351 | 0.044 | 0.237 | 0.146 | 0.337 | 0.146 | 0.337 |
| 3799.7 | 0.151 | 0.325 | 0.051 | 0.252 | 0.146 | 0.337 | 0.146 | 0.337 |
| 3803.7 | 0.079 | 0.281 | 0.074 | 0.261 | 0.146 | 0.337 | 0.146 | 0.337 |
| 3805.6 | 0.514 | 0.808 | 0.085 | 0.289 | 0.146 | 0.337 | 0.146 | 0.337 |
| 3808.7 | 0.182 | 0.382 | 0.047 | 0.246 | 0.146 | 0.337 | 0.146 | 0.337 |
| 3810.6 | 0.184 | 0.327 | 0.065 | 0.268 | 0.146 | 0.337 | 0.146 | 0.337 |
| 3998.0 | 0.136 | 0.329 | 0.126 | 0.320 | 0.151 | 0.343 | 0.140 | 0.343 |
| 4001.0 | 0.234 | 0.477 | 0.128 | 0.314 | 0.151 | 0.343 | 0.151 | 0.343 |
| 4003.9 | 0.163 | 0.361 | 0.146 | 0.342 | 0.151 | 0.343 | 0.133 | 0.343 |
| 4005.9 | 0.178 | 0.380 | 0.140 | 0.337 | 0.151 | 0.343 | 0.151 | 0.343 |
| 4010.9 | 0.140 | 0.332 | 0.174 | 0.388 | 0.151 | 0.343 | 0.151 | 0.343 |
| 4024.0 | 0.187 | 0.462 | 0.173 | 0.361 | 0.151 | 0.343 | 0.151 | 0.343 |
| 4024.9 | 0.158 | 0.354 | 0.159 | 0.344 | 0.151 | 0.343 | 0.158 | 0.354 |
| 4025.9 | 0.136 | 0.324 | 0.157 | 0.343 | 0.151 | 0.343 | 0.136 | 0.324 |
| 4028.9 | 0.137 | 0.327 | 0.160 | 0.347 | 0.151 | 0.343 | 0.137 | 0.327 |
| 4029.9 | 0.130 | 0.317 | 0.161 | 0.350 | 0.151 | 0.343 | 0.130 | 0.317 |
| 4030.9 | 0.136 | 0.320 | 0.166 | 0.357 | 0.151 | 0.343 | 0.136 | 0.320 |
| 4031.9 | 0.127 | 0.320 | 0.162 | 0.353 | 0.151 | 0.343 | 0.127 | 0.320 |

Continued on next page

Table A.1 – continued

| HJD (245 0000+) | Methods | | | | | | | |
|--------------------|---------|-------|-------|-------|-------|-------|-------|-------|
| | A | | B | | C | | D | |
| | k_v | k_y | k_v | k_y | k_v | k_y | k_v | k_y |
| 4035.9 | 0.154 | 0.355 | 0.173 | 0.364 | 0.151 | 0.343 | 0.154 | 0.355 |
| 4039.0 | 0.191 | 0.424 | 0.175 | 0.362 | 0.151 | 0.343 | 0.151 | 0.343 |
| 4048.8 | 0.154 | 0.332 | 0.178 | 0.364 | 0.151 | 0.343 | 0.151 | 0.343 |
| 4049.8 | 0.176 | 0.382 | 0.179 | 0.368 | 0.151 | 0.343 | 0.151 | 0.343 |
| 4050.8 | 0.179 | 0.380 | 0.189 | 0.379 | 0.151 | 0.343 | 0.151 | 0.343 |
| 4054.8 | 0.134 | 0.317 | 0.176 | 0.361 | 0.151 | 0.343 | 0.151 | 0.343 |
| 4055.8 | 0.146 | 0.340 | 0.179 | 0.368 | 0.151 | 0.343 | 0.151 | 0.343 |
| 4056.8 | 0.117 | 0.291 | 0.175 | 0.359 | 0.151 | 0.343 | 0.151 | 0.343 |
| 4057.8 | 0.134 | 0.317 | 0.179 | 0.367 | 0.151 | 0.343 | 0.151 | 0.343 |
| 4058.8 | 0.150 | 0.348 | 0.182 | 0.370 | 0.151 | 0.343 | 0.151 | 0.343 |
| 4059.8 | 0.131 | 0.304 | 0.187 | 0.376 | 0.151 | 0.343 | 0.151 | 0.343 |
| 4060.8 | 0.149 | 0.347 | 0.198 | 0.393 | 0.151 | 0.343 | 0.151 | 0.343 |
| 4061.8 | 0.147 | 0.350 | 0.199 | 0.393 | 0.151 | 0.343 | 0.151 | 0.343 |
| 4062.8 | 0.152 | 0.343 | 0.195 | 0.387 | 0.151 | 0.343 | 0.151 | 0.343 |
| 4064.8 | 0.144 | 0.343 | 0.195 | 0.387 | 0.151 | 0.343 | 0.151 | 0.343 |
| 4067.7 | 0.083 | 0.280 | 0.204 | 0.386 | 0.151 | 0.343 | 0.151 | 0.343 |
| 4069.7 | 0.198 | 0.389 | 0.221 | 0.409 | 0.151 | 0.343 | 0.151 | 0.343 |
| 4070.7 | 0.133 | 0.324 | 0.203 | 0.390 | 0.151 | 0.343 | 0.151 | 0.343 |
| 4071.7 | 0.152 | 0.341 | 0.199 | 0.385 | 0.151 | 0.343 | 0.151 | 0.343 |
| 4072.7 | 0.124 | 0.320 | 0.204 | 0.391 | 0.151 | 0.343 | 0.151 | 0.343 |
| 4074.7 | 0.129 | 0.320 | 0.132 | 0.319 | 0.151 | 0.343 | 0.151 | 0.343 |
| 4077.7 | 0.200 | 0.399 | 0.145 | 0.336 | 0.151 | 0.343 | 0.151 | 0.343 |
| 4079.7 | 0.105 | 0.262 | 0.143 | 0.334 | 0.151 | 0.343 | 0.151 | 0.343 |
| 4080.7 | 0.148 | 0.352 | 0.149 | 0.335 | 0.151 | 0.343 | 0.151 | 0.343 |
| 4081.8 | 0.175 | 0.381 | 0.151 | 0.340 | 0.151 | 0.343 | 0.175 | 0.381 |
| 4084.9 | 0.045 | 0.343 | 0.161 | 0.369 | 0.151 | 0.343 | 0.151 | 0.343 |
| 4086.8 | 0.156 | 0.354 | 0.185 | 0.414 | 0.151 | 0.343 | 0.156 | 0.354 |
| 4090.8 | 0.147 | 0.350 | 0.159 | 0.349 | 0.151 | 0.343 | 0.147 | 0.350 |
| 4093.7 | 0.183 | 0.382 | 0.157 | 0.331 | 0.151 | 0.343 | 0.183 | 0.382 |
| 4094.8 | 0.147 | 0.343 | 0.146 | 0.332 | 0.151 | 0.343 | 0.147 | 0.343 |
| 4095.7 | 0.129 | 0.321 | 0.143 | 0.338 | 0.151 | 0.343 | 0.151 | 0.343 |
| 4100.8 | 0.185 | 0.403 | 0.152 | 0.333 | 0.151 | 0.343 | 0.185 | 0.403 |
| 4101.7 | 0.116 | 0.302 | 0.147 | 0.358 | 0.151 | 0.343 | 0.116 | 0.302 |
| 4102.7 | 0.137 | 0.353 | 0.171 | 0.360 | 0.151 | 0.343 | 0.137 | 0.353 |
| 4103.7 | 0.156 | 0.373 | 0.172 | 0.329 | 0.151 | 0.343 | 0.156 | 0.373 |
| 4104.7 | 0.132 | 0.320 | 0.147 | 0.327 | 0.151 | 0.343 | 0.132 | 0.320 |
| 4105.7 | 0.136 | 0.338 | 0.145 | 0.377 | 0.151 | 0.343 | 0.136 | 0.338 |
| 4108.7 | 0.230 | 0.432 | 0.193 | 0.349 | 0.151 | 0.343 | 0.230 | 0.432 |
| 4116.7 | 0.158 | 0.364 | 0.162 | 0.361 | 0.151 | 0.343 | 0.158 | 0.364 |
| 4117.7 | 0.150 | 0.353 | 0.172 | 0.354 | 0.151 | 0.343 | 0.150 | 0.353 |
| 4124.7 | 0.129 | 0.315 | 0.170 | 0.361 | 0.151 | 0.343 | 0.129 | 0.315 |
| 4127.7 | 0.146 | 0.333 | 0.173 | 0.353 | 0.151 | 0.343 | 0.146 | 0.333 |

Continued on next page

Table A.1 – continued

| HJD (245 0000+) | Methods | | | | | | | |
|--------------------|---------|-------|-------|-------|-------|-------|-------|-------|
| | A | | B | | C | | D | |
| | k_v | k_y | k_v | k_y | k_v | k_y | k_v | k_y |
| 4128.7 | 0.178 | 0.342 | 0.169 | 0.356 | 0.151 | 0.343 | 0.178 | 0.342 |
| 4134.7 | 0.156 | 0.327 | 0.173 | 0.346 | 0.151 | 0.343 | 0.156 | 0.327 |
| 4135.7 | 0.139 | 0.305 | 0.164 | 0.342 | 0.151 | 0.343 | 0.151 | 0.343 |
| 4136.7 | 0.132 | 0.308 | 0.157 | 0.362 | 0.151 | 0.343 | 0.132 | 0.308 |
| 4140.7 | 0.150 | 0.302 | 0.171 | 0.375 | 0.151 | 0.343 | 0.150 | 0.302 |
| 4143.7 | 0.121 | 0.299 | 0.183 | 0.349 | 0.151 | 0.343 | 0.151 | 0.343 |
| 4146.7 | 0.269 | 0.539 | 0.145 | 0.321 | 0.151 | 0.343 | 0.151 | 0.343 |
| 4147.7 | 0.092 | 0.235 | 0.129 | 0.315 | 0.151 | 0.343 | 0.151 | 0.343 |
| 4152.7 | 0.050 | 0.229 | 0.130 | 0.316 | 0.151 | 0.343 | 0.151 | 0.343 |
| 4153.6 | 0.025 | 0.100 | 0.126 | 0.306 | 0.151 | 0.343 | 0.151 | 0.343 |
| 4154.7 | 0.170 | 0.348 | 0.118 | 0.316 | 0.151 | 0.343 | 0.151 | 0.343 |
| 4156.7 | 0.179 | 0.348 | 0.128 | 0.309 | 0.151 | 0.343 | 0.151 | 0.343 |
| 4157.7 | 0.123 | 0.285 | 0.121 | 0.313 | 0.151 | 0.343 | 0.151 | 0.343 |
| 4158.7 | 0.116 | 0.291 | 0.125 | 0.317 | 0.151 | 0.343 | 0.151 | 0.343 |
| 4160.7 | 0.172 | 0.332 | 0.132 | 0.326 | 0.151 | 0.343 | 0.151 | 0.343 |
| 4161.7 | 0.314 | 0.456 | 0.139 | 0.351 | 0.151 | 0.343 | 0.151 | 0.343 |
| 4169.7 | 0.148 | 0.304 | 0.157 | 0.358 | 0.151 | 0.343 | 0.151 | 0.343 |
| 4170.7 | 0.126 | 0.333 | 0.162 | 0.346 | 0.151 | 0.343 | 0.151 | 0.343 |
| 4171.7 | 0.125 | 0.303 | 0.156 | 0.347 | 0.151 | 0.343 | 0.151 | 0.343 |
| 4172.6 | 0.190 | 0.390 | 0.153 | 0.341 | 0.151 | 0.343 | 0.151 | 0.343 |
| 4173.6 | 0.103 | 0.275 | 0.152 | 0.333 | 0.151 | 0.343 | 0.151 | 0.343 |
| 4174.6 | 0.142 | 0.297 | 0.144 | 0.336 | 0.151 | 0.343 | 0.151 | 0.343 |
| 4175.6 | 0.183 | 0.365 | 0.146 | 0.365 | 0.151 | 0.343 | 0.151 | 0.343 |
| 4185.6 | 0.161 | 0.326 | 0.206 | 0.422 | 0.151 | 0.343 | 0.151 | 0.343 |
| 4187.6 | 0.264 | 0.417 | 0.174 | 0.371 | 0.151 | 0.343 | 0.151 | 0.343 |
| 4189.6 | 0.111 | 0.319 | 0.194 | 0.381 | 0.151 | 0.343 | 0.151 | 0.343 |
| 4370.9 | 0.194 | 0.411 | 0.109 | 0.313 | 0.148 | 0.333 | 0.148 | 0.333 |
| 4397.9 | 0.127 | 0.322 | 0.103 | 0.298 | 0.148 | 0.333 | 0.127 | 0.322 |
| 4402.0 | 0.012 | 0.534 | 0.127 | 0.324 | – | 0.333 | 0.148 | 0.333 |
| 4404.0 | 0.027 | 0.246 | 0.127 | 0.324 | 0.148 | 0.333 | 0.143 | 0.334 |
| 4406.0 | 0.090 | 0.330 | 0.115 | 0.309 | 0.148 | 0.333 | 0.130 | 0.317 |
| 4413.0 | 0.061 | 0.235 | 0.143 | 0.352 | 0.148 | 0.333 | 0.148 | 0.333 |
| 4414.0 | 0.123 | 0.317 | 0.141 | 0.347 | 0.148 | 0.333 | 0.148 | 0.333 |
| 4416.0 | 0.160 | 0.383 | 0.128 | 0.323 | 0.148 | 0.333 | 0.136 | 0.319 |
| 4419.0 | 0.109 | 0.314 | 0.128 | 0.321 | 0.148 | 0.333 | 0.148 | 0.333 |
| 4423.0 | 0.138 | 0.350 | 0.137 | 0.332 | 0.148 | 0.333 | 0.132 | 0.315 |
| 4426.0 | 0.144 | 0.327 | 0.143 | 0.341 | 0.148 | 0.333 | 0.148 | 0.333 |
| 4428.0 | 0.077 | 0.241 | 0.147 | 0.341 | 0.148 | 0.333 | 0.175 | 0.370 |
| 4438.0 | 0.126 | 0.324 | 0.132 | 0.322 | 0.148 | 0.333 | 0.130 | 0.315 |
| 4439.0 | 0.138 | 0.309 | 0.128 | 0.319 | 0.148 | 0.333 | 0.121 | 0.307 |
| 4440.0 | 0.118 | 0.306 | 0.130 | 0.319 | 0.148 | 0.333 | 0.124 | 0.306 |
| 4459.8 | 0.152 | 0.318 | 0.157 | 0.341 | 0.148 | 0.333 | 0.152 | 0.318 |

Continued on next page

Table A.1 – continued

| HJD (245 0000+) | Methods | | | | | | | |
|--------------------|---------|-------|-------|-------|-------|-------|-------|-------|
| | A | | B | | C | | D | |
| | k_v | k_y | k_v | k_y | k_v | k_y | k_v | k_y |
| 4460.8 | 0.111 | 0.324 | 0.165 | 0.352 | 0.148 | 0.333 | 0.111 | 0.324 |
| 4461.8 | 0.210 | 0.386 | 0.178 | 0.365 | 0.148 | 0.333 | 0.210 | 0.386 |
| 4462.8 | 0.117 | 0.295 | 0.168 | 0.346 | 0.148 | 0.333 | 0.117 | 0.295 |
| 4465.8 | 0.138 | 0.323 | 0.164 | 0.348 | 0.148 | 0.333 | 0.138 | 0.323 |
| 4466.8 | 0.125 | 0.301 | 0.166 | 0.354 | 0.148 | 0.333 | 0.125 | 0.301 |
| 4476.8 | 0.136 | 0.323 | 0.162 | 0.346 | 0.148 | 0.333 | 0.136 | 0.323 |
| 4482.7 | 0.175 | 0.365 | 0.201 | 0.392 | 0.148 | 0.333 | 0.148 | 0.333 |
| 4483.8 | 0.117 | 0.290 | 0.200 | 0.391 | 0.148 | 0.333 | 0.117 | 0.290 |
| 4484.7 | 0.111 | 0.289 | 0.203 | 0.400 | 0.148 | 0.333 | 0.111 | 0.289 |
| 4485.7 | 0.126 | 0.303 | 0.106 | 0.293 | 0.148 | 0.333 | 0.126 | 0.303 |
| 4486.7 | 0.206 | 0.373 | 0.113 | 0.305 | 0.148 | 0.333 | 0.206 | 0.373 |
| 4502.7 | 0.187 | 0.340 | 0.109 | 0.296 | 0.148 | 0.333 | 0.187 | 0.340 |
| 4503.7 | 0.133 | 0.310 | 0.100 | 0.285 | 0.148 | 0.333 | 0.133 | 0.310 |
| 4504.7 | 0.132 | 0.307 | 0.097 | 0.281 | 0.148 | 0.333 | 0.132 | 0.307 |
| 4505.7 | 0.134 | 0.317 | 0.096 | 0.283 | 0.148 | 0.333 | 0.134 | 0.317 |
| 4508.7 | 0.231 | 0.435 | 0.111 | 0.296 | 0.148 | 0.333 | 0.231 | 0.435 |
| 4509.7 | 0.159 | 0.346 | 0.108 | 0.293 | 0.148 | 0.333 | 0.159 | 0.346 |
| 4516.7 | 0.164 | 0.358 | 0.109 | 0.298 | 0.148 | 0.333 | 0.164 | 0.358 |
| 4523.7 | 0.144 | 0.328 | 0.105 | 0.295 | 0.148 | 0.333 | 0.144 | 0.328 |
| 4524.7 | 0.134 | 0.325 | 0.107 | 0.297 | 0.148 | 0.333 | 0.148 | 0.333 |
| 4530.7 | 0.143 | 0.361 | 0.120 | 0.312 | 0.148 | 0.333 | 0.148 | 0.333 |
| 4533.7 | 0.214 | 0.389 | 0.132 | 0.322 | 0.148 | 0.333 | 0.148 | 0.333 |
| 4536.7 | 0.165 | 0.386 | 0.146 | 0.344 | 0.148 | 0.333 | 0.148 | 0.333 |
| 4544.7 | 0.136 | 0.339 | 0.142 | 0.336 | 0.148 | 0.333 | 0.148 | 0.333 |
| 4550.7 | 0.173 | 0.395 | 0.180 | 0.385 | 0.148 | 0.333 | 0.148 | 0.333 |
| 4551.7 | 0.150 | 0.353 | 0.165 | 0.365 | 0.148 | 0.333 | 0.148 | 0.333 |
| 4553.7 | 0.223 | 0.432 | 0.162 | 0.360 | 0.148 | 0.333 | 0.148 | 0.333 |
| 4555.7 | 0.170 | 0.384 | 0.161 | 0.356 | 0.148 | 0.333 | 0.148 | 0.333 |
| 4564.6 | 0.152 | 0.259 | 0.190 | 0.384 | 0.148 | 0.333 | 0.148 | 0.333 |
| 4565.6 | 0.248 | 0.417 | 0.220 | 0.419 | 0.148 | 0.333 | – | 0.333 |
| 4566.6 | 0.201 | 0.302 | 0.223 | 0.418 | 0.148 | 0.333 | – | 0.333 |
| 4728.9 | 0.236 | 0.494 | 0.123 | 0.325 | 0.140 | 0.328 | 0.140 | 0.328 |
| 4729.9 | 0.206 | 0.346 | 0.136 | 0.343 | 0.140 | 0.328 | 0.140 | 0.328 |
| 4730.9 | 0.142 | 0.344 | 0.125 | 0.329 | 0.140 | 0.328 | 0.140 | 0.328 |
| 4731.9 | 0.146 | 0.377 | 0.123 | 0.323 | 0.140 | 0.328 | 0.140 | 0.328 |
| 4734.9 | 0.123 | 0.312 | 0.147 | 0.358 | 0.140 | 0.328 | 0.140 | 0.328 |
| 4736.9 | 0.190 | 0.428 | 0.133 | 0.338 | 0.140 | 0.328 | 0.140 | 0.328 |
| 4737.9 | 0.142 | 0.337 | 0.156 | 0.372 | 0.140 | 0.328 | 0.140 | 0.328 |
| 4738.9 | 0.128 | 0.320 | 0.182 | 0.419 | 0.140 | 0.328 | 0.140 | 0.328 |
| 4740.9 | 0.252 | 0.507 | 0.226 | 0.485 | 0.140 | 0.328 | 0.140 | 0.328 |
| 4743.9 | 0.278 | 0.565 | 0.124 | 0.316 | 0.140 | 0.328 | 0.140 | 0.328 |
| 4745.9 | 0.189 | 0.388 | 0.127 | 0.314 | 0.140 | 0.328 | 0.140 | 0.328 |

Continued on next page

Table A.1 – continued

| HJD (245 0000+) | Methods | | | | | | | |
|--------------------|---------|-------|-------|-------|-------|-------|-------|-------|
| | A | | B | | C | | D | |
| | k_v | k_y | k_v | k_y | k_v | k_y | k_v | k_y |
| 4746.9 | 0.175 | 0.341 | 0.129 | 0.319 | 0.140 | 0.328 | 0.140 | 0.328 |
| 4747.9 | 0.034 | 0.167 | 0.124 | 0.316 | 0.140 | 0.328 | 0.140 | 0.328 |
| 4752.9 | 0.108 | 0.324 | 0.141 | 0.335 | 0.140 | 0.328 | 0.140 | 0.328 |
| 4753.9 | 0.248 | 0.469 | 0.141 | 0.338 | 0.140 | 0.328 | 0.140 | 0.328 |
| 4754.9 | 0.195 | 0.414 | 0.132 | 0.327 | 0.140 | 0.328 | 0.140 | 0.328 |
| 4755.9 | 0.154 | 0.334 | 0.125 | 0.314 | 0.140 | 0.328 | 0.140 | 0.328 |
| 4756.9 | 0.133 | 0.394 | 0.125 | 0.317 | 0.140 | 0.328 | 0.140 | 0.328 |
| 4757.9 | 0.110 | 0.274 | 0.128 | 0.322 | 0.140 | 0.328 | 0.140 | 0.328 |
| 4758.9 | 0.177 | 0.371 | 0.132 | 0.325 | 0.140 | 0.328 | 0.140 | 0.328 |
| 4760.9 | 0.091 | 0.239 | 0.136 | 0.333 | 0.140 | 0.328 | 0.140 | 0.328 |
| 4767.8 | 0.081 | 0.244 | 0.163 | 0.363 | 0.140 | 0.328 | 0.081 | 0.244 |
| 4768.8 | 0.091 | 0.226 | 0.161 | 0.361 | 0.140 | 0.328 | 0.091 | 0.226 |
| 4769.9 | 0.257 | 0.496 | 0.193 | 0.408 | 0.140 | 0.328 | 0.257 | 0.496 |
| 4770.8 | 0.255 | 0.497 | 0.190 | 0.407 | 0.140 | 0.328 | 0.255 | 0.497 |
| 4771.8 | 0.131 | 0.343 | 0.166 | 0.370 | 0.140 | 0.328 | 0.131 | 0.343 |
| 4772.8 | 0.190 | 0.385 | 0.166 | 0.368 | 0.140 | 0.328 | 0.140 | 0.328 |
| 4773.8 | 0.186 | 0.363 | 0.142 | 0.332 | 0.140 | 0.328 | 0.186 | 0.363 |
| 4774.8 | 0.143 | 0.339 | 0.157 | 0.352 | 0.140 | 0.328 | 0.140 | 0.328 |
| 4775.8 | 0.199 | 0.403 | 0.149 | 0.336 | 0.140 | 0.328 | 0.140 | 0.328 |
| 4776.8 | 0.101 | 0.295 | 0.142 | 0.328 | 0.140 | 0.328 | 0.101 | 0.295 |
| 4777.8 | 0.132 | 0.311 | 0.135 | 0.320 | 0.140 | 0.328 | 0.132 | 0.311 |
| 4778.8 | 0.117 | 0.296 | 0.140 | 0.328 | 0.140 | 0.328 | 0.117 | 0.296 |
| 4785.8 | 0.132 | 0.280 | 0.155 | 0.348 | 0.140 | 0.328 | 0.132 | 0.280 |
| 4786.8 | 0.109 | 0.291 | 0.157 | 0.344 | 0.140 | 0.328 | 0.109 | 0.291 |
| 4787.8 | 0.127 | 0.320 | 0.167 | 0.358 | 0.140 | 0.328 | 0.127 | 0.320 |
| 4788.8 | 0.148 | 0.341 | 0.155 | 0.345 | 0.140 | 0.328 | 0.140 | 0.328 |
| 4789.8 | 0.149 | 0.351 | 0.169 | 0.362 | 0.140 | 0.328 | 0.149 | 0.351 |
| 4790.8 | 0.142 | 0.346 | 0.167 | 0.360 | 0.140 | 0.328 | 0.142 | 0.346 |
| 4800.8 | 0.139 | 0.321 | 0.110 | 0.289 | 0.140 | 0.328 | 0.139 | 0.321 |
| 4801.8 | 0.109 | 0.302 | 0.107 | 0.288 | 0.140 | 0.328 | 0.109 | 0.302 |
| 4810.7 | 0.098 | 0.249 | 0.129 | 0.306 | 0.140 | 0.328 | 0.098 | 0.249 |
| 4821.7 | 0.089 | 0.284 | 0.114 | 0.297 | 0.140 | 0.328 | 0.089 | 0.284 |
| 4822.7 | 0.123 | 0.297 | 0.113 | 0.295 | 0.140 | 0.328 | 0.123 | 0.297 |
| 4830.7 | 0.122 | 0.284 | 0.121 | 0.303 | 0.140 | 0.328 | 0.122 | 0.284 |
| 4831.7 | 0.139 | 0.330 | 0.121 | 0.305 | 0.140 | 0.328 | 0.140 | 0.328 |
| 4832.7 | 0.122 | 0.290 | 0.128 | 0.308 | 0.140 | 0.328 | 0.140 | 0.328 |
| 4833.7 | 0.114 | 0.303 | 0.129 | 0.311 | 0.140 | 0.328 | 0.114 | 0.303 |
| 4838.7 | 0.033 | 0.241 | 0.122 | 0.301 | 0.140 | 0.328 | 0.140 | 0.328 |
| 4839.7 | 0.133 | 0.287 | 0.117 | 0.297 | 0.140 | 0.328 | 0.133 | 0.287 |
| 4840.6 | 0.134 | 0.326 | 0.120 | 0.300 | 0.140 | 0.328 | 0.134 | 0.326 |
| 4841.6 | 0.057 | 0.224 | 0.135 | 0.319 | 0.140 | 0.328 | 0.140 | 0.328 |
| 4842.6 | 0.180 | 0.395 | 0.133 | 0.315 | 0.140 | 0.328 | 0.140 | 0.328 |

Continued on next page

Table A.1 – continued

| HJD (245 0000+) | Methods | | | | | | | |
|--------------------|---------|-------|-------|-------|-------|-------|-------|-------|
| | A | | B | | C | | D | |
| | k_v | k_y | k_v | k_y | k_v | k_y | k_v | k_y |
| 4844.6 | 0.162 | 0.353 | 0.133 | 0.312 | 0.140 | 0.328 | 0.162 | 0.353 |
| 4846.6 | 0.136 | 0.332 | 0.134 | 0.316 | 0.140 | 0.328 | 0.136 | 0.332 |
| 4856.6 | 0.148 | 0.341 | 0.133 | 0.315 | 0.140 | 0.328 | 0.148 | 0.341 |
| 4860.6 | 0.148 | 0.330 | 0.144 | 0.329 | 0.140 | 0.328 | 0.148 | 0.330 |
| 4861.6 | 0.117 | 0.332 | 0.151 | 0.339 | 0.140 | 0.328 | 0.140 | 0.328 |
| 4862.6 | 0.160 | 0.323 | 0.161 | 0.353 | 0.140 | 0.328 | 0.140 | 0.328 |
| 4863.6 | 0.138 | 0.316 | 0.168 | 0.360 | 0.140 | 0.328 | 0.138 | 0.316 |
| 4864.6 | 0.046 | 0.223 | 0.154 | 0.340 | 0.140 | 0.328 | 0.140 | 0.328 |
| 4865.6 | 0.131 | 0.322 | 0.148 | 0.331 | 0.140 | 0.328 | 0.131 | 0.322 |
| 4873.6 | 0.143 | 0.325 | 0.138 | 0.316 | 0.140 | 0.328 | 0.143 | 0.325 |
| 4875.6 | 0.083 | 0.166 | 0.158 | 0.343 | 0.140 | 0.328 | 0.083 | 0.166 |
| 4881.6 | 0.135 | 0.334 | 0.179 | 0.370 | 0.140 | 0.328 | 0.140 | 0.328 |
| 4888.6 | 0.120 | 0.304 | 0.148 | 0.330 | 0.140 | 0.328 | 0.140 | 0.328 |

A.1.2 Observed residuals

Table A.2: Observed residuals in mag between measurements and multisine fit for the first, second and third observing period in the y filter.

| HJD (245 000)+ | Methods | | | | Notes |
|-------------------|---------|-------|-------|-------|-------|
| | A | B | C | D | |
| 3792 | 5.970 | 5.711 | 5.885 | 5.848 | |
| 3797 | 4.724 | 5.588 | 3.965 | 3.466 | |
| 3798 | 4.511 | 5.617 | 4.312 | 4.220 | |
| 3799 | 4.048 | 4.396 | 4.362 | 4.040 | |
| 3800 | 4.913 | 4.294 | 5.312 | 5.119 | |
| 3804 | 4.085 | 4.453 | 3.200 | 3.606 | |
| 3806 | 6.993 | 4.099 | 3.727 | 3.580 | |
| 3809 | 7.106 | 6.286 | 6.795 | 6.254 | |
| 3811 | 6.867 | 8.839 | 7.932 | 7.003 | |
| 3998 | 4.210 | 4.248 | 4.612 | 4.324 | |
| 4001 | 5.305 | 3.856 | 4.444 | 4.279 | |
| 4004 | 5.068 | 5.054 | 4.852 | 5.113 | |
| 4006 | 4.925 | 5.196 | 5.121 | 5.026 | |
| 4011 | 8.355 | 8.370 | 6.885 | 6.660 | |
| 4024 | 5.948 | 6.077 | 5.731 | 6.266 | |
| 4025 | 3.563 | 3.420 | 3.533 | 3.224 | |
| 4026 | 5.275 | 5.136 | 5.181 | 5.348 | |
| 4029 | 7.780 | 7.789 | 7.802 | 6.781 | |
| 4030 | 4.570 | 4.487 | 4.458 | 4.126 | |
| 4031 | 4.001 | 4.378 | 4.019 | 4.157 | |
| 4032 | 7.846 | 7.592 | 7.659 | 7.808 | |

Continued on next page

Table A.2 – continued

| HJD (245 000)+ | Methods | | | | Notes |
|-------------------|---------|-------|-------|-------|-------|
| | A | B | C | D | |
| 4036 | 5.563 | 5.344 | 5.541 | 5.473 | |
| 4039 | 5.498 | 5.688 | 3.001 | 2.924 | |
| 4049 | 4.192 | 4.250 | 3.200 | 3.043 | |
| 4050 | 6.749 | 6.912 | 6.788 | 6.470 | |
| 4051 | 8.382 | 8.102 | 7.923 | 6.744 | |
| 4055 | 4.983 | 4.964 | 4.642 | 4.816 | |
| 4056 | 5.097 | 5.067 | 5.126 | 5.266 | |
| 4057 | 4.171 | 4.935 | 4.651 | 4.699 | |
| 4058 | 4.497 | 4.253 | 3.934 | 4.253 | |
| 4059 | 4.589 | 4.647 | 3.654 | 4.361 | |
| 4060 | 3.852 | 4.816 | 4.212 | 4.174 | |
| 4061 | 3.436 | 4.518 | 3.638 | 3.701 | |
| 4062 | 6.606 | 5.798 | 6.754 | 6.520 | |
| 4063 | 6.623 | 6.640 | 6.008 | 4.392 | |
| 4065 | 4.844 | 4.230 | 4.618 | 4.790 | |
| 4068 | 4.522 | 4.157 | 3.794 | 4.161 | |
| 4070 | 8.512 | 9.313 | 7.597 | 7.741 | |
| 4071 | 4.403 | 4.978 | 3.689 | 4.539 | |
| 4072 | 5.491 | 5.340 | 5.524 | 3.912 | |
| 4073 | 3.246 | 4.571 | 3.800 | 3.670 | |
| 4075 | 3.695 | 3.794 | 3.516 | 3.349 | |
| 4078 | 3.435 | 3.129 | 3.001 | 3.070 | |
| 4080 | 6.039 | 5.553 | 5.501 | 5.399 | |
| 4081 | 5.778 | 2.605 | 2.545 | 2.700 | |
| 4082 | 5.046 | 5.047 | 5.012 | 5.112 | |
| 4085 | 8.700 | 5.512 | 5.831 | 2.024 | |
| 4087 | 6.886 | 6.777 | 6.885 | 6.691 | |
| 4091 | 5.490 | 5.353 | 5.174 | 5.310 | |
| 4094 | 5.008 | 4.961 | 5.371 | 5.019 | |
| 4095 | 4.759 | 4.742 | 3.937 | 4.712 | |
| 4096 | 4.926 | 4.979 | 5.102 | 4.845 | |
| 4101 | 5.071 | 4.863 | 4.854 | 4.939 | |
| 4102 | 5.348 | 5.485 | 5.808 | 5.438 | |
| 4103 | 5.521 | 5.542 | 5.549 | 5.522 | |
| 4104 | 4.697 | 4.792 | 4.033 | 4.683 | |
| 4105 | 4.288 | 4.311 | 4.405 | 4.236 | |
| 4106 | 4.971 | 5.011 | 5.099 | 5.115 | |
| 4109 | 5.893 | 5.738 | 5.773 | 6.043 | |
| 4117 | 5.515 | 5.540 | 5.529 | 5.313 | |
| 4118 | 4.391 | 4.599 | 4.517 | 4.597 | |
| 4125 | 5.961 | 6.054 | 6.250 | 6.057 | |
| 4128 | 3.409 | 3.183 | 3.540 | 3.396 | |
| 4129 | 6.226 | 6.277 | 6.574 | 6.267 | |

Continued on next page

Table A.2 – continued

| HJD (245 000)+ | Methods | | | | Notes |
|-------------------|---------|-------|-------|-------|----------------------|
| | A | B | C | D | |
| 4135 | 4.607 | 4.161 | 4.453 | 3.917 | |
| 4136 | 4.029 | 4.384 | 4.211 | 4.233 | |
| 4137 | 5.205 | 5.444 | 5.566 | 4.390 | |
| 4141 | 7.909 | 8.074 | 7.971 | 7.931 | |
| 4144 | 3.989 | 3.777 | 3.863 | 3.758 | |
| 4147 | 5.042 | 4.606 | 4.712 | 4.642 | |
| 4148 | 6.975 | 6.141 | 5.945 | 5.898 | |
| 4153 | 5.504 | 5.370 | 5.519 | 5.583 | |
| 4154 | 4.512 | 3.244 | 3.020 | 3.704 | |
| 4155 | 5.057 | 5.402 | 5.249 | 5.329 | |
| 4157 | 4.646 | 4.831 | 4.741 | 4.801 | |
| 4158 | 4.707 | 4.767 | 4.574 | 4.714 | |
| 4159 | 6.258 | 6.237 | 6.322 | 6.219 | |
| 4161 | 6.384 | 6.536 | 6.258 | 4.913 | |
| 4162 | 7.883 | 4.124 | 3.606 | 4.270 | |
| 4170 | 7.018 | 6.734 | 7.183 | 7.144 | |
| 4171 | 5.661 | 6.401 | 6.432 | 6.052 | |
| 4172 | 5.499 | 5.541 | 5.851 | 4.653 | |
| 4173 | 3.894 | 3.932 | 3.885 | 3.751 | |
| 4174 | 6.419 | 5.997 | 5.841 | 5.990 | |
| 4175 | 4.710 | 4.872 | 5.106 | 4.869 | |
| 4176 | 3.277 | 2.915 | 3.039 | 2.942 | |
| 4179 | 9.082 | 3.291 | 2.585 | 3.145 | |
| 4186 | 7.375 | 5.639 | 7.017 | 7.244 | |
| 4188 | 5.125 | 3.825 | 3.687 | 3.721 | |
| 4190 | 3.047 | 3.046 | 2.722 | 2.678 | |
| 4371 | 3.401 | 3.932 | 2.930 | 3.645 | |
| 4398 | 6.885 | 6.858 | 6.525 | 6.520 | |
| 4402 | 3.200 | 5.004 | – | 5.263 | bad C1–C2 |
| 4404 | 2.778 | 4.523 | 5.000 | 4.717 | |
| 4406 | 4.270 | 5.173 | 5.652 | 5.595 | |
| 4413 | 9.448 | 7.268 | 7.502 | 7.143 | |
| 4414 | 2.887 | 3.463 | 3.365 | 3.490 | |
| 4416 | 2.761 | 2.523 | 2.243 | 2.471 | |
| 4419 | – | – | – | – | measured during dawn |
| 4423 | 3.597 | 3.572 | 3.465 | 3.616 | |
| 4426 | 7.669 | 7.453 | 6.770 | 7.620 | |
| 4428 | 9.519 | 8.208 | 8.076 | 7.422 | |
| 4438 | 5.332 | 5.256 | 5.405 | 5.237 | |
| 4439 | 3.727 | 3.508 | 4.062 | 3.740 | |
| 4440 | 6.079 | 5.921 | 6.569 | 5.761 | |
| 4460 | 5.117 | 5.216 | 5.068 | 5.139 | |
| 4461 | 6.888 | 7.043 | 6.748 | 6.905 | |

Continued on next page

Table A.2 – continued

| HJD (245 000)+ | Methods | | | | Notes |
|-------------------|---------|--------|-------|-------|-----------|
| | A | B | C | D | |
| 4462 | 6.138 | 6.029 | 5.170 | 6.078 | |
| 4463 | 6.046 | 6.797 | 5.148 | 5.554 | |
| 4466 | 5.041 | 5.057 | 5.114 | 5.054 | |
| 4467 | 4.821 | 5.302 | 5.060 | 4.556 | |
| 4477 | 4.632 | 4.868 | 4.336 | 4.498 | |
| 4483 | 5.435 | 5.197 | 5.642 | 5.115 | |
| 4484 | 6.898 | 6.707 | 6.935 | 6.986 | |
| 4485 | 7.217 | 7.885 | 7.197 | 6.839 | |
| 4486 | 6.533 | 6.375 | 6.330 | 6.221 | |
| 4487 | 6.784 | 6.727 | 6.574 | 6.505 | |
| 4503 | 5.652 | 4.809 | 5.325 | 5.658 | |
| 4504 | 5.092 | 5.214 | 5.062 | 5.026 | |
| 4505 | 6.215 | 6.416 | 5.846 | 5.968 | |
| 4506 | 5.331 | 5.224 | 4.735 | 4.636 | |
| 4509 | 6.865 | 6.507 | 6.463 | 6.896 | |
| 4510 | 5.179 | 5.046 | 4.824 | 5.426 | |
| 4517 | 7.188 | 6.808 | 6.878 | 5.447 | |
| 4524 | 4.891 | 4.142 | 5.243 | 5.047 | |
| 4525 | 4.861 | 5.265 | 4.763 | 4.663 | |
| 4531 | 2.947 | 3.344 | 2.925 | 3.094 | |
| 4534 | 6.059 | 6.049 | 5.497 | 6.028 | |
| 4537 | 6.185 | 5.990 | 6.291 | 6.220 | |
| 4545 | 5.498 | 5.552 | 6.247 | 5.873 | |
| 4551 | 4.166 | 4.046 | 3.838 | 4.064 | |
| 4552 | 3.474 | 3.140 | 3.136 | 3.319 | |
| 4554 | 3.590 | 3.229 | 3.231 | 3.301 | |
| 4556 | 5.101 | 4.917 | 4.601 | 4.666 | |
| 4565 | 4.426 | 4.916 | 4.342 | 4.287 | |
| 4566 | 6.530 | 7.538 | 9.518 | – | bad C1–C2 |
| 4567 | 10.556 | 11.188 | 8.433 | – | bad C1–C2 |

A.2 Figures

A.2.1 Light curves of EE Cam

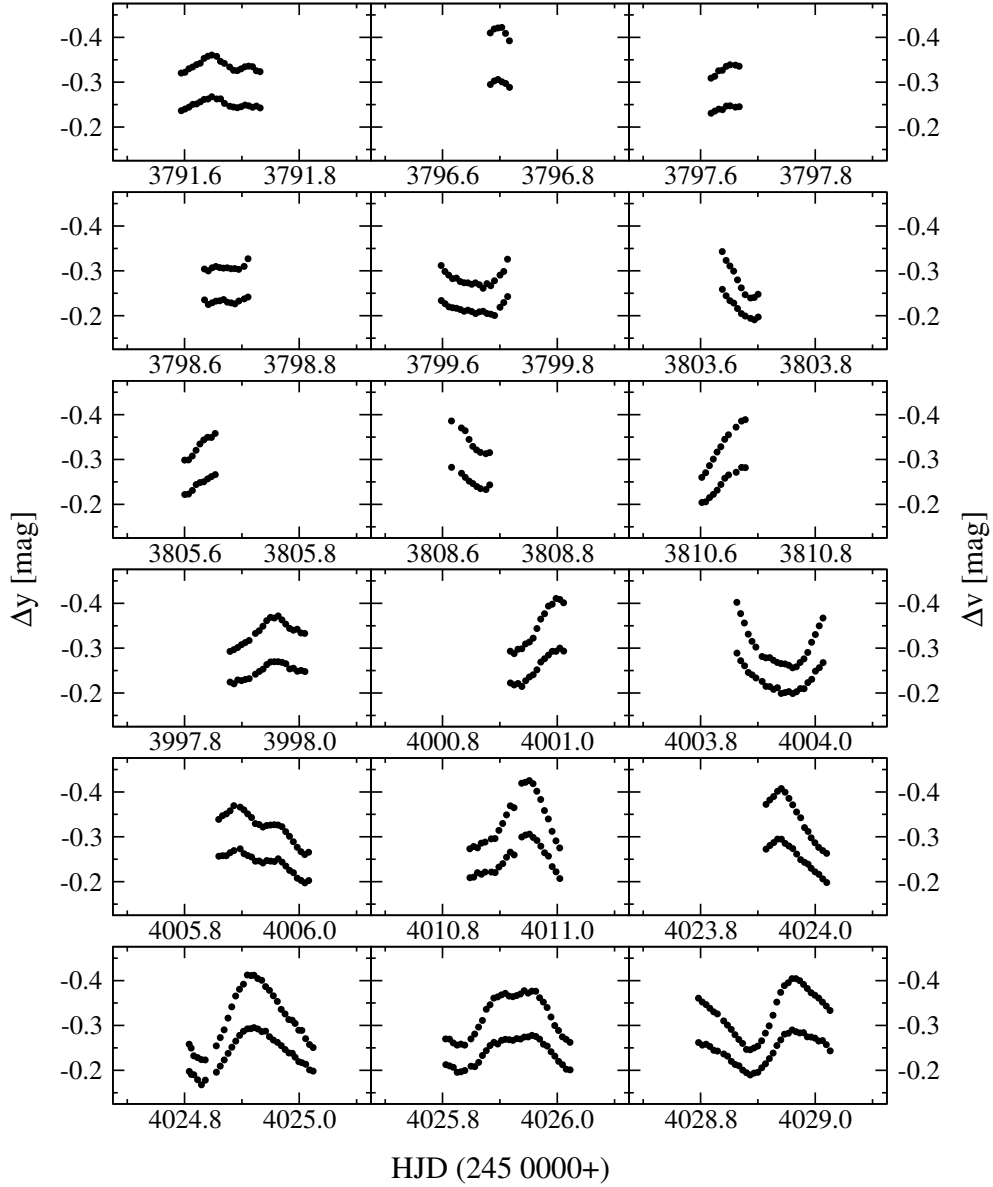


Figure A.1: EE Cam light curves (V-C1 in v and y) obtained with the APT. Continued on next page.

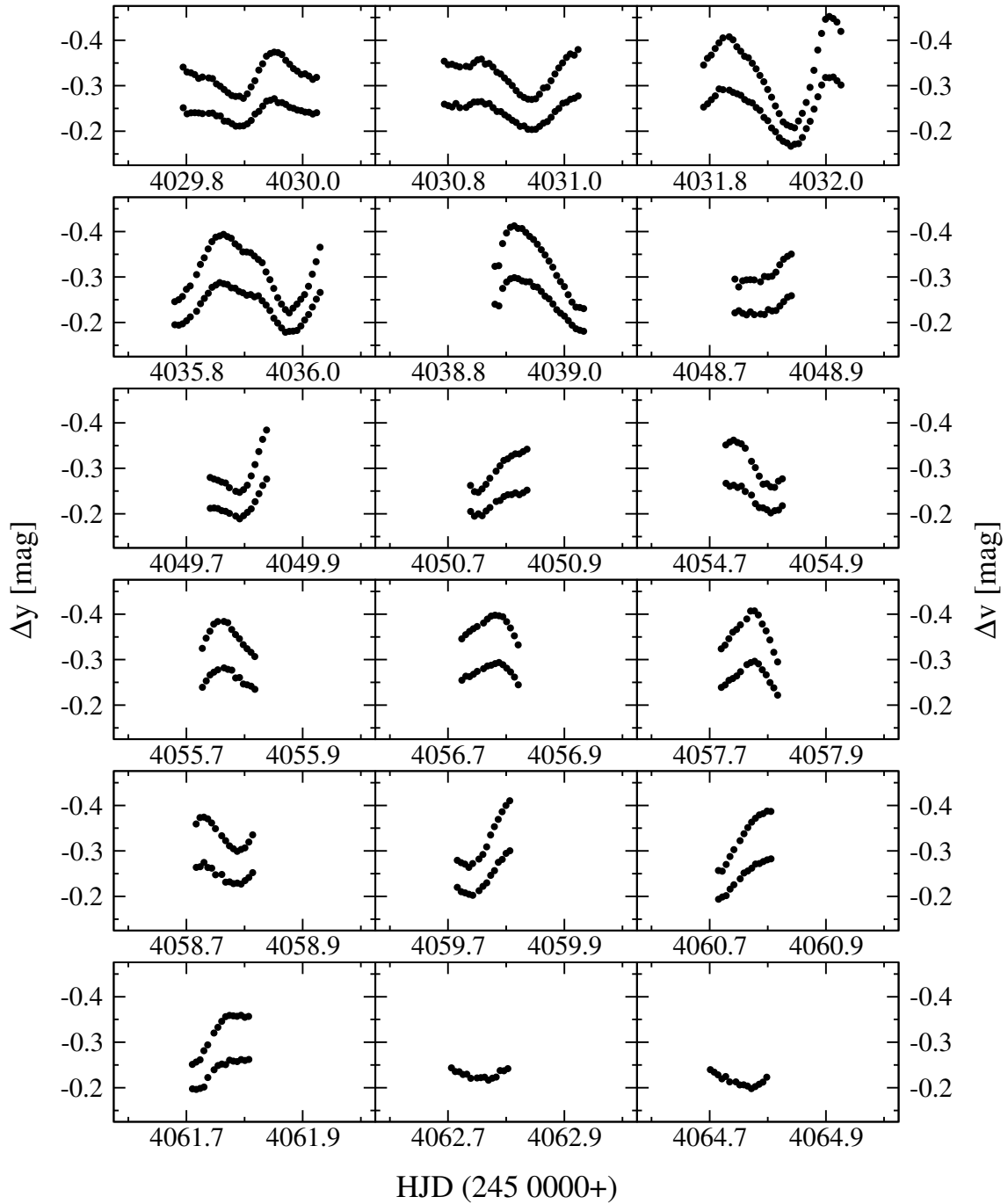


Figure A.1: Continued on next page.

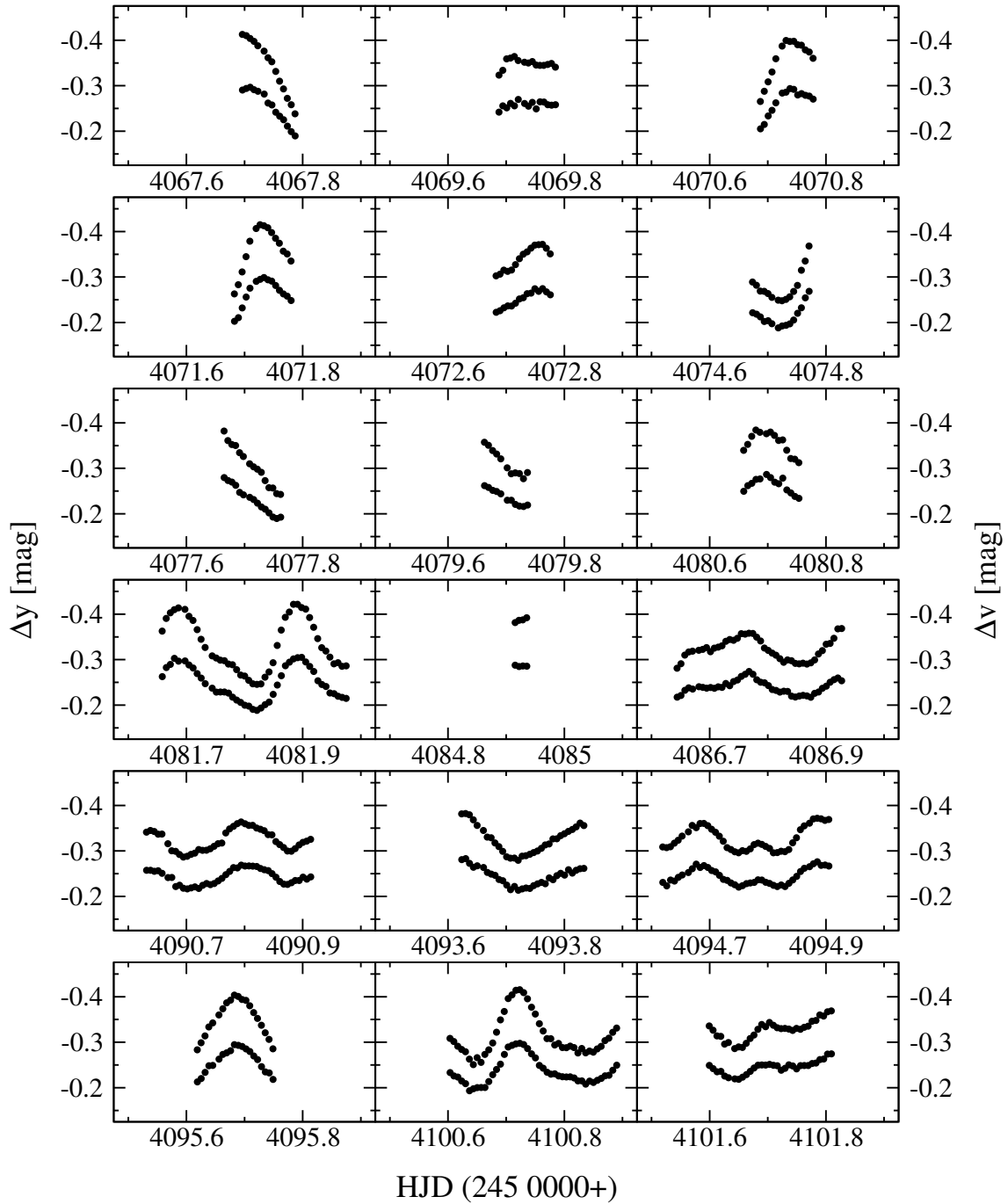


Figure A.1: Continued on next page.

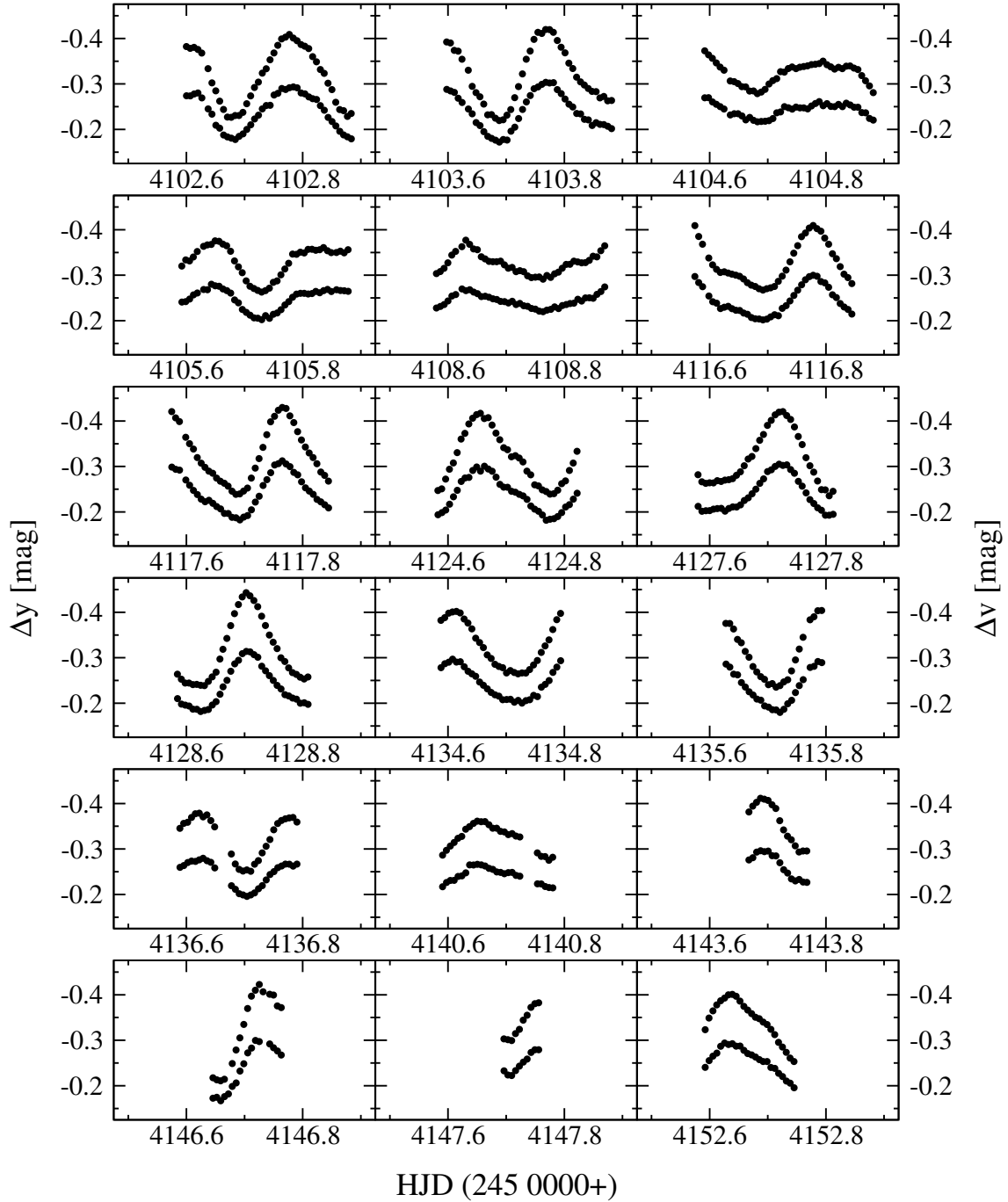


Figure A.1: Continued on next page.

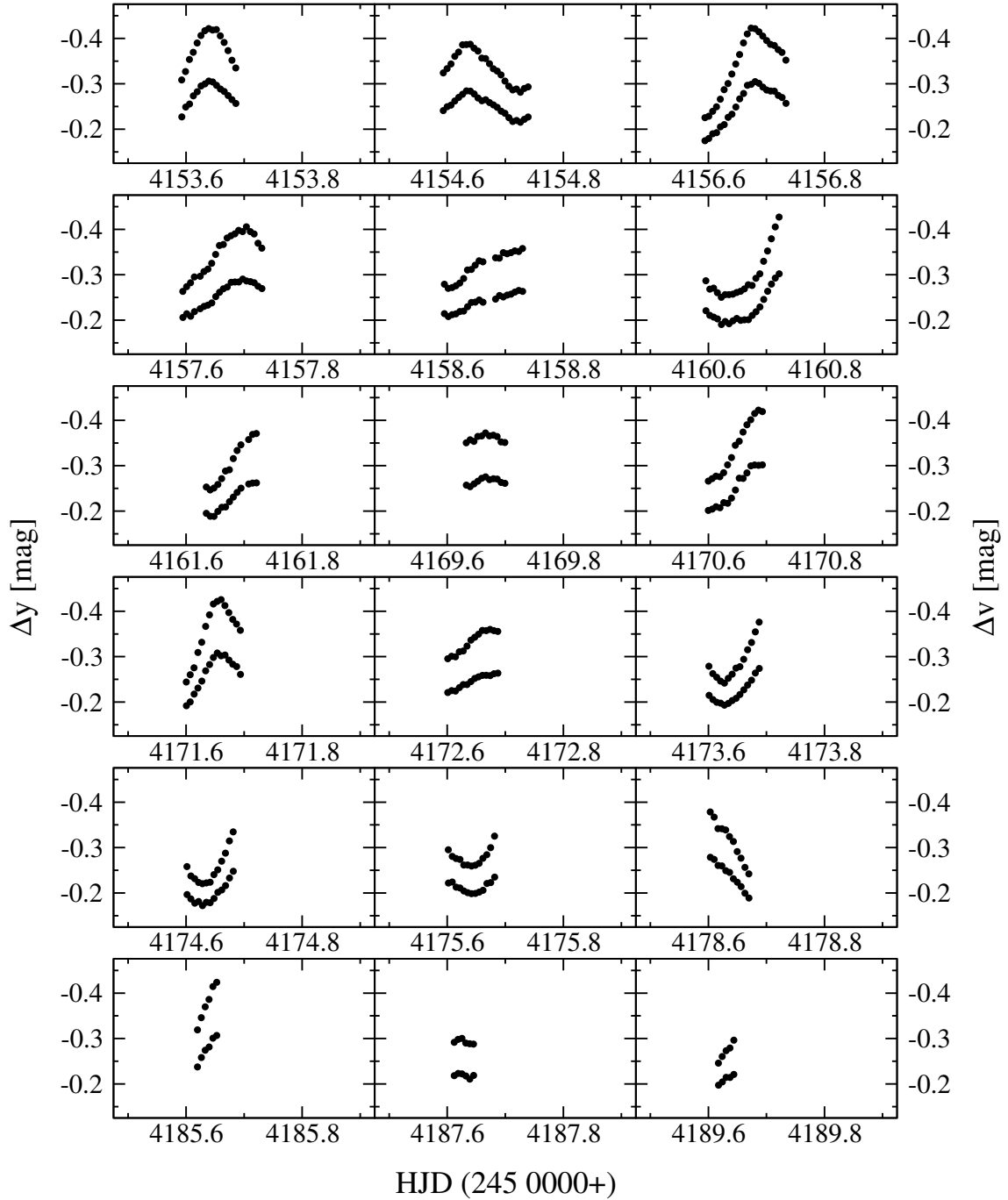


Figure A.1: Continued on next page.

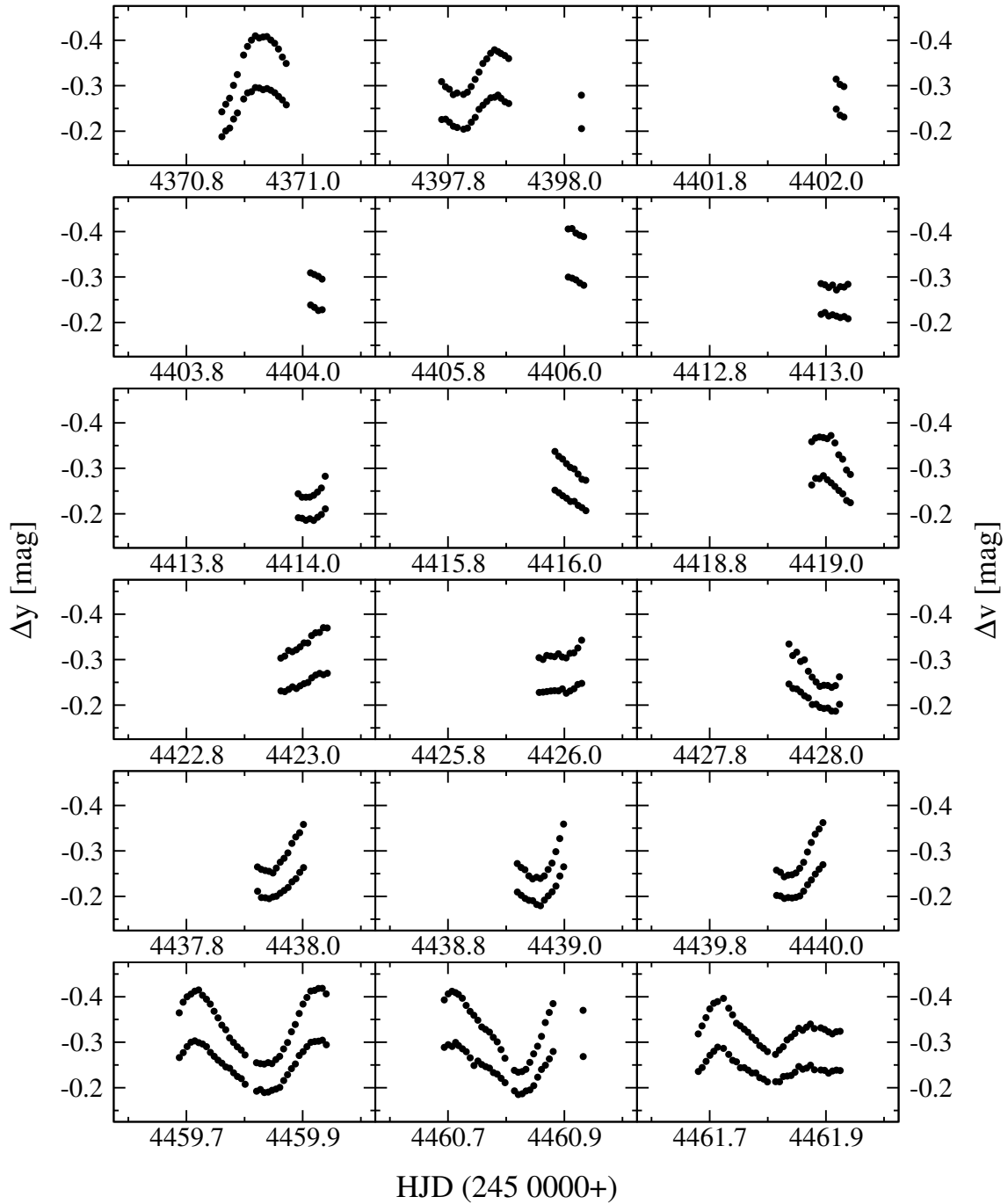


Figure A.1: Continued on next page.

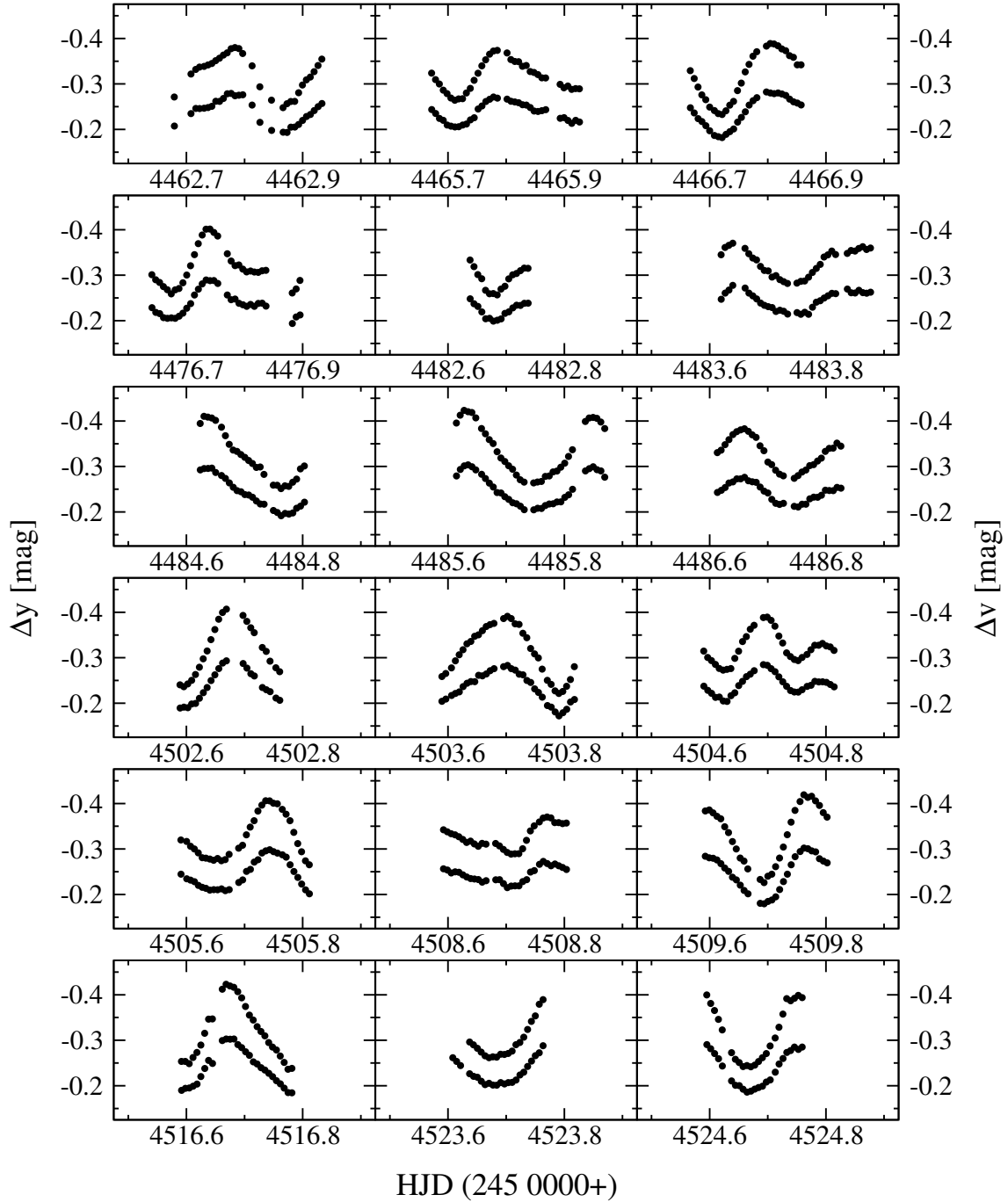


Figure A.1: Continued on next page.

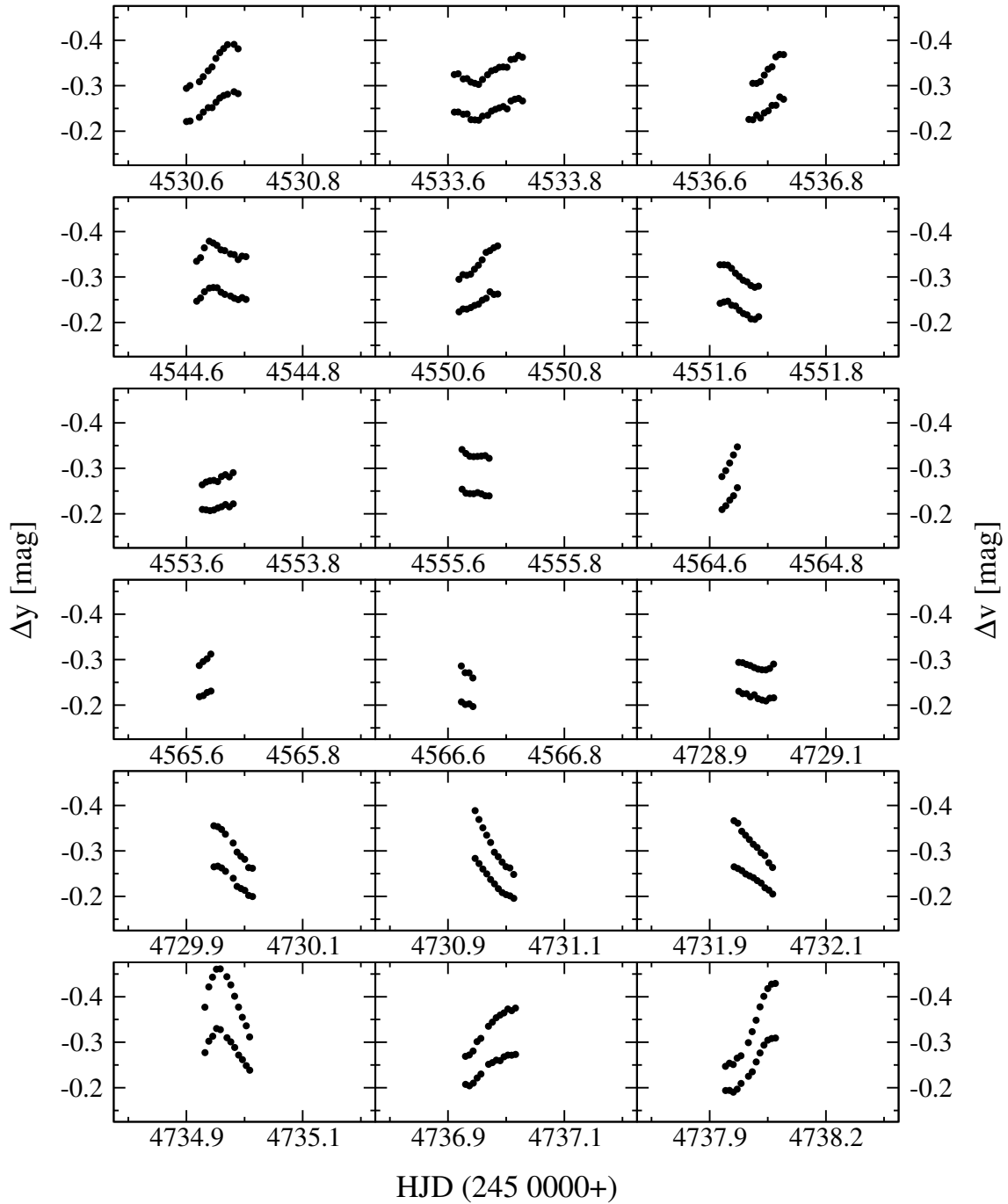


Figure A.1: Continued on next page.

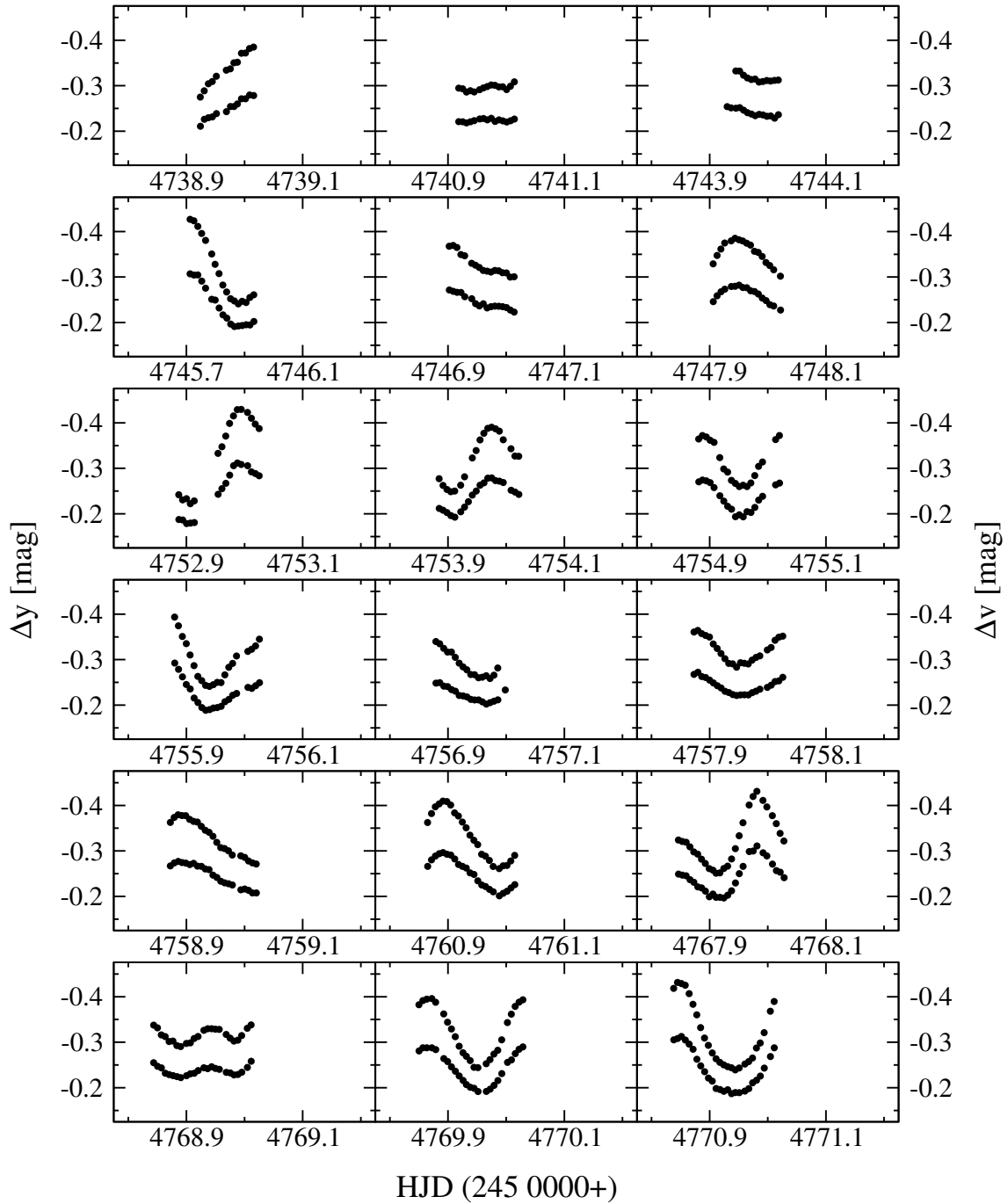


Figure A.1: Continued on next page.

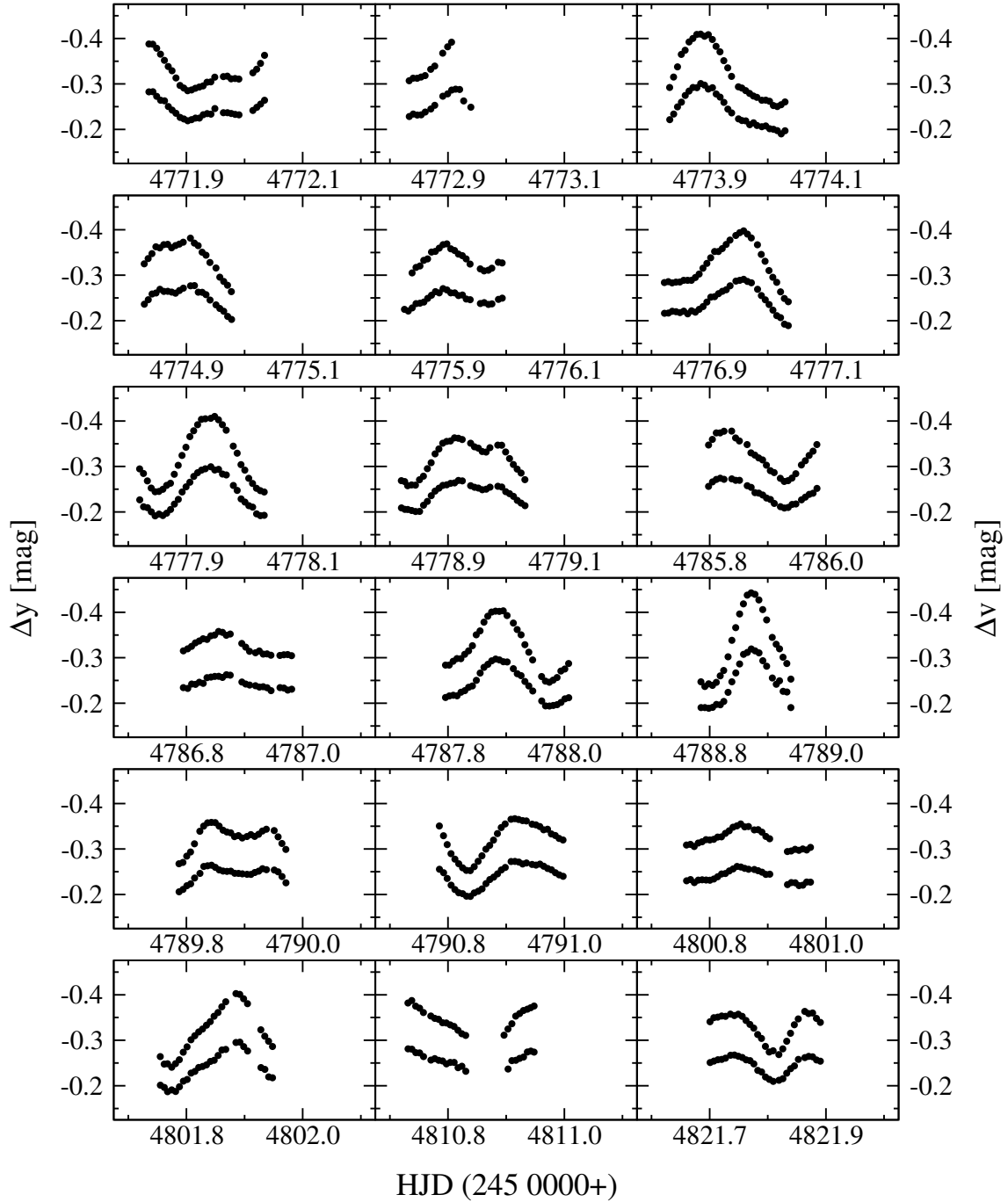


Figure A.1: Continued on next page.

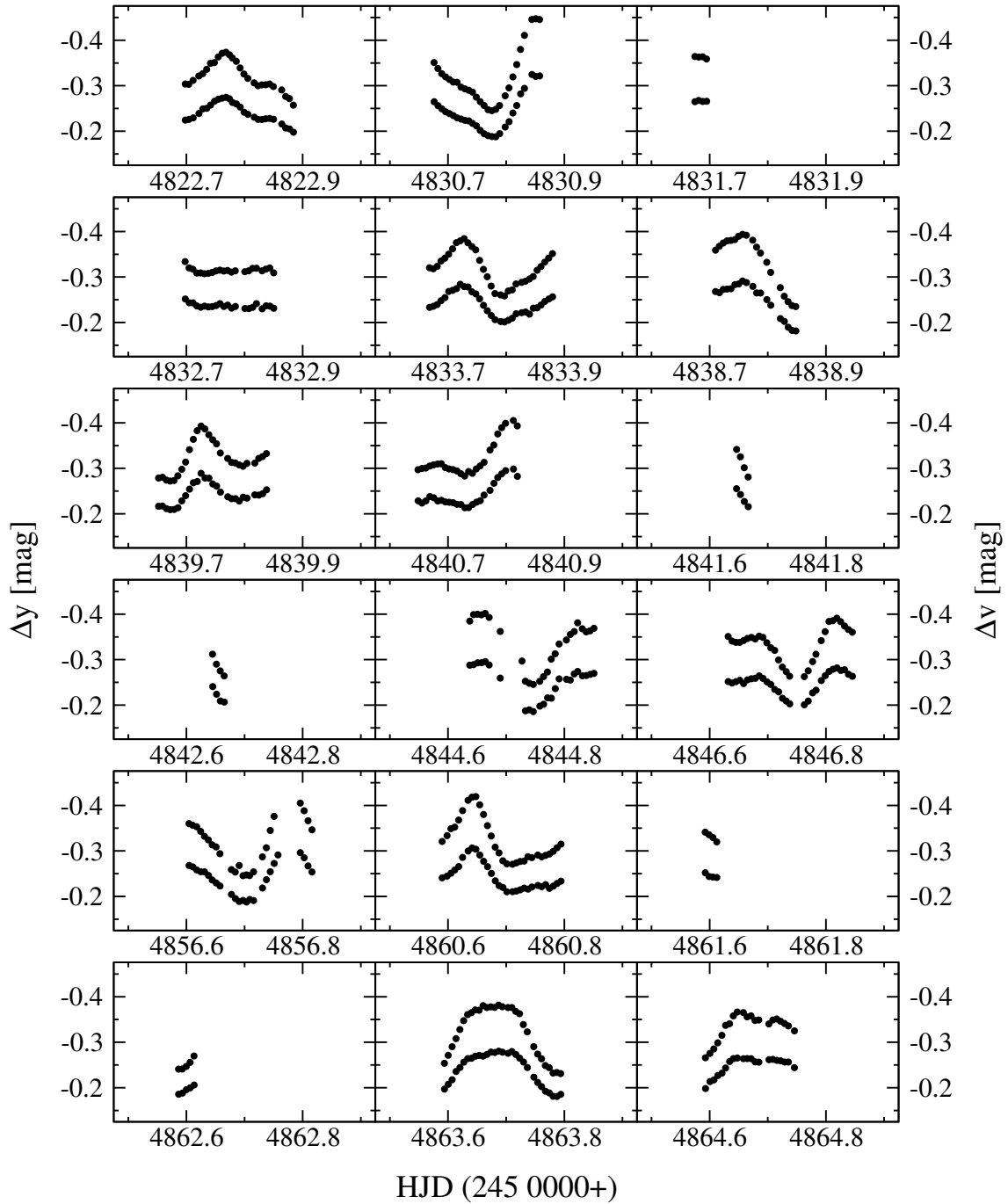


Figure A.1: Continued on next page.

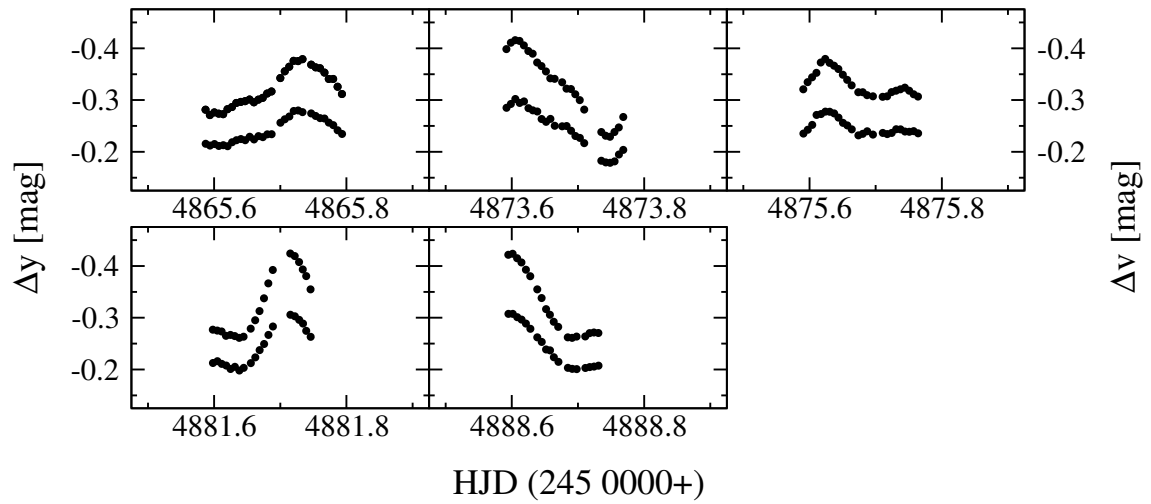


Figure A.1: EE Cam light curves (V-C1 in v and y) obtained with the APT.

References

- Aerts, C. 1996, 314, 115A
- Antoci, V., Breger, M., Rodler, F., Bischof, K., & Garrido, R. 2007, A&A, 463, 225
- Balona, L. A., Krisciunas, K., & Cousins, A. W. J. 1994, MNRAS, 270, 905
- Balona, L. A., & Evers, E. A. 1999, MNRAS, 302, 349
- Bessell, M. S. 1969, Astrophysical Journal Supplement, 18, 195
- Bessell, M. S. 1990, PASP, 102, 1181
- Bigot, L. & Dziembowski, W. A. 2002, A&A, 391, 235
- Breger, M. 1972, ApJ, 171, 539
- Breger, M., & Bregman, J. N. 1975, Astrophys. J., 200, 343
- Breger, M. 1979, PASP, 91, 5
- Breger, M., Stich, J., Garrido, R., et al. 1993, A&A, 271, 482
- Breger, M. 1993, Proceedings of the IAU Colloquium, 136, 106
- Breger, M. 2000a, The Impact of Large-Scale Surveys on Pulsating Star Research, ASP Conference Series 203; also IAU Colloquium # 176. Edited by L. Szabados and D. Kurtz, 421
- Breger, M. 2000b, Delta Scuti and Related Stars, Reference Handbook and Proceedings of the 6th Vienna Workshop in Astrophysics, held in Vienna, Austria, 4-7 August, 1999. ASP Conference Series, 210. Edited by Michel Breger and Michael Montgomery, 3
- Breger, M. 2003, Astrophysics and Space Science, 284, 137
- Breger, M., Lenz, P., Antoci, V., et al. 2005, A&A, 435, 955
- Breger, M. 2007, CoAst, 150, 25
- Breger, M., Rucinski, S. M., & Reegen, P. 2007, The Astronomical Journal, 134, 1994
- Breger, M., & Lenz, P. 2008, A&A, 488, 643
- Budding, E. 1993, An introduction to astronomical photometry, Cambridge University Press, Cambridge, Great Britain
- Christensen-Dalsgaard, J. 2003, <http://www.phys.au.dk/jcd/oscilnotes/>
- Christiansen, J. L., Derekas, A., Ashley, M. C. B., et al. 2007, MNRAS, 382, 239
- Crawford, D. L., & Barnes, J. V. 1970, AJ, 75, 978
- Deeming, T. J. 1975, Ap&SS, 36, 137
- Eggen, O. J. 1956, PASP, 68, 238

-
- Eggen, O. J. 1971, *Publ. Astron. Soc. Pac.*, 83, 762
- Guenther, D. B., Kallinger, T., Zwintz, K., et al. 2007, *The Astrophysical Journal*, 671, 581
- Henry, G. W., Fekel, F. C. 2005, *The Astronomical Journal*, 129, 2026
- Horne, J. H., & Baliunas, S. L. 1986, *ApJ*, 302, 757
- Johnson, H. L., & Morgan, W. W. 1951, *ApJ*, 114, 522
- Johnson, H. L. 1965, *ApJ*, 141, 923
- Jones, D. H. P., & Haslam, C. M 1966, *The Observatory*, 86, 34
- Kim, C., Jeon, Y.-B., & Kim, S.-L. 2002, *Astrophysics and Space Science*, 282, 731
- King, H., Matthews, J. M., Row, J. F., et al. 2006, *CoAst*, 148, 28
- Kristian, J., & Blouke, M. 1982, *SciAm*, 247, 10, 48
- Kurtz, D. W. 2006, *CoAst*, 147, 6
- Lamla, E. 1982, *Landoldt & Börnstein, Volume 2 Astronomy and Astrophysics*, 35
- Lenz, P. 2005, *Diploma Thesis*
- Lenz, P., & Breger, M. 2005, *CoAst*, 146, 53
- Lenz, P., Pamyatnykh, A. A., Breger, M., & Antoci, V. 2008, *A&A*, 478, 855
- Lopez de Coca, P., Garrido, R., Costa, V., & Rolland, A. 1984, *Inf.Bull.Var.Stars*, 2465
- Mantegazza, L., Poretti, E., & Bossi, M. 1994, *A&A*, 287, 95
- Marconi, M., Palla, F., & Ripepi, V. 2002, *CoAst*, 141, 13
- McCarthy, D. D. 1998, *Journal for the History of Astronomy*, 327
- Meeus, J. 1998, *Astronomical Algorithms*, Willmann-Bell, Inc, Richmond, 132
- Mittermayer, P., & Weiss, W. W. 2003, *A&A*, 407, 1097
- Montenbruck, O. 2001, *Grundlagen der Ephemeridenrechnung, Sterne und Weltraum*, Heidelberg
- Napiwotzki, R., Schönberner, D., & Wenske, V. 1993, *A&A*, 268, 653
- Nordström, B., Mayor, M., Andersen, J., et al. 2004, *A&A*, 418, 989
- Olsen, E. H. 1980, *A&AS*, 39, 205
- Perryman, M. A. C., Lindegren, L., Kovalevsky, J., et al. 1997, *A&A*, 323, 49
- Reegen, P., Kallinger, T., Frast, D., et al. 2006, *MNRAS*, 367, 1417
- Reegen, P. 2007, *A&A*, 467, 1353
- Reegen, P. 2000, *PhD thesis*
- Rodriguez, E. 1994, *CoAst*, 145, 42
- Rodriguez, E., Amado, P. J., Costa, V., et al. 2006, *Memorie della SAI*, 77, 478
- Rowe, J. F., Matthews, J. M., Cameron, C., et al. 2006, *CoAst*, 148, 34
- Rufener, F. 1986, *A&A*, 165, 275
- Scargle, J. D. 1982, *ApJ*, 263, 835
- Smith, H. J. 1955, *Astronomical Journal*, 60, 179

- Solano, E., & Fernley, J. 1997, A&A Supplement series, 122, 131
- Sterken, C., & Manfroid, J. 1992, *Astronomical Photometry*, Kluwer Academic Publishers, Netherlands
- Strassmeier, K. G., Boyd, L. J., Epanch, D. H., & Granzer, Th. 1997, *PASP*, 109, 697
- Suran, M., Goupil, M., Baglin, A., et al. 2001, *A&A*, 372, 233
- Zima, W. 1999, Master Thesis
- Zima, W., Lehmann, H., Stütz, Ch., Ilyin, I. V., & Breger, M. 2007, *A&A*, 471, 237
- Zwintz, K. 2008, *The Astrophysical Journal*, 673, 1088

Acknowledgements

First of all, I would like to express my gratitude to my advisor Michel Breger, who provided me with helpful suggestions and advice during the course of this work.

Special thanks go to my colleagues at the Institute of Astronomy:

- Victoria Antoci for proof-reading this work with so much patience,
- Paul Beck, who helped me with Latex and distracted me from this work when needed,
- Gerald Handler for providing his extinction coefficients and for many helpful suggestions,
- Patrick Lenz for sharing his expertise concerning Period04 and mode identification,
- Peter Reegen, who answered all my questions (and there were a lot), encouraged me constantly and improved this work considerably.

Last but not least, I want to thank my family and friends for their moral support, patience and encouragement during all these years.

Abstract – German

Die Erforschung der Entwicklung und des Aufbaus von pulsierenden Sternen ist ein fundamentales Gebiet der Astronomie. Um Aussagen über diese Eigenschaften treffen zu können ist es notwendig, das Innere der Sterne zu erforschen. Die Asteroseismologie bietet diese Möglichkeit, indem photometrischen Daten gewonnen werden, welche die Helligkeitsvariationen eines pulsierenden Sterns liefern. Mit Hilfe einer Frequenzanalyse ist es möglich, die Frequenzen, Amplituden und Phasen eines periodisch Veränderlichen zu bestimmen. Diese liefern die notwendigen Informationen über die Schallwellen, welche Auskunft über das Innere der Sterne geben. Anhand dieser Erkenntnisse können die stellaren Parameter und physikalischen Prozesse im Stern beschrieben werden. Schon vorhandene theoretische Modelle können nun auf den Stern angewandt werden, um diese zu bestätigen oder zu falsifizieren. Um eine ausreichende Genauigkeit der photometrischen Daten zu erreichen, muss man einige instrumentelle und atmosphärische Effekte und Rauschquellen berücksichtigen und, wenn möglich, korrigieren.

Diese Diplomarbeit beschäftigt sich vorwiegend mit der beobachtenden Asteroseismologie. Verschiedene Quellen von Rauschen als auch die einzelnen Schritte der Datenreduktion werden erläutert, und gebräuchliche Algorithmen sind angeführt. Ein großer Teil dieser Arbeit beschäftigt sich mit der Bestimmung des bestmöglichen Extinktionskoeffizienten. Dieser ist Voraussetzung für eine zufriedenstellende Korrektur der atmosphärischen Extinktion. Vier unterschiedliche Methoden zur Bestimmung dieses Koeffizienten werden auf photometrische Daten des δ Scuti Sterns EE Cam angewandt, welche mit dem Vienna Twin Automatic Photoelectric Telescopes (APT) zwischen 2006 und 2009 in vier Beobachtungssaisonen gewonnen wurden. Zusätzlich wurde für die reduzierten Daten der ersten drei Saisonen eine Frequenzanalyse durchgeführt.

Eine Beschreibung von pulsierenden Sternen, ihres inneren Aufbaus und der Anregungsmechanismen der Pulsation enthält Kapitel 1. Kapitel 2 liefert eine Beschreibung der Instrumente und Filter, welche verwendet werden, um photometrische Daten zu gewinnen. EE Cam wurde mit dem APT beobachtet, welches hier genauer beschrieben wird. Das Problem instrumentellen Rauschens und etwaige Lösungsvorschläge werden behandelt. Die einzelnen Schritte der Datenreduktion, welche auf alle photometrischen Daten angewandt werden muss, werden in Kapitel 3 beschrieben. Eine kurze Einführung in die Diskrete Fourier-Transformation und die Bestimmung der Frequenz, Phase und Amplitude liefert Kapitel 4. Zwei Computerprogramme zur Durchführung der Frequenzanalyse werden vorgestellt. Kapitel 5 enthält die Beobachtungsdetails, wie Sternparameter, Länge der Datensätze, Lichtkurven von EE Cam, usw. Hier werden auch die Resultate präsentiert und diskutiert.

Curriculum Vitae

Persönliche Daten

| | |
|---------------------|---------------------------------|
| Geburtsdatum | 08.12.1984 |
| Nachname | Klotz |
| Vorname | Daniela |
| Adresse | Obere Bahngasse 20/6, 1030 Wien |
| Telefon | +43/0650/8200644 |
| E-mail | klotz@astro.univie.ac.at |
| Nationalität | Italien |

Ausbildung

| | |
|------------------|--|
| 1990-1995 | Volksschule "Hermann von Gilm", Meran |
| 1995-1998 | Mittelschule "Meran III", Meran |
| 1998-2003 | Handelsoberschule, Meran |
| 2003 | Matura mit Auszeichnung bestanden |
| 2003-2004 | Studium der Anglistik, Universität Wien |
| 2004-2007 | Bakkalaureatstudium der Astronomie, Universität Wien |
| 2007 | Bakkalaureatsarbeit Messung der künstlichen Nachthimmelshelligkeit und Lichtverschmutzung |
| Juli 2007 | Abschluss des Bakkalaureatstudiums |
| 2007-2009 | Magisterstudium der Astronomie, Universität Wien |
| 2008-2009 | Magisterarbeit: " Optimizing extinction corrections in time series photometry |
| Mai 2009 | Erhalt eines Leistungsstipendiums |

Sonstiges

| | |
|---------------------|--|
| 2006-2007 | Nachhilfe in Englisch, Mathematik, BWL, Italienisch |
| 19. Mai 2007 | Teilnahme am Österreichischen Tag der Astronomie |
| seit 2007 | Editorial Assistant bei "Communications in Asteroseismology" |

- Februar 2008** Veröffentlichung der Bakkalaureatsarbeit
auf www.ambientesalute.org
- März 2008** Interview über Lichtverschmutzung im Radio Rai Sender Bozen
- April 2008** Artikel über Lichtverschmutzung mit Georg Zotti
veröffentlicht auf www.der-orion.com

Internationale Tagungen

- 5.-6. Oktober 2007** 7th European Symposium for the Protection
of the Night Sky, Bled
Vortrag über Lichtverschmutzung
- 22.-23. August 2008** 8th European Symposium for the Protection
of the Night Sky, Vienna
Technische Assistentin